Heterogeneous nitrate production mechanisms in intense haze events

Yuk Chun Chan

A thesis

submitted in partial fulfillment of the

requirements for the degree of

Master of Science

University of Washington

2021

Committee:

Becky Alexander

Lyatt Jaeglé

Joel A. Thornton

Program Authorized to Offer Degree:

Atmospheric Sciences

University of Washington

Abstract

Heterogeneous nitrate production mechanisms in intense haze events

Yuk Chun Chan

Chair of the Supervisory Committee:
Professor Becky Alexander
Department of Atmospheric Sciences

The importance of heterogeneous (multi-phase) reactions between trace gases and particulates in controlling the tropospheric chemistry of reactive nitrogen oxides and driving the production of nitrate has long been recognized. However, less is known about how different chemical mechanisms contribute to nitrate production in intense haze events. I analyze the wintertime observations of reactive nitrogen oxides and isotopic composition of nitrate in Beijing, China, where intense haze events frequently occurred in the first two decades of the 21st century. The observation data are compared to predictions from the GEOS-Chem 3-D chemical transport model. The analysis shows that the mechanism that involves N_2O_5 most likely dominates nitrate production in wintertime Beijing, while the mechanism that involves NO_2 is a major source of

uncertainty in the model. I conduct a critical review of previous laboratory studies of NO_2 uptake on different surfaces and explain the origins of the model uncertainty.

TABLE OF CONTENTS

LIST OF FIGURES

LIST OF TABLES

ACKNOWLEDGEMENTS

Over the course of this master thesis project, my advisor Becky Alexander has been a marvelous mentor and provided me with unfailing guidance and support. She is my role model for being a scientist who achieves a great balance in research, teaching, mentoring, community services, and family. I look forward to exploring the other subjects in science with her in the next stage of the graduate program and beyond. I would like to thank my master committee members Lyatt Jaeglé and Joel Thornton for their very helpful inputs at various stages of the project. I would like to thank my research collaborators at the other institutes for providing observation data and model code essential for completing this project. I would like to thank GRAD-18 Cohort for their support along the graduate school processes. I would like to acknowledge the funding support from National Science Foundation Grant AGS 1644998.

Chapter 1. INTRODUCTION

Nitrate is an important component of tropospheric aerosols on Earth. It is produced by the oxidation of NO_2 via different pathways in the atmosphere. The formation of nitrate on aerosols, clouds, and other surfaces via heterogeneous (multi-phase) reactions is of great interest to atmospheric chemists and air-quality researchers because of their importance during haze events, but many key processes remain uncertain.

In Chapter 2, observations of ^{17}O excess nitrate ($\Delta^{17}O(NO_3^-)$) and other chemistry metrics in Beijing and China, one of the regions that experienced the most intense haze events in the early 21st century, are analyzed to improve our understanding of the heterogeneous nitrate production mechanisms. The observations are compared to the 3-D simulations of nitrate formation produced by the GEOS-Chem chemical transport model in different model experiments, in which we vary the important chemistry parameters for nitrate production. This chapter has been submitted to *Journal of Geophysical Research: Atmospheres* as a paper manuscript for potential publication as a research article.

In Chapter 3, I review the current literature on the NO_2 uptake on aerosols, which is identified as an uncertain nitrate-production pathway in intense haze in Chapter 2. Different hypothesized mechanisms are introduced, and their uncertainties are evaluated critically.

Chapter 2. HETEROGENEOUS NITRATE PRODUCTION MECHANISMS IN INTENSE HAZE EVENTS IN NORTH CHINA

This chapter has been submitted to Journal of Geophysical Research: Atmospheres on the 29th January 2021. The supplementary information for the manuscript is included as Appendix A. Figures and tables have been re-numbered to adjust to the thesis format.

Yuk-Chun Chan, Mathew J. Evans, Pengzhen He, Christopher D. Holmes, Lyatt Jaeglé, Prasad Kasibhatla, Xue-Yan Liu, Tomás Sherwen, Joel A. Thornton, Xuan Wang, Zhouqing Xie, Shuting Zhai, and Becky Alexander, Heterogeneous nitrate production mechanisms in intense haze events in North China, Submitted to *Journal of Geophysical Research: Atmospheres*

ABSTRACT

Studies of wintertime air quality in North China show that particulate-nitrate pollution persists despite rapid reduction in NO_x emissions. This intriguing NO_x-nitrate relationship may originate from non-linear nitrate-formation chemistry, but it is unclear which feedback mechanisms dominate in North China. In this study, we re-interpret the wintertime observations of ^{17}O excess of nitrate ($\Delta^{17}O(NO_3^-)$) in Beijing using the GEOS-Chem (GC) chemical transport model to estimate the importance of various nitrate-production pathways and how their contributions change with the intensity of haze events. We also analyze the relationships between other metrics of NO_y chemistry and [$PM_{2.5}$] in observations and model simulations. We find that the model on average

has a negative bias of – 0.9 ‰ and − 36% for $\Delta^{17}O(NO_3^-)$ and $[O_{x,major}]$(≡ $[O_3]$ + $[NO_2]$ + [p-NO_3^-]), respectively, while overestimating the nitrogen oxidation ratio ($[NO_3^-]/([NO_3^-]+ [NO_2])$) by +0.12 in intense haze. The discrepancies become larger in more intense haze. We attribute the model biases to an overestimate of NO_2-uptake on aerosols and an underestimate in wintertime O_3 concentrations. Our findings highlight a need to address uncertainties related to heterogeneous chemistry of NO_2 in air-quality models. The combined assessment of observations and model results suggest that N_2O_5 uptake in aerosols and clouds is the dominant nitrate-production pathway in wintertime Beijing, but its rate is limited by ozone under high-NO_x-high-$PM_{2.5}$ conditions. Nitrate production rates may continue to increase as long as $[O_3]$ increases despite reduction in $[NO_x]$, creating a negative feedback that reduces the effectiveness of air pollution mitigation strategies.

2.1 INTRODUCTION

Haze events, which are episodes of high concentrations of particulate matter (PM) in the lower troposphere, are common in many metropolitan areas around the world. Industrial activities, heavy traffic, and weak ventilation all favor the occurrence of haze events near population centers. North China, in particular, has been affected by intense wintertime haze in recent decades (An et al., 2019; Y.-L. Zhang & Cao, 2015). Frequent outbreaks of haze events can lead to short-term surges in premature mortality and long-term reduction in life expectancy (Y. Chen et al., 2013; Lelieveld et al., 2015; C. Song et al., 2017). An important source of fine-mode PM ($PM_{2.5}$, particulate matter with a diameter of less than 2.5 μm) during haze events is chemical reactions that oxidize gas-

phase pollutants into $PM_{2.5}$. To mitigate haze events in metropolitan areas effectively, we must understand the chemical mechanisms driving this secondary production of $PM_{2.5}$.

Nitrate is becoming the dominant inorganic component of $PM_{2.5}$ over China in recent years, especially during wintertime haze events (Fu et al., 2020; Itahashi et al., 2018; H. Li et al., 2019; Y. Sun et al., 2020; Xu et al., 2019; Zhou et al., 2019). The Chinese government implemented a series of clean air policies since the year 2010 that imposed stricter controls on the emissions of SO_2, NO_x ($NO+NO_2$), and primary PM (Zheng et al., 2018). As a result, wintertime sulfate concentration decreased substantially by about 60% from 2014 to 2017 (H. Li et al., 2019; Zhou et al., 2019). A similar long-term concentration reduction was not observed in particulate nitrate ($p\text{-}NO_3^-$) despite a steady decline in NO_x emission in the 2010s (Fu et al., 2020; Itahashi et al., 2018; H. Li et al., 2019; Xu et al., 2019). Analysis of the aerosol sampled in Beijing in 2017 showed that nitrate contributes 25-35% to fine-mode-PM mass during wintertime haze events (H. Li et al., 2019; Xu et al., 2019), which is higher than similar observations in 2014 (<20%) (H. Li et al., 2019). In the eastern US and northern China, the concentration of wintertime secondary aerosol, including nitrate and sulfate, also responds weakly to the reduction of NO_x and SO_2 emissions, which is largely attributed to non-linear chemical feedbacks (Huang et al., 2020; Le et al., 2020; Leung et al., 2020; Shah et al., 2018; Y. Sun et al., 2020). In light of the emerging importance of nitrate in PM pollution in North China, it is essential to understand the chemistry of nitrate production during wintertime haze events in order to implement effective air pollution mitigation strategies.

Reactions of reactive nitrogen oxides ($NO_y \equiv NO_x + NO_3 + 2\times$dinitrogen pentoxide ($N_2O_5$) + nitryl chloride ($ClNO_2$) + gas-phase nitric acid (HNO_3) + particulate nitrate ($p\text{-}NO_3^-$) + nitrous acid (HONO) + halogen nitrates (ξNO_3, where ξ = Br, Cl, or I) + peroxynitric acid (HNO_4) + peroxyacylnitrates (PANs) + other organic nitrates ($RONO_2$)) control both nitrate production and oxidant budgets in North China (See Figure **2-1** and Table **A-1**). Production of NO_3^- (total nitrate $NO_3^- = HNO_3 + p\text{-}NO_3^-$) is the main sink of NO_x in polluted urban air (Kenagy et al., 2018; Shah et al., 2020). In Beijing, the majority of locally produced HNO_3 quickly converts into $p\text{-}NO_3^-$ via thermodynamically controlled gas-particle partitioning (Ding et al., 2019). The dominant chemical pathway for nitrate production varies diurnally and seasonally. During the daytime, the oxidation of NO_2 by hydroxyl radical (OH) (Figure **2-1**b, R4) dominates nitrate production, whereas the reactions of nitrate radical (NO_3) (Figure **2-1**b, R8-12), including N_2O_5 uptake (Figure **2-1**b, R10-11), dominate at night (Alexander et al., 2020). Shah et al. (2020) showed that N_2O_5 uptake and OH oxidation contribute similarly to NO_x loss (33% vs. 43% in 2017) over summertime in central-eastern China, which is similar to the global annual average (41-42% vs. 28-41%) (Alexander et al., 2020). In winter, on the contrary, N_2O_5 uptake dominates over OH oxidation (51% vs. 23%) (Shah et al., 2020). The conversion of NO_x to NO_3^- is coupled to many other reactive species in the atmosphere, including ozone, peroxy radicals (RO_2), and HONO. For instance, the production of NO_3 radical requires ozone (Figure **2-1**b **b**, R6); yet the efficiency of ozone production is, in turn, controlled by the amount of NO_x and peroxy radicals. Meanwhile, the uptake of NO_2 on aerosols (Figure **2-1**b, R5) and photolysis of $p\text{-}NO_3^-$ can produce HONO, which yields OH readily upon photolysis and may control the tropospheric oxidizing capacity under haze conditions (L. Li et al., 2018; Z. Tan et al., 2019; J. Zhang et al., 2019). A comprehensive representation of nitrate chemistry in models is necessary for accurate predictions of air quality in winter.

While heterogeneous chemistry (i.e., multi-phase reactions) of NO_y is critical to wintertime nitrate production in urban air, its complexity represents a major source of uncertainty in many air-quality models. The uptake of NO_2 on aerosols, which has been presumed to be a sink of NO_x and a source of NO_3^- and HONO in models, was re-examined in recent modeling studies. Holmes et al. (2019) decreased the uptake coefficients of NO_2 ($\gamma(NO_2)$) in their model after considering the lower estimates of $\gamma(NO_2)$ reported in more recent laboratory studies. Jaeglé et al. (2018) showed that changing the HONO yield of NO_2 uptake to 100% (no HNO_3 formation) improves the simulation of NO_y chemistry over wintertime Northeast United States. A global model study by Alexander et al. (2020) demonstrated that NO_2 uptake has the largest potential influence over North China. For N_2O_5 uptake on aerosol, the efficiency of nitrate formation is sensitive to the chemical composition (e.g., $[Cl^-]$, $[p\text{-}NO_3^-]$, and thickness of organic coating), pH, and water content of aerosols (Bertram & Thornton, 2009; Gaston et al., 2014; Tham et al., 2016; Xia et al., 2019; Zhou et al., 2018). Laboratory-based predictions of the uptake coefficient of N_2O_5 ($\gamma(N_2O_5)$) on aerosols often differ from the observation-based estimates by orders of magnitudes (e.g., McDuffie et al., 2018; C. Yu et al., 2019). In addition to reactions on aerosol surfaces, recent modeling studies also suggest that uptake of NO_y in cloud droplets is an overlooked sink of NO_x (Holmes et al., 2019). Cloud uptake of NO_y contributes up to 25% NO_x loss at higher latitudes annually (Alexander et al., 2020; Holmes et al., 2019). Given the large number of remaining uncertainties in heterogeneous chemistry of NO_y, models need additional observational constraints for improving the representation of these chemical processes in air quality models.

The oxygen isotopic composition of nitrate provides an independent piece of information related to the formation of nitrate. In particular, ^{17}O excess ($\Delta^{17}O$) in nitrate, which is determined solely by the relative importance of ozone to other oxidants during the oxidation of the members of NO_y family (Michalski et al., 2003), has proven to be a promising proxy for quantifying nitrate-production mechanisms in various environmental contexts (e.g., Alexander et al., 2020; Geng et al., 2017; Savarino et al., 2013). Three studies have reported observations of $\Delta^{17}O(NO_3^-)$ in North China during winter haze events (He et al., 2018; W. Song et al., 2020; Yan-Li Wang et al., 2019). Their analyses of the observations suggested that uptake of N_2O_5 and the oxidation of volatile organic compounds (VOCs) by NO_3 radicals (Figure **2-1**b, R12) dominate wintertime nitrate production near Beijing. However, their interpretation of the observations relies on highly simplified models of nitrate production and several assumptions about the concentration of radicals in urban air. In this study, we use a 3-D chemical transport model with coupled HO_x-NO_x-VOC-ozone-halogen-aerosol tropospheric chemistry to re-interpret the observations of $\Delta^{17}O(NO_3^-)$ in North China in order to gain insight into the mechanisms of NO_y chemistry during winter haze events.

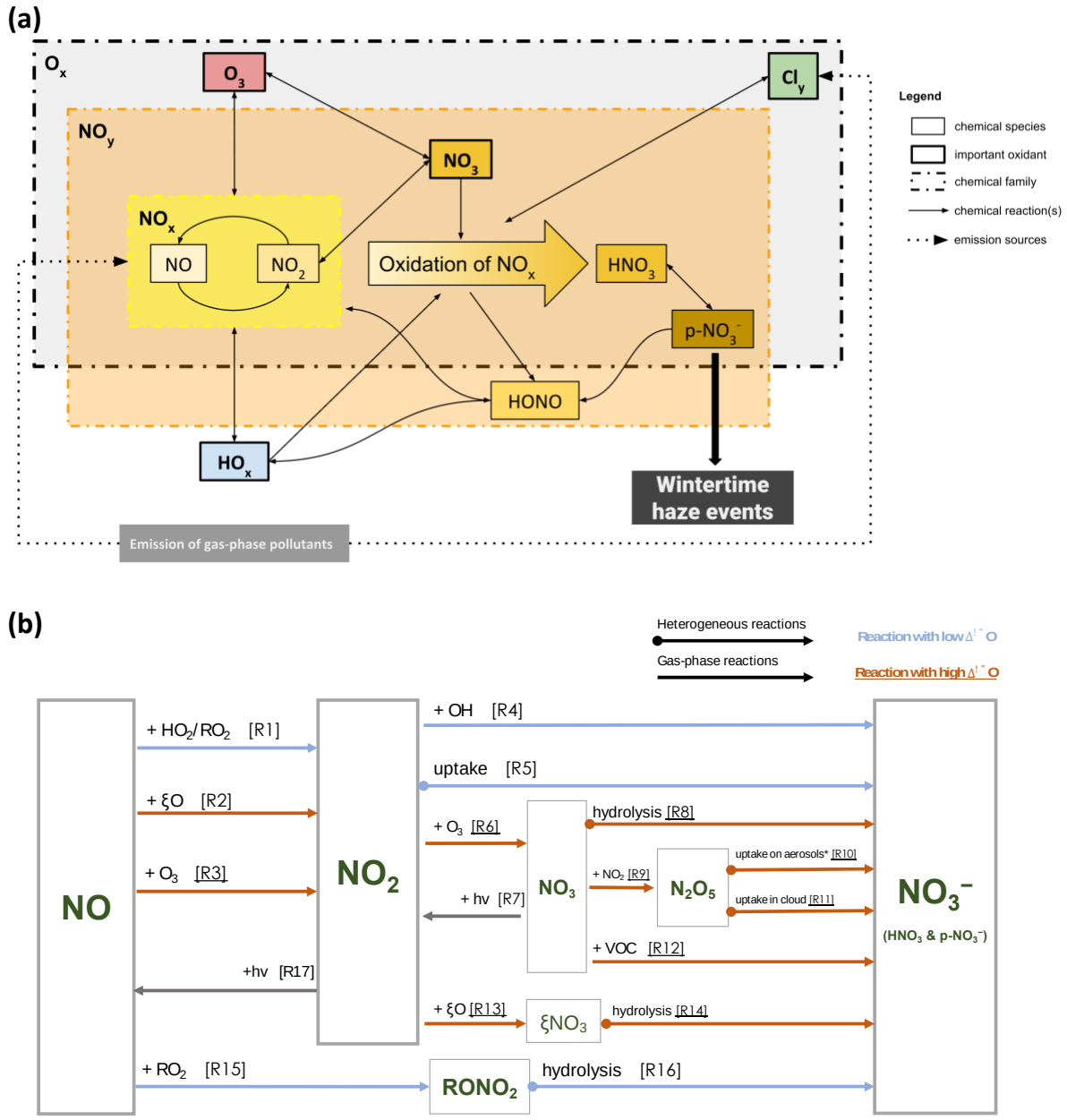

Figure 2-1 Simplified schematic of the chemistry of nitrate production in urban air. 1(a) is the schematic of the coupling of nitrate production and the emission of gas-phase pollutants, the NOy chemical family, the budget of odd oxygen species, and PM pollution. 1(b) is the schematic of nitrate production pathways in the model and important intermediate species from the oxidation of NOx to NO3− ([NO3−] = [HNO3] + [p-NO3−]). "ξ" stands for the halogens (Cl/ Br/I), while "VOC" stands for volatile organic compounds. N2O5 uptake on aerosols (R10) can undergo two possible pathways, depending on the chloride content in

the aerosol. The chemical equation and other details of the reactions R1 to R17 can be found in Table **A-1**.

2.2 DATA AND METHODS

2.2.1 *Measurements of $\Delta^{17}O(NO_3^-)$, aerosol, and trace gases during Beijing in winter 2014-15*

Observations of $\Delta^{17}O(NO_3^-)$ in Beijing were previously published in He et al. (2018), Y. Wang et al. (2019), and W. Song et al. (2020) and are briefly described here. Most of the aerosol samples were collected in the Beijing metropolitan area from October 2014 to January 2015 and later sent to IsoLab at the University of Washington for isotopic analysis. The location of the measurement sites is shown in Figure S1(a). He et al. (2018) and W. Song et al. (2020) used collection intervals of about 12 hours for each aerosol sample, whereas Y. Wang et al. (2019) used 23 hours. The aerosol filters collected both HNO_3 and p-NO_3^-, so the observed $\Delta^{17}O(NO_3^-)$ contains $\Delta^{17}O$ signals from both species (He et al., 2018). We compute the daily mean of $\Delta^{17}O(NO_3^-)$ from these published measurements and obtain a dataset with 51 data points between 1 October 2014 and 15 January 2015.

To evaluate the modeled concentration of $PM_{2.5}$, p-NO_3^-, NO_2, and ozone in Beijing, we use measurements of these species reported in He et al. (2018), Y. Wang et al. (2019), and W. Song et al. (2020). We also consider similar measurements at other Beijing air-quality stations that are operated by the China Ministry of Ecology and Environment as a complementary dataset (location of these sites are shown in Figure **A-1**(a)). These air-quality measurements are publicly available on https://quotsoft.net/air (last accessed on 26 January 2021).

2.2.2 *GEOS-Chem 3-D Chemical Transport Model simulations*

We use the three-dimensional global chemical transport model GEOS-Chem (version 12.7.0; hereafter GC) to simulate the evolution of haze events in winter 2014-15. This version of the GC model code is accessible from https://doi.org/10.5281/zenodo.3634864 (last accessed on 26 January 2021). The model considers detailed HO_x-NO_x-VOC-ozone-halogen-aerosol chemistry in the troposphere (Fisher et al., 2018; Kasibhatla et al., 2018; Sherwen et al., 2017; X. Wang et al., 2019, 2020). The Fast-JX module in GC calculates aerosol radiative effects and photolysis rates (Eastham et al., 2014; Neu et al., 2007). The partitioning between the HNO_3 and p-NO_3^- is determined by an aerosol thermodynamic equilibrium module ISORROPIA II (Fountoukis & Nenes, 2007). The deposition schemes for trace gases and aerosols in GC are described in Y. Wang et al. (1998), Liu et al. (2001), L. Zhang et al. (2001), and Jaeglé et al. (2018). Earlier versions of GC have been used extensively to investigate NO_x and PM pollution in metropolitan areas (e.g., Jaeglé et al., 2018; Shah et al., 2020).

The NO_y chemistry in GC has been updated substantially in recent versions of the model. Holmes et al. (2019) modified the uptake coefficients for NO_2, NO_3, and N_2O_5 on different aerosols based on recent laboratory studies. In particular, $\gamma(NO_2)$ on sulfate-nitrate-ammonium (SNA) aerosol has been set to 5×10^{-6}, which is a factor-of-20 reduction compared to the previous work. The latest versions of GC also incorporated the uptake of NO_2, NO_3 and N_2O_5 in cloud droplets, following the entrainment-limited scheme described in Holmes et al. (2019) for partly cloudy conditions. For the uptake of N_2O_5 on SNA aerosol, the latest version of GC now considers the inhibiting effects of organic coating through the parametrization described in McDuffie et al. (2018), which was

built on top of the Bertram and Thornton (2009) scheme to calculate the reaction probability of N_2O_5 on aerosol. Particulate-nitrate photolysis described in Kasibhatla et al. (2018) is currently an optional feature in GC and is switched off by default. For gas-phase NO_y chemistry, the latest updates include the reactions of C1-C3 alkyl nitrate, as described in Fisher et al. (2018). While the previous studies independently showed that these chemistry updates improved the representation of NO_y in the model, no study to date has yet examined the combined effects of these updates on model simulations of wintertime haze events in China.

In this study, we use version 12.7.0 of GC as our "base model". Driven by GEOS-FP meteorological data assimilation products with a native horizontal resolution of 0.25° x 0.3125° and 72 vertical levels, the base simulation was run at a coarser spatial resolution (4° latitude x 5° longitude and 47 vertical levels) to attain global coverage. We also performed nested-grid regional simulations for East Asia at a higher horizontal resolution (0.25° latitude x 0.3125° longitude) by using output from the corresponding global simulations as boundary conditions (See Figure **A-1**(b) and Figure **A-1**(c) for grid size and boundaries). The model simulates the mixing of chemical species in the planetary boundary layer using the non-local mixing scheme from Lin and McElroy (2010). Anthropogenic emissions of reactive gases and aerosols over the United States, Canada, Asia, and Africa are from the regional emissions inventories EPA/NEI2011, APEI, MIX, and DICE-Africa, respectively (M. Li et al., 2017; Marais & Wiedinmyer, 2016). NO_x emissions from MEIC (the emission inventory for China in MIX framework) between 2005 and 2018 have recently been validated by the satellite retrievals of NO_2 columns in Shah et al. (2020) and showed a good agreement. Emissions in the rest of the world are from the Community Emissions Data System (CEDS) inventory (Hoesly et al., 2018). Biomass burning emissions are from the Global Fire

Emissions Database (GFED 4.1s) (van der Werf et al., 2017). Lightning-NO_x emissions in the model are estimated based on a satellite lightning climatology described in Murray et al. (2012). Soil-NO_x emissions are estimated offline using the algorithm described in Hudman et al. (2012). The model simulation period is from August 2014 to January 2015, in which the first two months are used for "spinning-up" the model. To address the uncertainty in NO_y chemistry, we conduct a series of model sensitivity experiments at 4° latitude x 5° longitude resolution. The detailed configurations for these simulations are described in Section 3.2.2 and Section A.1.2.

2.2.3 *Calculation of $\Delta^{17}O(NO_3^-)$ in model simulations*

Following the approach of Alexander et al. (2020), we use local chemical production rates to calculate $\Delta^{17}O(NO_3^-)$, by which we assume that $\Delta^{17}O(NO_3^-)$ is controlled by local NO_x cycling and nitrate production (See Figure **A-2**). This method works well for intense haze events in wintertime North China, where most NO_3^- is produced locally over the North China Plain (See Figure **A-3**). The $\Delta^{17}O$ in tropospheric ozone ($\Delta^{17}O(O_3)$) is assumed to be 26‰ based on recent measurements (Vicars & Savarino, 2014). We assume that only the terminal oxygen atom of ozone is transferred during oxidation reactions; hence the $\Delta^{17}O$ value of the oxygen atom transferred is equal to 39‰ ($= \frac{3}{2} \times 26‰$, denoted as $\Delta^{17}O(O_3^*)$) (Morin et al., 2011). For calculation of $\Delta^{17}O(NO_2)$, we assume isotopic equilibration during the daytime for all nitrate production pathways. The longer lifetime of NO_x in wintertime North China (≈ 21 to 27 hours estimated by Shah et al. (2020)) suggests that NO_x oxidation rates are slow enough to make this a reasonable assumption. Figure **A-2** also shows the assumed $\Delta^{17}O(NO_3^-)$ values for each nitrate formation pathway in the model.

2.2.4 *Other metrics for evaluating NO_y chemistry*

In addition to $\Delta^{17}O$, we also use the concentration and speciation of the odd oxygen family (O_x) to evaluate the performance of the model in simulating NO_y chemistry. In theory, O_x includes all the chemical species that cycle with ozone and atomic oxygen in the atmosphere via photochemical reactions and is highly coupled with the local nitrate production (Bates & Jacob, 2020; Lu et al., 2019; Womack et al., 2019).

Here, we define total O_x as the weighted sum of ozone and other species that cycle with ozone and atomic oxygen in the model:

$$O_x \equiv O_3 + NO_2 + 2NO_3 + 3N_2O_5 + HNO_3 + p\text{-}NO_3^- + PANs + RONO_2 + HNO_4 + \xi O + \xi NO_2 + 2\xi NO_3 + \sum_{n=2}^{5} n\xi_2 O_n + 2O\xi O$$

where ξ = Br, Cl, or I. Our definition of O_x is very similar to the one used in Bates and Jacob (2020), except that we (1) include p-NO_3^- and (2) exclude the short-lived radical species (e.g., $O(^1D)$ and Criegee intermediates) that have a negligible impact on total O_x abundances. We consider p-NO_3^- to be an O_x member because of the rapid equilibrium partitioning between HNO_3 and p-NO_3^- on fine-model aerosol and the potential importance of renoxification in urban air from the photolysis of p-NO_3^- (Bao et al., 2018; Kasibhatla et al., 2018; Yuhan Liu et al., 2019; Ye et al., 2017). Womack et al. (2019) also included p-NO_3^- in their definition of generalized odd

oxygen family. While GC can simulate and output all the species listed in our definition of O_x, most of the measurements in Beijing only include the concentration of O_3, NO_2, and p-NO_3^- (with possible interference of HNO_3, as explained in Section 2.1). The incomplete observations of O_x only have minor effects on our model-observation comparison because O_3, NO_2, and p-NO_3^- are the dominant (>95%) O_x species in wintertime Beijing in the model (See more detailed analysis in Section 2.3.1). We denote the sum of O_3, NO_2, and p-NO_3^- as $O_{x,major}$.

Since the speciation of O_x is sensitive to NO_y chemistry, we also compare the ratio of different O_x species in the observations and the model simulations. In particular, we compute the nitrogen oxidation ratio (NOR) using the mixing ratios of NO_2 and NO_3^-:

$$NOR \equiv \frac{[NO_3^-]}{[NO_3^-] + [NO_2]} = \frac{[p\text{-}NO_3^-] + [HNO_3]}{[p\text{-}NO_3^-] + [HNO_3] + [NO_2]}$$

NOR ranges from 0 (complete absence of NO_3^-) to 1 (complete oxidation of all NO_2). This dimensionless ratio indicates the efficiency of the oxidation of NO_x and is less prone to absolute errors in simulating NO_x concentrations (such as uncertainties in emissions). NOR has been widely used in the analysis of nitrate formation mechanisms in other studies (e.g., He et al., 2018; P. Liu et al., 2020; Shi et al., 2019; Xu et al., 2019).

2.2.5 *Haze-regime categorization*

To facilitate our analysis of the relationships between the chemistry metrics and the intensity of haze events, we categorize the data into four haze regimes according to the surface $PM_{2.5}$ concentration: "light haze" ($[PM_{2.5}] \leq 75$ μg m^{-3}), "moderate haze" events (75 μg m^{-3} $<[PM_{2.5}] \leq$ 150 μg m^{-3}), "severe haze" events (150 μg $m^{-3}<[PM_{2.5}] \leq 225$ μg m^{-3}), and "extreme haze" events ($[PM_{2.5}] > 225$ μg m^{-3}) (See Table **A-2** for the frequency of different haze regimes). For the observations, we compute the average of daily mean $[PM_{2.5}]$ observed at the Beijing air-quality stations (both urban and suburban stations, 22 stations in total) to determine the haze regime of a particular day. The inter-station average $[PM_{2.5}]$ can better reflect the intensity of regional haze events than the single-station measurements. For model data, we use the modeled, mean surface $[PM_{2.5}]$ over the Beijing gridbox in coarse-resolution simulations. It is noted that the choice of this categorization does not imply the existence of statistically significant differences between chemical metrics in different haze regimes or abrupt shifts in NO_y chemistry at regime boundaries (where $[PM_{2.5}] = 75$, 150, or 225 μg m^{-3}). Instead, this categorization is merely used for illustrating and communicating some general trends in NO_y chemistry as haze intensifies. Similar categorizations have also been adopted in other studies of nitrate pollution in Beijing (e.g., Fu et al., 2020; He et al., 2018; P. Liu et al., 2020). When we are referring to patterns that are seen across multiple haze regime, the terms "intense haze" ($[PM_{2.5}]>$ 75 μg m^{-3}) and "more intense haze" ($[PM_{2.5}]>$ 150 μg m^{-3}) are sometimes used.

2.3 RESULTS

2.3.1 *Observations of $\Delta^{17}O(NO_3^-)$ in Beijing*

A compilation of all available $\Delta^{17}O(NO_3^-)$ observations reveals a positive relationship between $\Delta^{17}O(NO_3^-)$ and $PM_{2.5}$ concentration in Beijing during winter 2014-15 (**Error! Reference source not found.**). The median of $\Delta^{17}O(NO_3^-)$ increases from 26.1‰ in light haze to 31.5‰ in extreme haze (**Error! Reference source not found.**b). Similar positive relationships between $\Delta^{17}O(NO_3^-)$ and [$PM_{2.5}$] have also been reported in He et al. (2018) and Y. Wang et al. (2019). The positive relationship can still be seen when we analyze daytime and nighttime measurements separately (Figure **A-4**). The lack of strong diurnal variability in $\Delta^{17}O(NO_3^-)$ in observations is consistent with the long lifetime of NO_x in wintertime North China shown by previous modeling studies (e.g., Shah et al., 2020). The higher $\Delta^{17}O(NO_3^-)$ measured in intense haze indicates that the relative importance of high-$\Delta^{17}O$ pathways involving O_3 increases with $PM_{2.5}$ concentration.

Error! Reference source not found. also shows that the variability of $\Delta^{17}O(NO_3^-)$ is larger on days with lower [$PM_{2.5}$]. The standard deviation (s.d.) of $\Delta^{17}O(NO_3^-)$ decreases from 3.7‰ in light haze to 1.7‰ intense haze. The observed smaller variability of $\Delta^{17}O(NO_3^-)$ in intense haze may be explained by the weaker ventilation and the overwhelming contribution of nitrate from local production (See Figure **A-3**). We also note that very high variability in $\Delta^{17}O(NO_3^-)$ is only seen in the light-haze observations from Y. Wang et al. (2019) (the corresponding s.d. is 3.9‰). Observations in He et al. (2018) and W. Song et al. (2020) show a similar variability in $\Delta^{17}O$ (the overall s.d. are 1.6‰ and 1.4‰, respectively) and do not contain the low $\Delta^{17}O(NO_3^-)$ values

(<26‰) reported by Y. Wang et al. (2019). Thus, we focus our analysis more on intense haze when the observations from all three studies are in better agreement on the magnitude and variability in $\Delta^{17}O(NO_3^-)$.

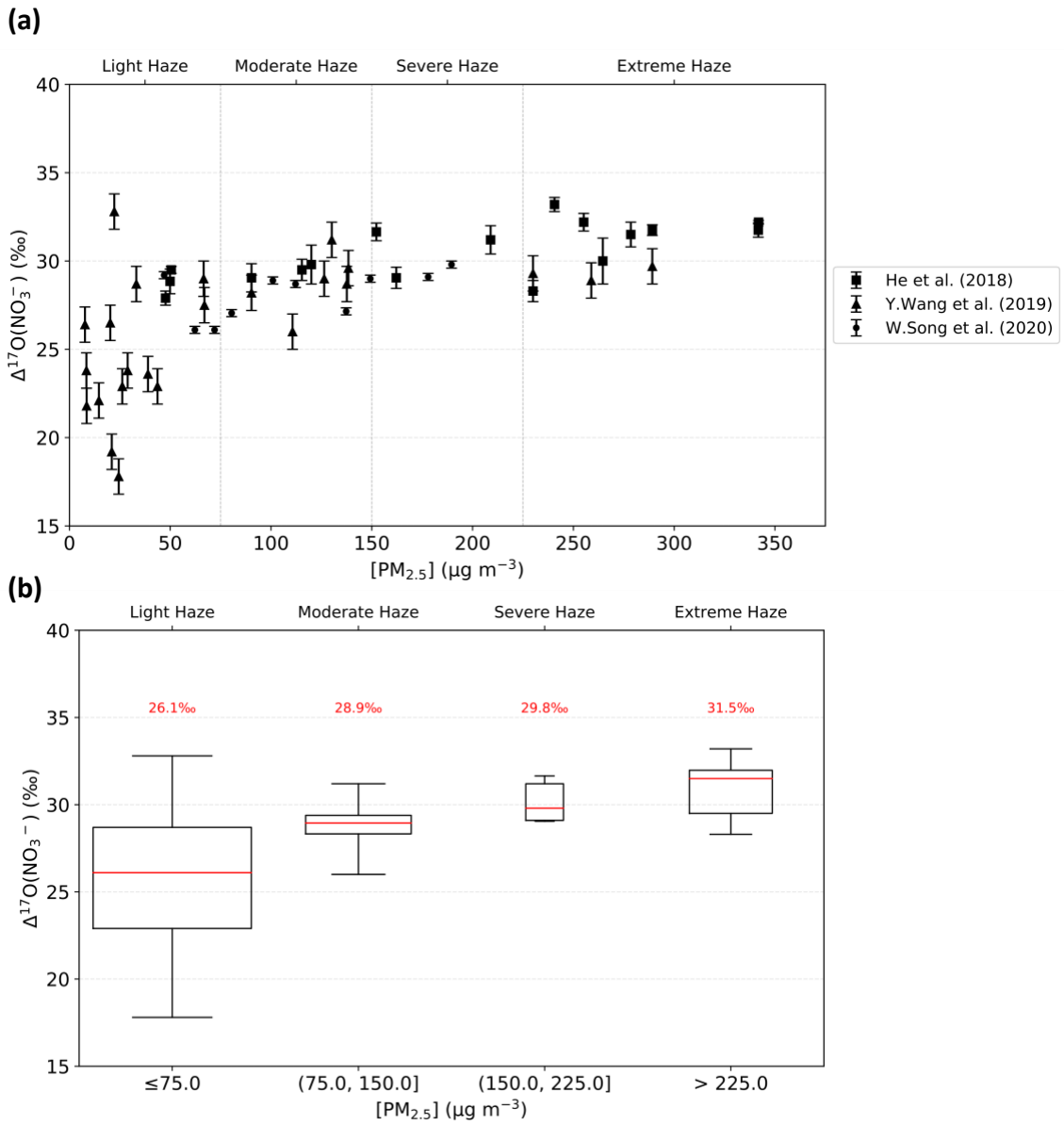

Figure 2-2 Observed relationship between $\Delta^{17}O(NO_3^-)$ and $PM_{2.5}$ concentration.

The scatter plot in 2(a) shows the daily-average measurements in He et al. (2018) (squares), Y. Wang et al. (2019) (triangles), and W. Song et al. (2020) (circles). The error bars represent the ± 2σ standard deviation uncertainty range for the $\Delta^{17}O$ measurements. The box plot in 2(b) shows the statistics of the observed $\Delta^{17}O(NO_3^-)$ in each haze regime. The red line indicates the median; the top and the bottom of the box indicate the 75th percentile and the 25th percentile, respectively; the whiskers indicate the maximum and the minimum. The width of boxes scales with the number of samples in each haze regime. The number in red above each box is the median of $\Delta^{17}O(NO_3^-)$ in each haze regime.

2.3.2 *Model Results*

2.3.2.1 Base Model

Figure 2-3 compares the magnitude of modeled and observed $\Delta^{17}O(NO_3^-)$ in Beijing in intense haze. While the modeled median $\Delta^{17}O(NO_3^-)$ in moderate haze (29.5‰) and severe haze (29.1‰) lie within the range of observations, most of the modeled $\Delta^{17}O(NO_3^-)$ in extreme haze (median = 27.3‰) are lower than the minimum value in the observations (28.3‰). The lower $\Delta^{17}O(NO_3^-)$ in extreme haze compared to moderate and severe haze means the base model predicts a negative relationship between $\Delta^{17}O(NO_3^-)$ and $[PM_{2.5}]$ in intense haze (Figure 2-3), which is the opposite relationship shown in the observations. Modeled median $\Delta^{17}O(NO_3^-)$ in moderate haze is 2.2‰ higher than that in extreme haze. Lower $\Delta^{17}O(NO_3^-)$ in extreme haze cannot be explained by the modeled difference in $\Delta^{17}O(NO_2)$, of which the median changes by less than 0.5‰ across different types of haze events (Figure **A-5**).

The base model also cannot reproduce a sufficient amount of O_x, the observed O_x speciation, nor the observed NOR in Beijing in intense haze (Figure 2-4 and Figure 2-5). Modeled [$O_{x,\ major}$] in intense haze is 36% lower than the observations on average. The bias in modeled [O_x] in North China is mainly caused by an underestimate of [NO_2] and [O_3] (Figure 2-4, and more discussion in Section 2.4.2). In extreme haze, the base model underestimates the mean of [NO_2] and [O_3] by 55% and 54%, respectively. The large model-observation discrepancy in [NO_2] cannot be explained by the long-known interference of NO_z species (members in the NO_y family that are not NO or NO_2) in chemiluminescence-based measurements (Lamsal et al., 2008; Reed et al., 2016), because both our model (see Figure **A-6**) and other observations suggest that non-NO_3^- gas-phase NO_z species' (e.g., PAN) concentration is small in comparison with [NO_x] in wintertime in Beijing (S. Chen et al., 2020; B. Zhang et al., 2017; G. Zhang et al., 2020; H. Zhang et al., 2014). The underestimate of NO_2 leads to a modeled overestimate of NOR (0.33) in intense haze compared to the observations (0.21). The discrepancy between modeled and observed NOR increases with [$PM_{2.5}$]. In extreme haze, the modeled median NOR (0.50) is higher than the observed maximum (0.47) (Figure **2-5**).

The base model's bias in $\Delta^{17}O(NO_3^-)$, [O_x], and NOR persists even when a higher horizontal spatial resolution is used. The range of the chemical metrics increases with model resolution, but the median and the mean remain largely unchanged (Figure **2-3**, Figure **2-4** and Figure **2-5**). The relationship between modeled $\Delta^{17}O(NO_3^-)$ and [$PM_{2.5}$] is still negative in intense haze (Figure **2-3**). Moreover, the extended range of modeled $\Delta^{17}O(NO_3^-)$ still cannot capture the maximum and minimum in observations. A similar model underestimate of mean [O_x] during intense haze events

is seen in both the regional-level and the site-level comparison (Figure 2-4 and Figure **A-7**). The nested-grid simulation predicts a slightly lower median NOR (− 0.01, − 0.05, and − 0.07 in moderate, severe, and extreme haze, respectively), but the modeled NOR is still too high compared to the observations (Figure 2-5). The comparison between nested-grid and global simulations suggests that low horizontal spatial resolution is not the fundamental cause for the model's bias in NO_y chemistry over North China. Comparison of observed and modeled mixed layer depths also suggests that the bias in the thickness of vertical mixing layer is not a cause of the model biases in trace gas concentrations (See Figure **A-8**).

In the base simulation, the major low-$\Delta^{17}O$ pathways in Beijing are gas-phase oxidation of NO_2 by OH and NO_2 uptake on aerosols, which contribute 34.4% and 19.0 % to nitrate production on average over winter 2014-15, respectively (Figure 2-6). The major high-$\Delta^{17}O$ pathways are N_2O_5 uptake on aerosols (33.6%) and clouds (11.3%) (Figure 2-6). The relative importance of high-$\Delta^{17}O$ pathways and low-$\Delta^{17}O$ pathways remains at around a ratio of 1:1 from light haze to severe haze events. In extreme haze, the contribution from NO_2 uptake increases sharply to 35.9% and becomes higher than N_2O_5 uptake on aerosols and clouds (30.0%), resulting in relatively low values of $\Delta^{17}O(NO_3^-)$ (Figure 2-6).

The model-observation comparison of the $\Delta^{17}O(NO_3^-)$ in extreme haze suggests that the standard version of GC either overestimates the contribution of low-$\Delta^{17}O$ pathways and/or underestimates the contribution of high-$\Delta^{17}O$ pathways as $PM_{2.5}$ increases. In the base simulation, the modeled reduction in $\Delta^{17}O(NO_3^-)$ in extreme haze is driven by an increase in NO_2 uptake rate and a decrease in N_2O_5 uptake on aerosols (Figure 2-6a), suggesting that the modeled rate of NO_2 uptake is too

high and/or the rate of N_2O_5 uptake is too low in extreme haze. It is also possible that the model underestimates the contribution of the other high-$\Delta^{17}O$ nitrate production pathways, such as reactions between NO_3 and VOCs (Figure **2-1**b, R12) and the hydrolysis of halogen nitrates (Figure **2-1**b, R14). However, further analysis and model sensitivity simulations suggest that either these reactions are negligible and/or cannot resolve the model biases in the chemical metrics because of the limited supply of NO_3 and N_2O_5 in intense haze (Refer to Section A.1.1 and A.1.2.2 in SI).

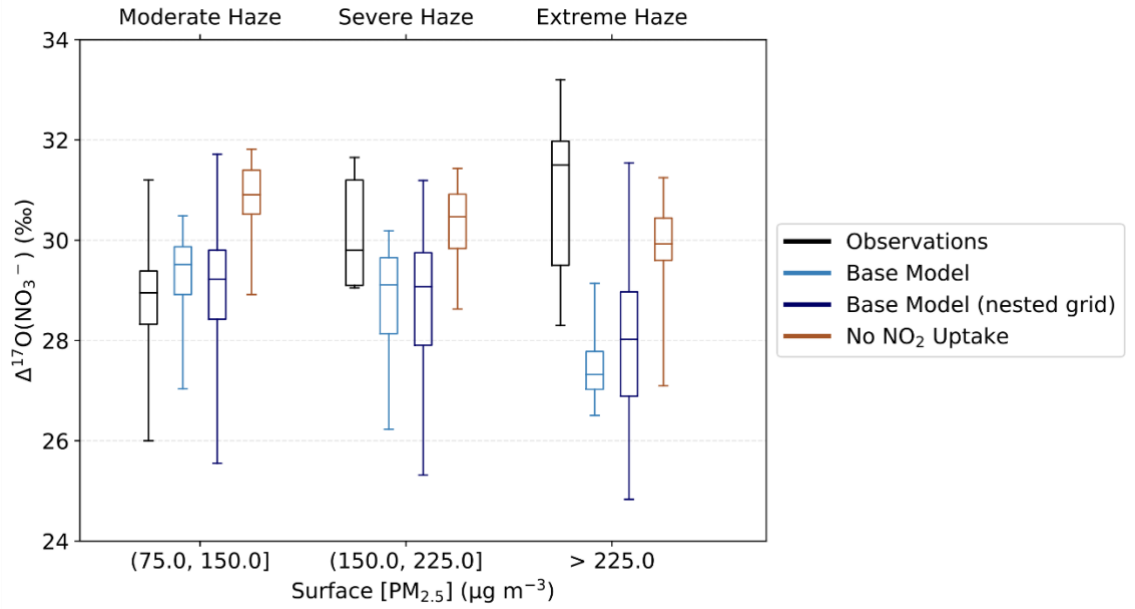

Figure 2-3. Comparison of $\Delta^{17}O(NO_3^-)$ in observations and model simulations under different haze regimes.

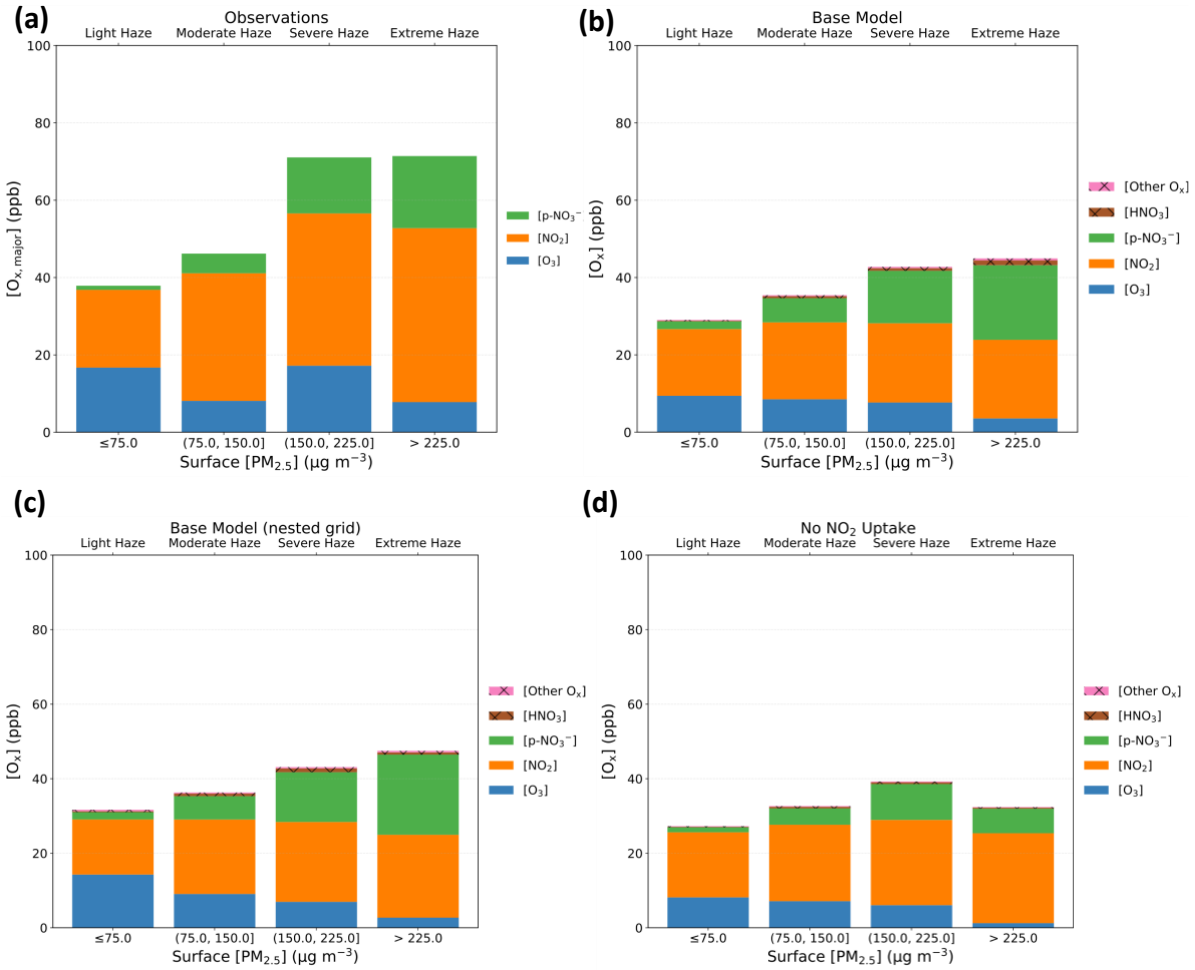

Figure 2-4. Concentration and speciation of O_x under different haze regimes in (a) observations, (b) base simulation, (c) nested-grid base simulation, (d) No NO_2 Uptake simulation.

Hatching (x-filled bars) indicates the O_x species that were not measured at the observation sites.

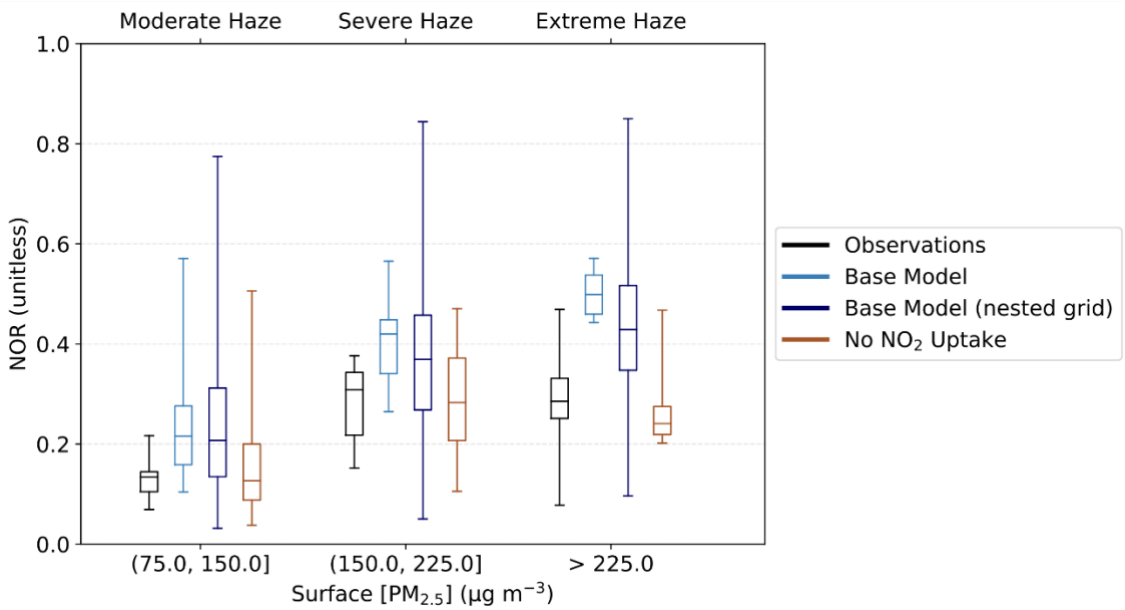

Figure 2-5. Comparison of nitrogen oxidation ratio (NOR) in observations and model simulations under different haze regimes.

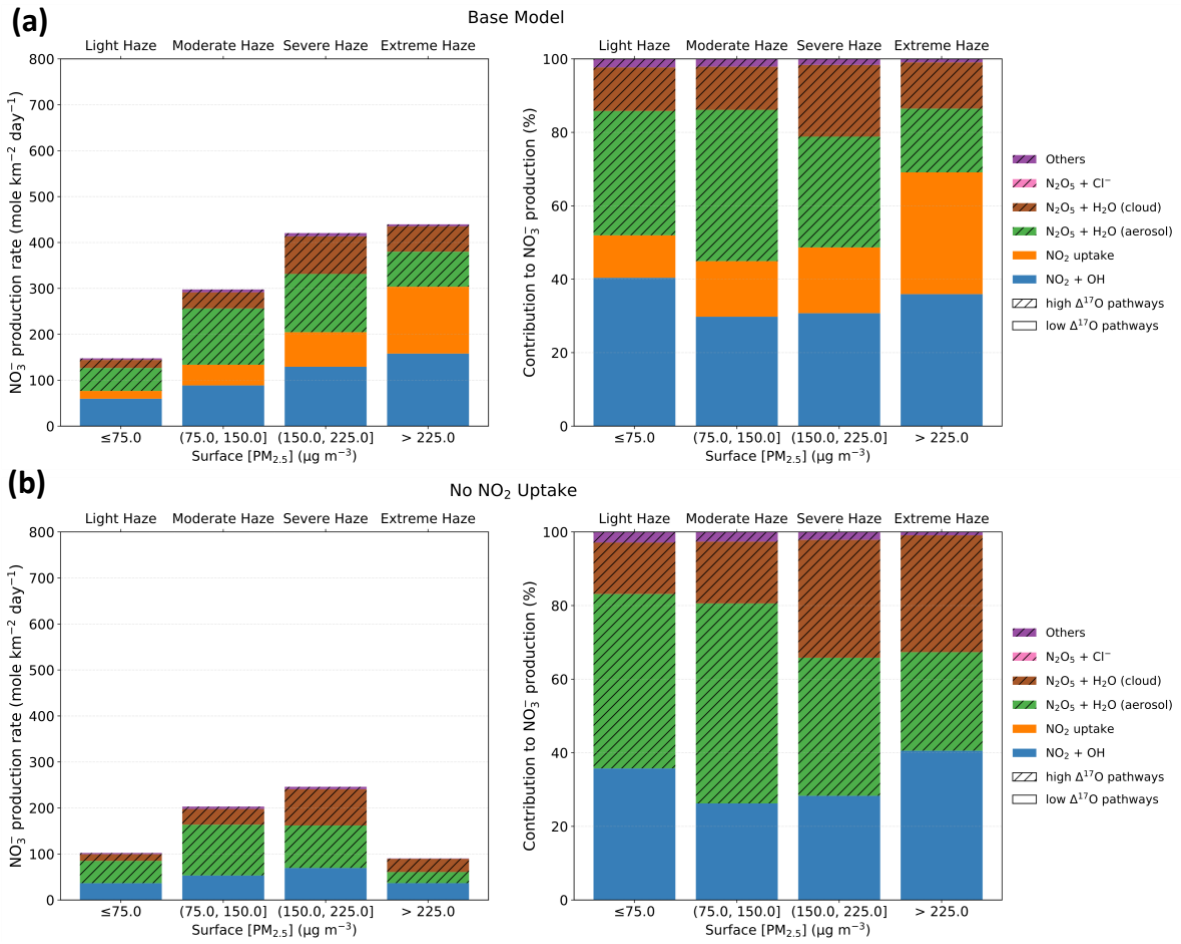

Figure 2-6. Average rate of different near-surface nitrate production pathways (left) and their relative contribution to nitrate formation in Beijing under different haze regimes (right) in (a) the base simulation and (b) No NO_2 Uptake simulation.

"Near-surface" is defined as the sum over the ten lowest vertical levels in model, which on average corresponds to the altitudes between 0 to 1300 m. Hatching (//-filled bars) indicates high-$\Delta^{17}O$ pathways.

2.3.2.2 No-NO_2-uptake model simulation

An overestimate of NOR combined with the models' low bias in $\Delta^{17}O$ suggests an overestimate of NO_2 uptake (a low-$\Delta^{17}O$ heterogeneous pathway). Although a high bias in NOR could also suggest an underestimate of renoxification, a model sensitivity study allowing for efficient photolysis of p-NO_3^- shows that this explanation cannot resolve the model biases (Refer to Section A.1.2.1). To evaluate the role of NO_2 uptake on the three chemistry metrics, we perform a sensitivity simulation in which the reaction is removed from the model by setting the uptake coefficients of NO_2 uptake on all types of aerosol and clouds to zero (i.e., $\gamma(NO_2) = 0$).

Without NO_2 uptake, the model predicts higher $\Delta^{17}O(NO_3^-)$ relative to the base model simulation under all haze regimes (Figure **2-3**). The average increase in modeled $\Delta^{17}O(NO_3^-)$ in intense haze is 1.5 ‰, and the largest increase is found in extreme haze: the modeled median $\Delta^{17}O(NO_3^-)$ increases by 2.6 ‰ compared to the base simulation. Most of the modeled $\Delta^{17}O(NO_3^-)$ in extreme haze now lie inside the range of observations. The simulation without NO_2 uptake predicts the median $\Delta^{17}O(NO_3^-)$ in extreme haze to be 29.9‰, which is closer to the observations (31.5‰). However, the model now overestimates the $\Delta^{17}O(NO_3^-)$ in moderate haze. The median $\Delta^{17}O(NO_3^-)$ in moderate haze in the model is 30.9‰, which is 2.0‰ higher than the observations. Similar to the base simulation, the simulation without NO_2 uptake predicts a decrease in $\Delta^{17}O(NO_3^-)$ as $[PM_{2.5}]$ increases. The negative relationship is driven by the sharp decrease in the rate of N_2O_5 production and nitrate production via N_2O_5 uptake in extreme haze (Figure 2-6).

The model without NO_2 uptake shows better agreement with observations of O_x speciation and NOR but still underestimates the total O_x concentration (Figure 2-4 and Figure 2-5). The average NOR in intense haze in the model is 0.22, which is very close to the observations (0.21). The modeled NOR in extreme haze spans within the observed range for all haze regimes (Figure **2-5**). Modeled [O_x] is not sensitive to the change in NO_2 uptake, except in extreme haze. [O_x] in extreme haze decreases from 41.0 ppb in the base simulation to 34.6 ppb in the simulation with no NO_2 uptake. This worsens the underestimate of modeled [O_x].

The reduction in NOR relative to the base model simulation is due to a reduction in the nitrate-production rate in all haze regimes, but especially during extreme haze (Figure 2-6). This is driven mainly by the absence of NO_2 uptake as a nitrate-production pathway, but also due to a decrease in nitrate production via NO_2 + OH. The decrease in nitrate production via NO_2 + OH is driven by the lack of HONO production from NO_2 uptake, the photolysis of which was a major source of OH in the model. The rate of N_2O_5 uptake remains relatively unchanged, except for a decrease during extreme haze (Figure 2-7). This increases the relative importance of N_2O_5 uptake resulting in an increase in $\Delta^{17}O(NO_3^-)$ during all haze regimes compared to the base model, especially during more intense haze events.

The results from the simulation without NO_2 uptake demonstrates that model discrepancies in $\Delta^{17}O(NO_3^-)$ and O_x as seen in the base simulation cannot be solely explained by the uncertainty in the efficiency of NO_2 uptake. Even when we completely eliminate the contribution of nitrate production from the NO_2 uptake pathway, the existing high-$\Delta^{17}O$ pathways in the model still cannot contribute enough to reproduce the observed range of $\Delta^{17}O(NO_3^-)$ in severe haze and

extreme haze. This model sensitivity simulation also shows that the supply of [NO_2] is not a rate-limiting factor for N_2O_5 uptake in Beijing. As less NO_2 is converted into NO_3^- due to the absence of NO_2 uptake pathway, the modeled [O_3] becomes more depleted as [NO_x] increases (Figure 2-4). In the presence of excess NO_x, the low [O_3] in the model slows down the production of NO_3 radicals via $NO_2 + O_3$, which ultimately limits the rate of N_2O_5 production via $NO_2 + NO_3$ and nitrate production via N_2O_5 uptake. Compared with the base simulation, the simulation without NO_2 uptake predicts lower N_2O_5 production and lower nitrate production via N_2O_5 uptake on aerosols and clouds in extreme haze (Figure **2-7**), further supporting that O_3 is the limiting factor for N_2O_5 production and uptake.

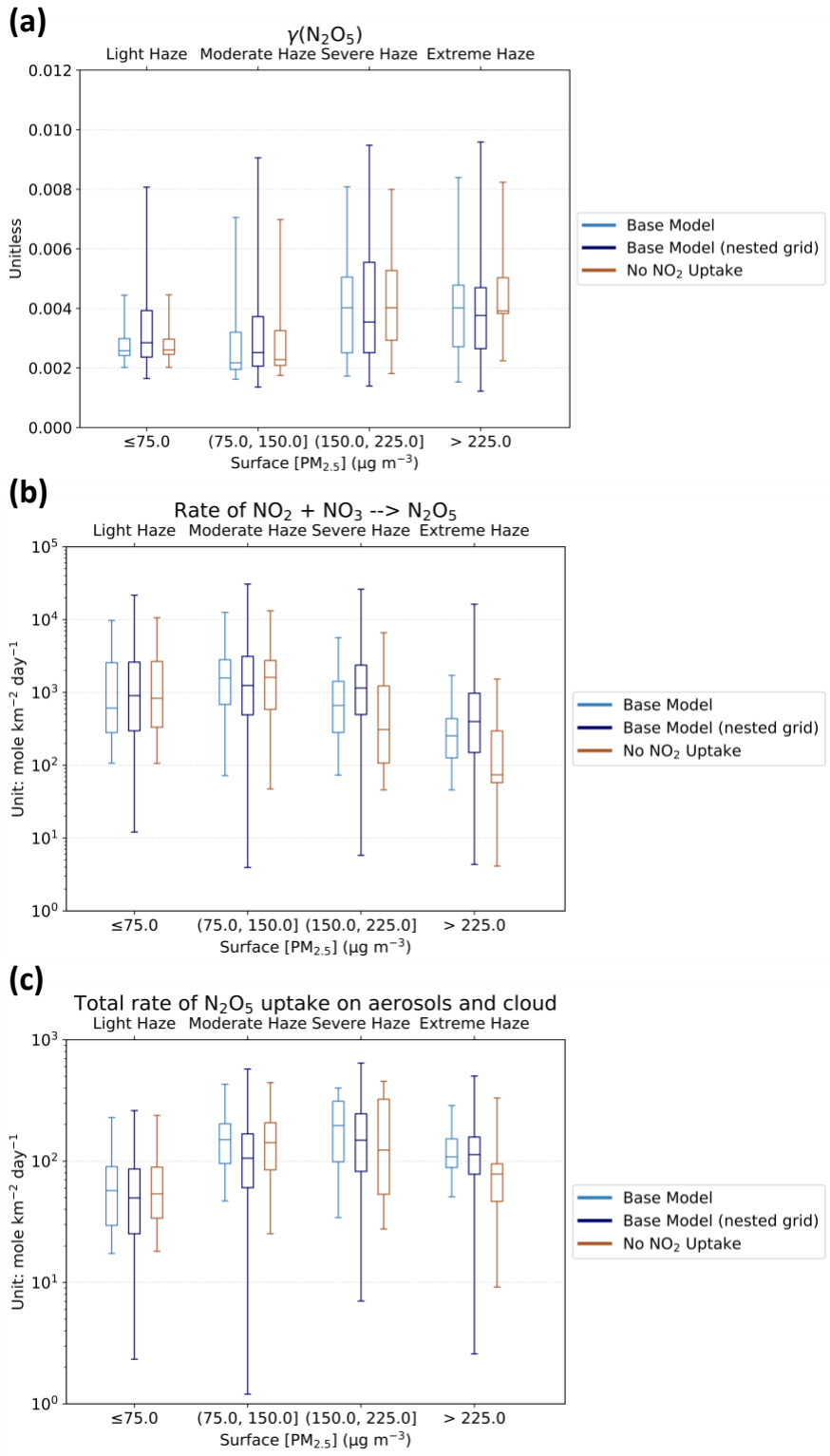

Figure 2-7. Factors controlling the near-surface rate of nitrate production via N_2O_5 hydrolysis in simulations and their dependence on [$PM_{2.5}$].

2-7(a) shows the average uptake coefficient of N_2O_5 on aerosols. 2-7(b) shows the average rate of N_2O_5 production. 2-7(c) shows the average total rate of N_2O_5 uptake on aerosols and cloud.

2.4 DISCUSSION

2.4.1 *Model sensitivity to uncertainties in NO_2 uptake on aerosol*

The model results presented in Section 2.3 and Section A.1.2 show that modeled NOR and $\Delta^{17}O(NO_3^-)$ are most sensitive to NO_2 uptake. In NO_x-rich air, we expect to see positive relationships between $[HO_x]$ and $[O_3]$ because of their coupling via the cycling of NO_x (Bates & Jacob, 2020). As modeled O_3 concentration increases, NO more likely reacts with O_3 to produce NO_2, as a result, more HO_x becomes available for other reactions, including nitrate production, and vice versa. The competing effects of HO_x- and ozone-related nitrate-production pathways explain why modeled $\Delta^{17}O(NO_3^-)$ is not very sensitive to changes in various chemical parameters, with the exception of $\gamma(NO_2)$. NO_2 uptake, which carries a low-$\Delta^{17}O$ signature, is the only important nitrate-production pathway in the base model that converts NO_2 into NO_3^- without involving HO_x or ozone directly (Figure **2-1**b). Additional model simulations increasing the HONO yield resulting from NO_2 uptake on aerosol to 100%, as well as model simulations including various combinations of the three model sensitivity studies described in Section 2.3.2 and Section A.1.2, further show that $\Delta^{17}O(NO_3^-)$ and NOR are most sensitive to $\gamma(NO_2)$ (Figure **A-9** and Figure **A-10**). The extra HONO produced from NO_2-uptake yielding 100% HONO increases OH and the rate of NO_2 + OH and simultaneously promotes nitrate production via N_2O_5 uptake through HO_x-O_3 coupling effects (See Figure **A-11**), but the modeled $[O_x]$ is still low compared to the observations (Figure **A-12**). Among all the model simulations performed, only those with $\gamma(NO_2) = 0$ improve model agreement with both observed $\Delta^{17}O(NO_3^-)$ and NOR during more intense haze events (Figure **A-9** and Figure **A-10**).

In addition to the isotopic constraints, results from some laboratory and field studies also support the choice of a lower $\gamma(NO_2)$. The current GC parametrization sets $\gamma(NO_2, \text{black carbon})=10^{-4}$, which is 20 times higher than $\gamma(NO_2, \text{SNA})$. Laboratory studies of NO_2(g) uptake on soot or carbonaceous surfaces suggested that heterogeneous reactions can rapidly consume the organic adsorbates and/or surface groups (Ammann et al., 1998; Bröske et al., 2003; Gerecke et al., 1998; Kalberer et al., 1999; Kleffmann et al., 1999), with rates of NO_2 uptake decreasing to negligible levels within minutes to hours (Gerecke et al., 1998; Kalberer et al., 1999; Kleffmann et al., 1999). For SNA aerosols, laboratory studies by F. Tan et al. (2016) and F. Tan et al. (2017) found that the rate of NO_2 uptake decreases with increasing RH when aerosols contain $CaCO_3$ due to formation of insoluble $CaSO_4 \cdot nH_2O$ on aerosol surfaces at higher RH. A potential suppressing effect of high-RH conditions on NO_2 uptake may help to explain the positive relationship between $\Delta^{17}O(NO_3^-)$ and $[PM_{2.5}]$ in observations. P. Liu et al. (2020) used the RH-dependence of NO_2 uptake to explain the negative relationship between NOR and RH when RH is above 60% in their Beijing observations. However, we cannot replicate their finding using our observations, which show a positive relationship between NOR and RH across all RH conditions (Figure **A-13**). Given the large uncertainties of NO_2 uptake under atmospheric conditions and its large influence on nitrate production, HONO production, and $[O_x]$ in extreme haze, future studies should investigate the dominant mechanisms of NO_2 uptake on ambient aerosols and seek additional observational constraints during more intense haze events.

2.4.2 *Possible causes of modeled underestimate in wintertime [O_x] in North China and their potential influence on NO_y chemistry*

The model bias in wintertime ozone is critical for the simulation of [O_x] and nitrate production via N_2O_5 uptake. NO_2 and ozone are the major components of [O_x], but the base model underestimates their concentration in Beijing, especially during intense haze events. Modeled [NO_x] increases with [$PM_{2.5}$] in Beijing, and NO becomes the primary NO_x species in severe and extreme haze (Average [NO]/[NO_x] ratios are 0.55 and 0.66, respectively, in the base model. See Figure **A-6**). The high [NO]/[NO_x] ratio on more polluted days is also evident in other wintertime observations in Beijing (Lu et al., 2019; Jiaqi Wang et al., 2017; G. Zhang et al., 2020). Under NO_x-saturated regime, the daytime cycling of NO and NO_2 is mainly controlled by the rates of NO + O_3 reaction (R3, a.k.a. ozone titration) and NO_2 photolysis. As predicted by the Leighton Relationship, [NO_2]/[NO] ratio is linearly proportional to [O_3] at photochemical steady state. From this basic theoretical perspective, the model bias in wintertime ozone should at least partly explain the underestimate in [NO_2] in our simulations. The actual NO_x-O_3 relationship may deviate from Leighton's prediction because of the complicated interaction between aerosols and radiation, which can affect the photolysis of NO_2 and O_3 (Hollaway et al., 2019; W. Wang et al., 2019). As explained in Section 2.3.2, low [O_3] can also limit nitrate production via N_2O_5 uptake in NO_x-rich air. Since ozone is a secondary pollutant that plays a central role in tropospheric chemistry, the formation of ozone is inevitably sensitive to many different chemical processes. The particulate-nitrate-photolysis and chlorine-chemistry simulations show improvement in reproducing [O_3] in intense haze in Beijing compared to the base simulation, but none of the proposed updates to NO_y and Cl_y chemistry investigated here can completely correct the model's overall bias in O_x in

Beijing (See Figure **A-12** and Section A.1.2). In this section, we discuss other chemical processes that may explain the modeled underestimate in wintertime [O_3] and [O_x].

2.4.2.1 Aerosol uptake of HO_2 radicals

The uptake of HO_2 radicals on aerosols has been suggested as a key process in driving the observed trends of ozone in China in the 2010s (Jie Li et al., 2018; Ke Li, Jacob, Liao, Shen, et al., 2019; Ke Li, Jacob, Liao, Zhu, et al., 2019). Aerosols can scavenge gas-phase HO_2 radicals reducing [HO_x] and inhibiting ozone production. As pollution-control policies in China have reduced ambient [$PM_{2.5}$] in the 2010s, less HO_2 is scavenged by aerosols, resulting in increases in the ozone production efficiency. This theory on HO_x-O_3-aerosol interactions is consistent with the increasing trend of summertime ozone observed in China (Ke Li, Jacob, Liao, Shen, et al., 2019; Ke Li, Jacob, Liao, Zhu, et al., 2019).

Despite the potential impacts of aerosol uptake of HO_2 on ozone in urban air, the efficiency of this chemical process is still highly uncertain and may strongly depend on the content of aqueous transition-metal ions, the acidity, and the size of the aerosol (Guo et al., 2019; Mao et al., 2013; Thornton & Abbatt, 2005). To estimate the largest possible influence of HO_2 uptake on model bias in [O_x] in intense haze, we consider the extreme case of $\gamma(HO_2) = 0$ on all aerosols (Denote as no HO_2 uptake simulation). Disabling the uptake of HO_2 on aerosols increases the modeled median [$O_{x,\,major}$] by 9.5% in intense haze, but this is smaller than the corresponding change resulting from introducing p-NO_3^- photolysis into the model (+24%) (See Figure **A-12** and Section A.1.2). The

model still fails to reproduce the high level of [O_x] in observations in intense haze. The overall effect of HO_2 uptake on NOR and $\Delta^{17}O(NO_3^-)$ are small in comparison with the models with $\gamma(NO_2) = 0$ (See Figure **A-9** and Figure **A-10**). Our simulation results show that the uncertainty in $\gamma(HO_2)$ is not of primary importance to the model bias in simulating [O_x], NOR, and $\Delta^{17}O(NO_3^-)$ in Beijing.

2.4.2.2 Wintertime emissions of volatile organic compounds in North China

The roles of VOCs in nitrate production have been highlighted in recent studies of nitrate pollution in urban air (Fu et al., 2020; He et al., 2018; Shah et al., 2020; W. Song et al., 2020; Yan-Li Wang et al., 2019; Womack et al., 2019). In Section A.1.1, we showed that the direct effects of VOCs on nitrate formation are likely small in wintertime Beijing. However, VOCs can still modulate nitrate production rates by influencing ozone formation (Huang et al., 2020; Womack et al., 2019). VOCs accelerate the production of O_3 in NO_x-rich urban air. Reduction in VOC emissions has been proposed as a key strategy for mitigating wintertime nitrate pollution in Beijing and in Utah (Lu et al., 2019; Womack et al., 2019). Because of the potential importance of [VOCs] in nitrate production during intense haze events, we investigate the model bias in simulating wintertime [VOCs] in Beijing and examine whether a bias in [VOCs] can explain the model-observation discrepancy in terms of [O_x].

Emitted from biomass burning and fossil fuels, aromatic compounds are often considered to be the largest contributor to ozone formation in metropolitan areas in China (J. Sun et al., 2018; Yan et

al., 2017; D. Yu et al., 2020). The concentration of aromatics in general positively correlates with [$PM_{2.5}$] in the model (Table **A-3**), consistent with observations in North China (Chengtang Liu et al., 2017; Sheng et al., 2018; J. Sun et al., 2018). However, the model underestimates the concentration of aromatics compared to the observations, except for xylene. The mean concentration of benzene in the base simulation is lower than the wintertime observations in Beijing by a factor of 2 (Table **A-3**). Le et al. (2020) showed that a 30% increase in the emissions of VOCs from conventional anthropogenic sources can increase the wintertime [O_3] by about 10% in their model. Model bias in wintertime VOC emissions from industry and transportation could be an important reason for the underestimate of modeled [O_x] during intense haze events.

Recent studies suggested that the manufacture and consumption of volatile chemical products (VCPs) can be an overlooked anthropogenic VOC-emission source in air-quality models (e.g., McDonald et al., 2018). Throughout the product life cycle, these VCPs emit many complex VOCs, including C≥4 alkanes, alcohols, and terpenes, and may account for about half of the VOC reactivity with OH in Los Angeles (McDonald et al., 2018). Comparison of the concentration of these VCP-related VOCs in the base simulation with wintertime observations in Beijing shows a model underestimate of the concentration of alcohols, monoterpenes, and C≥4 alkanes in Beijing (See Table **A-3**). However, without more observational constraints on the fluxes and speciation of VCP emissions in North China and their dependencies on atmospheric conditions, it is hard to conclude whether the model bias in [O_x] can be reduced by including emissions of VCPs in the simulations.

2.4.3 *Examination of the non-linearity in nitrate chemistry*

The weak response of particulate nitrate and other secondary aerosols to the reduction in NO_x emissions has been noted in studies of the long-term trends in wintertime air quality (e.g., H. Li et al., 2019; Shah et al., 2018; Xu et al., 2019), and more recently, in studies of air quality during the COVID-19 pandemic (Diamond & Wood, 2020; Huang et al., 2020; Le et al., 2020; Y. Sun et al., 2020). An astonishing example of the complexity of this NO_x-aerosol relationship can be found in the observations in North China from January to March in year 2020. Following a 40-60% reduction in the NO_x emissions over North China caused by COVID-19 lockdown, observed [$PM_{2.5}$], paradoxically, increased by 50% or more at several stations near Beijing (Huang et al., 2020; Le et al., 2020). Studies suggested that the surge is mostly driven by the production of secondary aerosols, including p-NO_3^- (Huang et al., 2020; Le et al., 2020).

Many studies attributed the persistence of high levels of p-NO_3^- to the non-linearity in atmospheric chemistry, but they hypothesized different mechanisms. Shah et al. (2018) suggested that NO_x and SO_2 emission reductions over the eastern United States has resulted in a gradual increase in aerosol alkalinity, which favors HNO_3-to-p-NO_3^- conversion and increases the fraction of p-NO_3^- in wintertime aerosols. We denote the non-linearity originated from the sensitivity of p-NO_3^- to aerosol-pH as the 'alkalinity-limited mechanism'. In contrast, studies in China observed an increase in [O_3] and production of secondary aerosols following the emission reductions during COVID-19 lockdown, which is likely caused by a reduction in ozone titration (Huang et al., 2020; Le et al., 2020). The enhancement in [O_3] increases the oxidizing capacity of the lower troposphere and promotes the production of secondary aerosols (Fu et al., 2020; Huang et al., 2020; Le et al.,

2020). We denote the non-linearity arising from the sensitivity of nitrate to NO_x-VOCs-ozone chemistry as the 'ozone-limited mechanism'.

To examine the relevance of ozone-limited mechanism in our model simulations of nitrate production, we analyze the relationship between nitrate production rate, [O_3], and [NO_x] during intense haze events for Beijing (Figure **2-8**). It is noted that the inter-model differences in our study orginates from the variations in the modeled chemistry. This is different from other studies like Huang et al. (2020), where they focused on the effects of changing emissions. Although the modeled [O_3], [NO_x], and nitrate production rate are considerably different among various experiments, a positive relationship between nitrate production rate and [O_3] during intense haze events can be identified in all the simulations with $\gamma(NO_2) = 0$. In contrast, all these simulations predict a negative relationship between the nitrate production rate and [NO_x], which can be attributed to the effects of ozone titration. The strong and postive correlation between the nitrate production rate and [O_3] predicted by our models is consistent with the theory of ozone-limited mechanism. Meanwhile, our simulations also show that the partitioning between p-NO_3^- and HNO_3 in Beijing is not sensitive to the intensity of haze events or the difference in NO_y chemistry parametrization (See Figure **A-14**). p-NO_3^- remains the dominant form of NO_3^- in all cases. The model prediction is also consistent with the estimated high aerosol pH (4.5 ± 0.7) in wintertime Beijing, which can be explained by the high NH_3 abundance in observations (Ding et al., 2019). Our model simulations confirm the importance of ozone-limited mechanism in wintertime North China and show that the positive relationship between [O_3] and nitrate production rate during intense haze events is robust regardless of the uncertainty in modeled NO_y chemistry after $\gamma(NO_2)$ is set to 0.

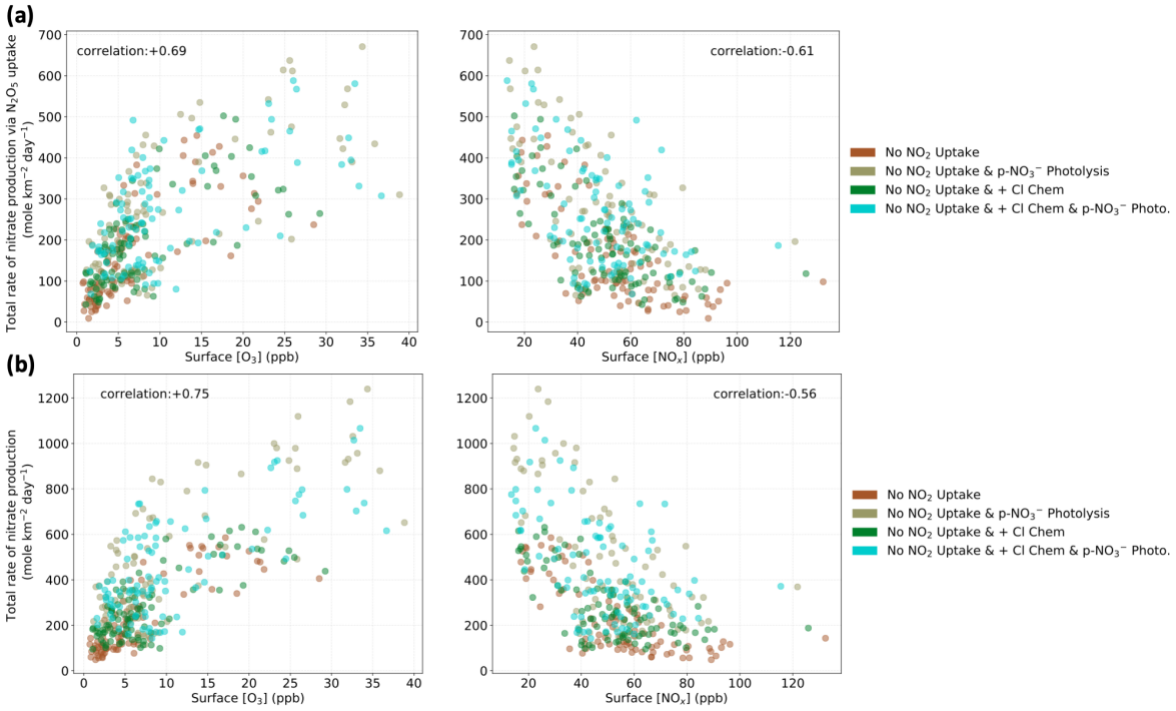

Figure 2-8. The relationship between [O_3], [NO_x], the rate of nitrate production via N_2O_5 uptake (2-8a), and the total rate of nitrate production (2-8b) during intense haze events in simulations without NO_2 uptake on aerosols.

The correlation coefficients shown in the figure are calculated using data from all the four model experiments. All the estimated linear-regression slopes are different from 0 at the 95% significance level.

2.5 CONCLUSIONS AND IMPLICATIONS

By analyzing the observations of $\Delta^{17}O(NO_3^-)$, NOR, and O_x in Beijing during winter 2014-15 and results from a global and regional chemical transport model, we examine the mechanisms for nitrate production in wintertime North China and how the underlying chemical processes vary with the intensity of haze events. $\Delta^{17}O(NO_3^-)$ indicates the dominance of high-$\Delta^{17}O$ oxidants (e.g., ozone) to low-$\Delta^{17}O$ oxidants (e.g., OH and RO_2) during NO_x-to-NO_3^- conversion, while NOR and O_x provide information about the efficiency of NO_y oxidation and the oxidizing capacity of the air. In intense haze, the base model underestimates $\Delta^{17}O(NO_3^-)$ and $[O_x]$ in Beijing by – 0.86 ‰ and − 36%, respectively, but overestimates NOR by +0.12. To investigate the relationship between model bias and uncertainty in chemistry, we perform model sensitivity experiments by varying several key parameters in NO_y chemistry in simulations. Our analysis of the model-observation discrepancy suggests a model overestimate in NO_2-uptake rate on aerosols and the underestimate in wintertime ozone may explain the model biases.

Our model sensitivity simulations show that modeled $\Delta^{17}O(NO_3^-)$ and NOR during highly polluted conditions are most sensitive to the parametrization of NO_2 uptake on aerosols. The $\Delta^{17}O(NO_3^-)$ observations in Beijing and its relationship with $[PM_{2.5}]$ suggest that the rate of NO_2 uptake is likely too high in the model, yielding too high nitrate- and HONO-production rates, especially in severe and extreme haze. Model simulations without NO_2 uptake better reproduce the observed $\Delta^{17}O(NO_3^-)$ and NOR in Beijing under high-$PM_{2.5}$ conditions. A NO_2 uptake mechanism that is suppressed by high RH may explain the positive relationship between $\Delta^{17}O(NO_3^-)$ and $[PM_{2.5}]$ in observations, but the supporting evidence for such a mechanism is currently inconclusive. Further

laboratory and observation-based studies are needed to constrain the reaction probability of NO_2 on ambient aerosols, with a focus on its role in nitrate and HONO formation.

Our simulations also reveal that nitrate production is largely limited by ozone during intense haze events in wintertime North China. After accounting for the uncertainty in NO_2 uptake on aerosols, our analysis suggests that N_2O_5 uptake in aerosols and clouds is the dominant mechanism for nitrate production in wintertime Beijing. Under high-NO_x-high-$PM_{2.5}$ conditions, [O_3] modulates the rate of N_2O_5 production and, subsequently, the rate of nitrate production via N_2O_5 uptake. The base model underestimates [O_3] and [O_x] during wintertime haze events. Uncertainty in heterogeneous chemical processes, such as renoxification via nitrate photolysis or $ClNO_2$ production and the scavenging of HO_x by aerosols, may contribute to the model bias in wintertime O_x, but our model sensitivity simulations show that adjusting related chemistry parameters cannot remove the bias even under extreme scenarios, suggesting processes other than chemistry (e.g., emissions of VCPs) may play a more important role. Both the reduction in [$PM_{2.5}$] and NO_x emissions have been shown to lead to increases in [O_3] in North China (Huang et al., 2020; Le et al., 2020; Ke Li, Jacob, Liao, Zhu, et al., 2019). Nitrate production rates may continue to increase as long as [O_3] increases despite decreases in [NO_x], creating a negative feedback that reduces the effectiveness of air pollution reduction strategies. Policies that result in a reduction of ambient O_3 concentrations, possibly through reductions in VOC emissions, will also reduce the formation of nitrate and its contribution to $PM_{2.5}$ during wintertime haze events.

Chapter 3. POSSIBLE MECHANISMS FOR NO2 UPTAKE AND THE ASSOCIATED UNCERTAINTIES

3.1 INTRODUCTION

NO_2 can undergo heterogeneous reactions in the presence of surfaces, but the rates and product yields are still quite uncertain. In Chapter 2, we demonstrate that the standard version of GEOS-Chem model (GC, version 12.7.0) likely overestimates rate of nitrate production via NO_2 uptake on aerosol, which leads to model bias in nitrogen oxidation ratio and $\Delta^{17}O(NO_3^-)$. Heterogeneous reactions of NO_2 on different surfaces have been studied by numerous laboratory studies, where nitrate, HONO, NO and N_2O have found in the reaction products. In the standard version of the GC model, the hydrolysis of NO_2 on aerosols is parametrized as:

$$NO_2 \rightarrow 0.5\ HNO_3 + 0.5\ HONO \qquad \text{(R3.1)}$$

In the GC parametrization, the uptake coefficient of NO_2 ($\gamma(NO_2)$) is a function of aerosol type and ranges from 10^{-8} (for dust, cloud water, and dry sea salt) to 10^{-4} (for black carbon and wet sea salt).

Given the low solubility of NO_2 in liquid water (Sander, 2015), the direct uptake of NO_2 on typical aerosols and clouds is usually regarded as an inefficient process. The overall inefficiency of NO_2 uptake is reflected in the rather low $\gamma(NO_2)$ reported in the more recent studies (Ammann et al., 2013; Crowley et al., 2010). Nevertheless, the influence of the multiphase reactions of NO_2 may still be large in the real atmosphere since the concentration of NO_2 is orders of magnitude higher than that of non-nitrate NO_z species in many environments. In addition, laboratory studies showed

the uptake of NO_2 can be much more efficient under certain conditions (e.g., in the presence of organic compounds and metal oxides), some of which can occur in the real atmosphere. These efficient mechanisms for NO_2 uptake may explain some of the observations of [NO_2], [HONO], and [p-NO_3^-], but the complexity in these mechanisms also introduces uncertainties into the model simulations of nitrate production. In this chapter, we review different NO_2- uptake mechanisms proposed in the literature and how the discrepancy among these mechanisms can affect the modeled uptake coefficient, product yields, and $\Delta^{17}O$.

3.2 CATEGORIZATION OF THE PROPOSED NO_2-UPTAKE MECHANISMS

A large variety of NO_2-uptake mechanisms have been proposed in the literature. Most of these mechanisms are derived from the interpretations of the results of laboratory experiments (See Table 3.1), which come with different focuses and limitations. To ease the comparison, we try to group the proposed NO_2-uptake mechanisms into five categories.

Table 3.1. Summary of the experimental conditions and findings in all the laboratory studies on NO_2 uptake referred in Section 3.2.

Reference	**Surface type(s)**	**Experimental conditions and measurement techniques**	**NO_y products observed**	**Overall Reaction order for NO_2**	**Reported $\gamma(NO_2)$**	**Mechanism(s) for NO_2 uptake**
Sakamaki et al. (1983)	Inner wall of the chamber (mostly coated with tetrafluoroethylene-perfluoroalkyl vinyl ether copolymer (PFA), with some quart, glass, and metal components)	- Evacuable and bakable smog chamber - Pressure in the chamber = 760 Torr - Use ^{18}O-label water to monitor the flow of oxygen in the reactions. - Fourier transform infrared (FTIR) spectroscopy for identifying and measuring different gas-phase species	HONO (g) and NO (g)	First order	N/A	N/A
Svensson et al. (1987)	Inner wall of a batch reactor coated with Teflon film or stainless-steel sheet metal.	- Pressure in the chamber = 5 Pa $\approx 4\times10^{-2}$ Torr - Initial [NO_2 (g)] = 5 - 800 ppm - [H_2O (g)] = 1000 - 20000 ppm - FTIR spectroscopy	HONO (g) and NO (g)	First order	N/A	N/A
Chughtai et al. (1990)	Soot particles generated by combustion in laboratory conditions	- Total partial pressure of NO_2 (g) and N_2O_4 (g) is 120 Torr. - Experiments at various temperature (room temperature to 473 °C)	NO (g) and N_2O (g)	N/A	N/A	Redox reactions with reduced compounds and/or surface groups on soot particles

		with and without water vapor - FTIR spectroscopy				
Gerecke et al. (1998)	Soot particles generated by the combustion of ethylene, acetylene and toluene in laboratory conditions	- Pressure in the set-up = 10^{-6} Torr - Initial [NO_2 (g)] ≈10^{10} – 10^{13} molecule cm^{-3} - Knudsen cell connecting to an electron-impact quadrupole mass spectrometer	HONO (g) and NO (g)	N/A	- Initial γ ranges from 1.2×10^{-1} to 3×10^{-2}. - Initial γ decreases with increasing [NO_2 (g)].	Redox reactions with reduced compounds and/or surface groups on soot particles
Ammann et al. (1998)	Soot particles with an average diameter of 70 nm	- Flow reactor - Ambient pressure and room temperature in the set-up; RH = 50% and 0.5% - Initial [NO_2 (g)] = 12 ppbv - X-ray photoelectron spectroscopy (XPS) for characterizing the surface of soot particles	HONO (g)	N/A	- Estimated γ ranges from 1.1×10^{-2} to 3.3×10^{-4}.	Redox reactions with reduced compounds and/or surface groups on soot particles
Kalberer et al. (1999)	Soot aerosol produced by a spark discharge generator	- Use NO_2 (g) labeled by radioactive ^{13}N. - [NO_2 (g)] = 2 - 150 ppbv - Measurements done at various RH (0 – 70%) - Flow reactor connected to gamma radiation detectors for measuring NO_y species	HONO (g)	First order (assumed)	N/A	Redox reactions with reduced compounds and/or surface groups on soot particles

Kleffmann et al. (1999)	Commercial soot (with/ without treated with sulfuric acid) and freshly prepared soot	- Pressure in the set-up = 740 Torr - [NO_2 (g)] = 1 - 40 ppmv - Soot samples are placed between two Teflon filters in a Pyrex glass reactor, which is connected to tunable diode laser spectrometers and a NO_x monitor (Horiba, Model APNA- x 350E)	HONO (g) and NO (g)	First order	- Initial γ is in the order of 10^{-7}. - Steady-state γ is in the order of 10^{-8}.	Redox reactions with reduced compounds and/or surface groups on soot particles
Underwood et al. (2001)	Various metal oxide particles (α-Al_2O_3, γ-Al_2O_3, α-Fe_2O_3, γ-Fe_2O_3, TiO_2, SiO_2, MgO, and CaO) and mineral dust samples from China and Sahara	- Pressure in the set-up for determining uptake coefficient $\approx 10^{-6}$ Torr - Knudsen cell reactor connecting to a quadrupole mass spectrometer	NO (g)	First order (in their model)	- Initial γ ranges from about 10^{-8} to 10^{-4} after adjusting for the roughness of particles. - Highest and lowest initial γ are observed in α-Al_2O_3 (8.5×10^{-5}) and γ-Al_2O_3 (2.2×10^{-8}), respectively.	Surface-group reactions on metal oxides
Bröske et al. (2003)	Secondary organic aerosols (SOA) generated in laboratory conditions	- Both filter experiments and flow-tube experiments have been done. - [NO_2 (g)] = 100 – 300 ppbv in filter experiments and $\approx$ 200 ppbv in flow-tube experiment. - Ambient pressure, room temperature, and 50% RH in the flow-tube experiment.	HONO(g)	N/A	- Estimated upper limits for γ are between 7×10^{-7} and 9×10^{-6} in the flow-tube experiments.	Redox reactions with reduced compounds and/or surface groups on organic surfaces

		- [NO_x (g)] measured by a luminol nitrogen oxide analyzer (Unisearch, LMA-3D) - Long path absorption photometer (LOPAP) instrument is used for HONO measurement. - SOA is generated by the reactions of α- pinene, limonene, and catechol with ozone or those between toluene or limonene and OH.				
B. J. Finlayson-Pitts et al. (2003)	Wall of borosilicate glass long-path cells	- Ambient pressure in the set-up - [NO_2 (g)] ≈ 10^2 - 10^3 ppmv - Measurements at various RH - FTIR spectroscopy	Gas-phase species: HONO, NO, N_2O Surface species: HNO_3, N_2O_4, NO_2^+	First order	N/A	N_2O_4-intermediate reactions
Ramazan et al. (2004)	Wall of borosilicate glass long-path cells	- Ambient pressure and room temperature in the set-up - Set-up is irradiated by UV (320 to 400 nm) - [NO_2 (g)] ≈ 20 - 50 ppmv - Measurements at RH= 33, 39, and 57% - FTIR spectroscopy	Gas-phase species: HONO, NO	First order	N/A	N_2O_4-intermediate reactions
George et al. (2005)	Organic coating (benzophenone, catechol, anthracene, anthrarobin) on the wall of flow-tube reactor	- Ambient pressure, room temperature, and 20% RH in the set-ups	HONO (g)	First order (assumed)	- Estimates of γ are in the order of 10^{-6}. - γ is higher under UV radiation.	Redox reactions with reduced compounds and/or surface groups on organic surfaces

		- Initial [NO_2 (g)] ≈ 20 ppbv - Mercury lamb for UV irradiation (λ> 300 nm) - One flow tube is coupled with a quadrupole mass spectrometer. - Another simplified flow tube is coupled with LOPAP for HONO measurements.				
Stemmler et al. (2006)	Humic acid coatings on the wall of flow-tube reactor	- Room temperature and 20% RH in the set-up - [NO_2 (g)] ≈ 6 - 120 ppbv - Fluorescence lamps in the wavelength ranges of (300 - 420, 400-700 nm and 500 -700 nm). -The irradiance in the reactor ranges from 0 to 160 W m^{-2}.	HONO (g)	First order (assumed)	Estimated $\gamma = 2\times10^{-5}$	Redox reactions with reduced compounds and/or surface groups on organic surface
Gustafsson et al. (2006)	TiO_2 (anatase:rutile = 3:1)-particles inside a flow-tube reactor	- Initial [NO_2 (g)] ≈ 100 ppbv - Measurements of the consumption of NO_2 (g) is done by a chemiluminescence NO_x analyzer (API 200E). - Fluorescent lamps for UV irradiation (λ_{max}=365 nm). Light intensity inside the reactor was 1.6 mW cm^{-2}.	HONO	First order	- Estimated γ is 9.6×10^{-4} and 1.2×10^{-5} at RH =15% and 80%, respectively. - γ decreases with increasing RH.	Photoelectrochemical reactions on titanium dioxide surface

Ndour et al. (2008)	Substrates produced from Arizona test dust and grinded Saharan sand.	- Measurements are done at various [NO_2 (g)] (10 to 380 ppbv). - Halogen lamps (λ below 400 nm, 0.069 mW cm^{-2}) and fluorescence lamps (300 -420 mm, 13.4 mW cm^{-2}) for UV irradiation. - Measurements of the consumption of NO_2 (g) is done by a chemiluminescence NO_x analyzer (THERMO 42C).	HONO	First order	Estimated γ_{BET} ranges from 1.2×10^{-7} and 1.9×10^{-6}.	Photoelectrochemical reactions on titanium dioxide surface
Gustafsson et al. (2008)	Samples of mineral dust from the Gobi Desert	- Ultrahigh vacuum chamber - Temperature increases from 170 to 600 K. - Partial pressure of NO_2 during initial exposure = 10^{-6} Torr - XPS - Temperature-programmed desorption (TPD) mass spectrometry	Isotopologues of HONO (g)	First order	N/A	Surface-group reactions on metal oxides
Beaumont et al. (2009)	TiO_2 (anatase: rutile = 3:1)-coated wall inside a flow-tube reactor	- [NO_2 (g)] = 200 ppbv, RH =20%, and room temperature inside the set-up - Measurements of surface species based on diffuse reflectance	- Gas-phase species: HONO and H_2O_2 - Surface species: nitrate	N/A	N/A	Photoelectrochemical reactions on titanium dioxide surface

		infrared Fourier transform spectroscopy (DRIFTS) - Measurements of [H_2O_2 (g)] based on Selective oxidative dimerization of p-hydroxyphenyl acetic acid (POPHA) with peroxidase. - Measurements of the consumption of NO_2 (g) is done by a chemiluminescence NO_x analyzer (API 200E). - [HONO (g)] is determined by measured [NO_2 (g)] with and without Na_2CO_3 denuder in the set-up. - Fluorescent lamps for UV irradiation (λ_{max}=365 nm)				
Langridge et al. (2009)	Commercially available self-cleaning window glass (TiO_2-coated)	- Ambient pressure in the set-up - Initial [NO_2 (g)] = 69 ppbv - Range of RH: 8 - 70 % - Measurement of [NO_2 (g)] and [HONO (g)] is done by Broadband cavity enhanced absorption spectroscopy (BBCEAS) - Fluorescent lamps for UV irradiation (λ_{max}=365 nm, 6 W m^{-2})	HONO (g)	N/A	N/A	Photoelectrochemical reactions on titanium dioxide surface
H. J. Li et al. (2010)	- $CaCO_3$ particles (size ≈ 1 - 10 μm)	- Room temperature - Initial [NO_2 (g)] = 710 ppmv	HNO_3 and HONO	Second order at low RH	Initial γ is $(4.25\pm1.18)\times10^{-9}$ and $(2.54\pm0.13)\times10^{-9}$ in	Dry conditions: N_2O_4-intermediate reactions

	- SiO_2 particles (control set-up)	- DRIFTS - Ion chromatography (IC) - Scanning electron microscopy (SEM) - XPS	No nitrate formation in the control set-up	First order at high RH	dry and wet conditions, respectively	Wet conditions: direct reaction between H_2O (ads) and NO_2 (ads), and N_2O_4-intermediate reactions are also possible
Monge et al. (2010)	Fresh soot particles produced by a miniCAST soot generator using propane	- Ambient pressure, room temperature, and 30% RH in the set-up. - [NO_2 (g)] = 16 – 150 ppb - Measurements of the consumption of NO_2 (g) is done by a chemiluminescence NO_x analyzer (THERMO 42i). - Fluorescent lamps for UV irradiation (λ = 300 - 420 nm)	HONO (g) and NO (g)	N/A	- Average γ ranges from 4.3×10^{-8} to 5×10^{-7}. - γ decreases with increasing [NO_2 (g)]. - γ increases with increasing irradiance.	Redox reactions with reduced compounds and/or surface groups on soot particles
Kim & Kang (2010)	Ice film grown on Ruthenium (0001) surface	- Ultrahigh vacuum chamber - Temperature increases from 90 to 180 K - Highly purified NO_2 (g) in the chamber with a pressure of 10^{-9} Torr - Reactive ion scattering (RIS) - TPD mass spectrometry - Auger electron spectroscopy - Isotope-tagging (deuterium)	Various surface species	First order	N/A	Direct reaction between H_2O (ads) and NO_2 (ads) N_2O_4-intermediate reactions are not likely to be important

Chang Liu et al. (2012)	Various metal oxide particles (α-Al_2O_3, α-Fe_2O_3, TiO_2, SiO_2, MgO, CaO, and ZnO), $CaCO_3$ particles, and $CaSO_4$ particles	- Samples are first exposed to 200 ppmv of [NO_2 (g)] - Temperature in the set-up = 303 K - DRIFTS	Various surface species	N/A	N/A	- N_2O_4-intermediate reactions (in the presence of SO_2 and metal-oxide surfaces)
Yongchun Liu et al. (2015)	Kaolin and hematite particles	- Ambient pressure and room temperature in the set-up - [NO_2 (g)] = 150±5 ppbv - Measurements at various RH - Measurement of [NO_x (g)] is done by a chemiluminescence NO_x analyzer (THERMO 42i). - [HONO (g)] is determined by measured [NO_2 (g)] with and without Na_2CO_3 denuder in the set-up.	Gas-phase species: HONO, NO, HNO_3	First order	- For kaolin, initial γ is $(1.44\pm0.10)\times10^{-7}$ and $(3.10\pm1.14)\times10^{-8}$ at the RH of 7 and 74%, respectively. Steady-state γ is $(4.56\pm0.15)\times10^{-9}$ and $(4.26\pm0.06)\times10^{-9}$ at the RH of 7 and 74%, respectively. - For hematite, initial γ is $(1.58\pm0.13)\times10^{-6}$ and $(1.86\pm0.07)\times10^{-7}$ at the RH of 7 and 74%, respectively. Steady-state γ is $(1.24\pm0.18)\times10^{-8}$ and $(1.23\pm0.05)\times10^{-8}$ at the RH of 7 and 74%, respectively. - Higher γ is usually observed at RH=15-47%. Highest steady-state γ is observed on hematite particles at RH=47%.	- Surface-group reactions on metal oxides - One possible pathway involves N_2O_4-intermediate reactions
F. Tan et al., (2016)	Particles of $CaCO_3$-$(NH_4)_2SO_4$ mixtures	- Measurements at various RH (<1, 40, 60, and 85%)	Various surface species	N/A	- For pure $CaCO_3$ particles, the initial uptake coefficient	Surface-group reactions on metal oxides

		- FTIR spectroscopy - DRIFTS - IC			(based on geometric surface area) is $(1.04\pm0.04)\times10^{-5}$ and $(7.10\pm0.04)\times10^{-6}$ at dry condition and 85% RH, respectively. - For particles with 93 wt % -$(NH_4)_2\ SO_4$ and 7 wt % of $CaCO_3$, the initial uptake coefficient is $(4.90\pm0.36)\times10^{-6}$ and $(2.55\pm0.28)\times10^{-6}$ at dry condition and 85% RH, respectively. - γ decreases as the mass percentage of $(NH_4)_2\ SO_4$. - γ peaks at the RH of 40%.	
Kebede et al. (2016)	The Wall of a flow-tube reactor coated with substrates made of (i) samples of mineral dust from the Sahara Desert, soil from Arizona, and clay minerals, and (ii) standard iron oxides (Magnetite (Fe_3O_4/γ-Fe_2O_3), goethite (α -FeOOH), and hematite (α-Fe_2O_3))	- Coated-wall flow tube attached to a chemical ionization mass spectrometer (CIMS) for measuring HONO (g) formation - The pH of the slurries (powder of substrates and water/ ethanol solution) is measured using a pH meter and is adjusted using H_2SO_4 and NaOH solutions. The slurries is then used for coating the inner walls of flow tube.	HONO (g)	N/A	Estimated γ for iron-bearing dust samples ranges from 0.1×10^{-5} to 2.9×10^{-5} .	Redox reactions with metal ions/complexes

		- RH in the flow tube is kept at 50%. - [NO_2 (g)] = 40 or 50 ppbv - X-ray diffraction (XRD) analysis and XPS for the characterization of dust samples				
Ma et al. (2017)	MgO-coated wall inside a flow-tube reactor	- Ambient pressure and room temperature inside the flow-tube reactor - Chemiluminescence analyzers (THERMO 42i) for measuring [NO_x(g)] and determining [HONO(g)] - Measurements at various [NO_2 (g)] (about 20, 60, 100, and 160 ppbv) - Measurements at various [SO_2 (g)] (0, 40, 100, and 1000 ppbv) - DRIFTS for measuring surface species - IC for analyzing the ions on the reacted MgO surface	HONO (g), nitrate, and various surface species	First order	-For "fresh" MgO, γ is about 2.87×10^{-6} and 1.03×10^{-6} at [SO_2(g)] = 100 and 40 ppbv, respectively. - For SO_2-aged MgO, γ is about 5.28×10^{-6}. - γ does not depend on [NO_2(g)] and RH.	Surface-group reactions on metal oxides in the presence of SO_2 (g)
Chang Liu et al. (2017)	Nanoparticles of TiO_2 (amorphous, anatase, and rutile; average size is 50 nm)	- Room temperature in the set-up - [NO_2 (g)] = 200 ppmv - DRIFTS	Various surface species	N/A	N/A	Photoelectrochemical reactions on titanium dioxide surface

R. Li et al. (2020)	Iron oxide (hematite, magnetite, goethite) particles on PTFE filter	- Filters with iron oxide samples are placed in a flow-tube reactor connecting to a NO_x analyzer -Inner wall surface is coated with fluorinated ethylene propylene (FEP) to reduce the loss of NO_2 to the wall - [NO_2 (g)] = 15±1 and 2.5±0.1 ppmv - Measurements at various RH (0, 30, 60, and 90%) - SEM and inductively coupled plasma- mass spectrometer (ICP-MS) for the characterization of iron oxide samples before and after exposure to NO_2 (g)	Nitrate formed on surfaces	N/A	- γ for hematite is about 5×10^{-9} and 1×10^{-8} at [NO_2 (g)] = 15 and 2.5 ppmv, respectively. - γ for magnetite and goethite is about 2.8×10^{-8} and 4.4×10^{-8}, respectively. - γ has no strong dependence on RH.	The reference did not discuss the chemical mechanisms for NO_2 uptake in detail but cited other previous paper that discussed surface-group reactions on metal oxides and photo-enhanced mechanisms.

3.2.1 *N_2O_4-intermediate reactions*

B. J. Finlayson-Pitts et al. (2003) first described the potential importance of N_2O_4 in the heterogeneous hydrolysis of NO_2 in details and provided a completed mechanism to explain most of the findings from previous laboratory studies by then. The uptake mechanism can be summarized in three steps:

Step 1: Formation of N_2O_4 via dimerization of NO_2

The proposed uptake mechanism starts with the dimerization of NO_2, which is an exothermic reaction. Meanwhile, N_2O_4 can also undergo decomposition to form NO_2. A chemical equilibrium may exist between gas-phase NO_2 and N_2O_4 (R3.2).

$$NO_2\ (g) + NO_2\ (g) \rightleftharpoons N_2O_4\ (g) \qquad \text{(R3.2)}$$

The next step is the adsorption of N_2O_4 on surfaces, which is also a reversible process (R3.3). It is noted that N_2O_4 is much more soluble than NO_2 in water: its Henry's law constant is 2 to 3 orders of magnitude higher than that of NO_2 and is comparable to that of N_2O_5 (Sander, 2015).

$$N_2O_4\ (g) \rightleftharpoons N_2O_4\ (ads) \qquad (R3.3)$$

For chemical equations in this chapter, the symbol "(ads)" indicates species adsorbed on the surface.

Step 2: Isomerization of N_2O_4 (ads) and backward reaction

It is proposed that symmetric N_2O_4 (O_2NNO_2) adsorbed on surfaces can undergo isomerization to form an asymmetric reaction intermediate $ONONO_2$ (R4). To explain why the heterogeneous hydrolysis of NO_2 appears to be first order with respect to NO_2 in most of the laboratory studies, B. J. Finlayson-Pitts et al. (2003) hypothesized that $ONONO_2$ (ads) reacts quickly with NO_2 (g) to convert back to N_2O_4 (ads) (R5). Combining the stoichiometry from R3.2 to R3.5, it can be shown that the steady state concentration of $ONONO_2$ is directly proportional to $[NO_2]$.

$$N_2O_4\ (ads) + H_2O \rightarrow ONONO_2\ (ads) + H_2O \qquad (R3.4)$$

$$ONONO_2\ (ads) + NO_2\ (g) \rightarrow N_2O_4\ (ads) + NO_2\ (g) \qquad (R3.5)$$

B. J. Finlayson-Pitts et al. (2003) also considered the scenarios in which N_2O_4 (ads) is not in equilibrium with NO_2(g). They modified the hypothesized isomerization reaction to explain the observed reaction order in laboratory experiments (R3.6):

$$N_2O_4\ (ads) + NO_2\ (g) \rightarrow ONONO_2\ (ads) + NO_2\ (g) \qquad (R3.6)$$

Step 3: Autoionization of $ONONO_2$ (ads) and subsequent hydrolysis

The mechanism proceeds by the autoionization of $ONONO_2$ (ads) to form a complex $NO^+NO_3^-$ (ads) (R3.7). This complex can react with water to produce HONO and HNO_3 (R3.8). Some of the HONO produced can convert back to gas phase and leave the surfaces. The predicted flow of oxygen atom from H_2O to HONO is consistent with some early isotope-labeling studies of NO_2 hydrolysis using $H_2{}^{18}O$, in which $H^{18}ONO$ is the major isotopologue produced from the reaction (Sakamaki et al., 1983; Svensson et al., 1987). Results from some molecular simulations also supported the occurrence of this hypothesized step and suggested that autoionization (R3.7) is very fast for $ONONO_2$ within water clusters (Miller et al., 2009).

$ONONO_2$ (ads) → $NO^+NO_3^-$ (ads) (R3.7)

$NO^+ NO_3^-$ (ads) + H_2O (ads) → HONO (g/ads) + HNO_3 (ads) (R3.8)

In the original mechanism proposed by B. J. Finlayson-Pitts et al. (2003), HONO and HNO_3 can also undergo other reactions to generate NO, NO^+, and N_2O_4.

Similar mechanisms that involve N_2O_4 have been adapted in many later studies (Barbara J. Finlayson-Pitts, 2009; H. J. Li et al., 2010; Chang Liu et al., 2012; Yongchun Liu et al., 2015; Ramazan et al., 2004). Ramazan et al. (2004) argued that the observed production of NO_2(g)

from the photolysis of adsorbed nitrate in laboratory studies could be understood by "reversing" the reactions in the mechanism proposed in B. J. Finlayson-Pitts et al. (2003). To explain the findings from the laboratory studies of NO_2 on $CaCO_3$ surface under dry condition, H. J. Li et al. (2010) suggested N_2O_4 (ads) can reacts with an altered form of adsorbed water on $CaCO_3$ surface (R3.9 and R3.10).

$$H_2O\ (ads) + \text{oxygen-vacancy site} \rightarrow \text{--(OH)H (ads)} \qquad (R3.9)$$

$$\text{--(OH)H (ads)} + N_2O_4\ (ads) \rightarrow HNO_3\ (ads) + HONO\ (g) + \text{oxygen-vacancy site} \qquad (R3.10)$$

Yongchun Liu et al. (2015) also considered the formation of nitrate and nitrite (NO_2^-) via a potential reaction between adsorbed N_2O_4 and the $\text{--}O^-$ surface groups on metal oxides in their investigation of the uptake of NO_2 on kaolin and hematite. However, it is important to note that this reaction of adsorbed N_2O_4 is not a necessary step in their proposed mechanism.

B. J. Finlayson-Pitts et al. (2003)'s interpretation of laboratory findings and their proposed mechanism have faced challenges from the later studies (e.g., Gustafsson et al., 2008; Kim & Kang, 2010). Gustafsson et al. (2008) argued that B. J. Finlayson-Pitts et al. (2003) might have overestimated the importance of N_2O_4 because most of the early laboratory studies had used an unrealistically high [NO_2 (g)] (at ppm levels) in the experimental set-ups. They repeated the isotope-labeling experiment using a lower [NO_2(g)] and failed to detect $H^{18}ONO$ in the reaction products. Indeed, their set-up produces $H^{16}ONO$ exclusively. Responding to the criticisms from Gustafsson et al. (2008), B. J. Finlayson-Pitts (2009) pointed out that (i) the very low pressure

and temperature condition ($P=10^{-10}$ mbar; T=170 K) used in the experimental set-up of Gustafsson et al. (2008) also could not mimic the real atmosphere, and (ii) results from Gustafsson et al. (2008) do not exclude the possibility of N_2O_4 formation via sequential reactions. Kim & Kang (2010) studied the uptake of NO_2 on ice surfaces at low temperature and the conclude that N_2O_4 is not an important immediate in NO_2 hydrolysis on surfaces. Their laboratory findings showed that (i) N_2O_4 (ads) only occurs in the presence of NO_2 multilayer at 90K and (ii) N_2O_4 (ads) correlates inverse with HONO production.

Direct uptake of N_2O_4 (g) on surfaces is not likely to be important under typical conditions in wintertime Beijing. At T = 273 K (average winter temperature in Beijing), the equilibrium constant for inter-conversion between NO_2 (g) and N_2O_4 (g) (R3.3) is of the order of 10^{-18} cm^3 $molecule^{-1}$ (computed using the kinetic data from Atkinson et al. (2004)). At [NO_2 (g)] ≈ 100 ppbv (common in extreme haze), [N_2O_4 (g)]$_{equilibrium}$ is about 0.6 pptv, which is orders of magnitude lower than [N_2O_5 (g)] observed in China (usually ranges from 10^1 to 10^3 pptv). Although the formation of N_2O_4 (ads) via the reactions between two adsorbed NO_2 on surfaces may occur and promote the production of nitrate and HONO (g) via R3.4 - R3.8, more kinetic studies are required to evaluate the importance of this possible pathway in the lower troposphere.

3.2.2 *Surface-group reactions on metal oxides*

Mechanisms that involve surface groups have been proposed more commonly among the studies of NO_2 uptake on metal oxides (Gustafsson et al., 2008; Yongchun Liu et al., 2015; Ma et al., 2017; F. Tan et al., 2016; Underwood et al., 2001). To explain how NO_2 reacts on dust samples

without involving N_2O_4, Gustafsson et al. (2008) proposed that NO_2 (a) can reacts with H (ads) and OH (ads) resulted from the dissociative chemisorption of water on dust surface (R3.11) to produce HNO_3 (R3.12) and HONO (R3.13). Meanwhile, B. J. Finlayson-Pitts (2009) questioned the relevance of R8 to the real atmosphere by stating that water unlikely undergoes thermal dissociation on natural surfaces under atmospheric conditions.

$$H_2O\ (ads) \rightarrow OH\ (ads) + H\ (ads) \qquad (R3.11)$$

$$NO_2\ (ads) + OH\ (ads) \rightarrow HNO_3\ (ads) \rightarrow HNO_3\ (g) \qquad (R3.12)$$

$$NO_2\ (ads) + H\ (ads) \rightarrow HONO\ (ads) \rightarrow HONO\ (g) \qquad (R3.13)$$

Since NO_2 (g) usually outnumbers the surface groups on metal oxides, NO_2 uptake will stop if all the active sites on surfaces are occupied. Besides, other species may also compete for the surface groups and inhibit the adsorption of NO_2. Therefore, more completed mechanisms have to explain how surface groups can be regenerated as the uptake of NO_2 proceeds. To account for the continuous production of HONO from the uptake of NO_2 on iron minerals, Yongchun Liu et al. (2015)'s mechanism is based upon cycling of --O^- group and --OH group in the presence of water (R3.14 to R3.16).

$$M\text{--}O^- + NO_2\ (g) \rightarrow MO\text{-}NO_2^-\ (ads) \qquad (R3.14)$$

$$M\text{--}O^- + H_2O\ (g/ads) \rightarrow M\text{--}OH + OH^-\ (ads) \qquad (R3.15)$$

$$MO\text{-}NO_2^- \text{ (ads)} + M\text{--}OH \text{ (ads)} \rightarrow M\text{--}O^- + HONO \text{ (g)} + MO\text{-}OH \text{ (ads)} \quad \text{(R3.16)}$$

It is noted that the symbol "M" in the chemical equations stands for metal atom.

In some cases, the bulk constituents and/or the presence of other trace gases can also modulate the interactions between NO_2 (g) and the surface groups. F. Tan et al. (2016) studied the heterogeneous reactions of NO_2 with $CaCO_3$-$(NH_4)_2SO_4$ mixture and proposed a mechanism that involves cycling of -OH surface group via interactions between the NO_3^- (ads) and other species in the mixture (Ca^{2+}, NH_4^+, and SO_4^{2-}). The first step of the mechanism is the formation of --OH·· NO_2 (ads) intermediate (R3.17) and the production of NO_3^-(ads) (R3.18-R3.20).

$$NO_2 \text{ (g)} + \text{--OH} \rightarrow \text{--OH}\cdot\cdot\ NO_2 \text{ (ads)} \quad \text{(R3.17)}$$

$$\text{--OH}\cdot\cdot\ NO_2 \text{ (ads)} + \text{--OH}\cdot\cdot\ NO_2 \text{ (ads)} \rightarrow NO_3^- \text{ (ads)} + NO_2^- \text{ (ads)} + H_2O \text{ (ads/g)} \quad \text{(R3.18)}$$

$$NO_2^- \text{ (ads)} + NO_2^- \text{ (ads)} \rightarrow NO_3^- \text{ (ads)} + NO \text{ (g)} \quad \text{(R3.19)}$$

$$NO_2^- \text{ (ads)} + NO_2 \text{ (g)} \rightarrow NO_3^- \text{ (ads)} + NO \text{ (g)} \quad \text{(R3.20)}$$

The regeneration of --OH groups depends on a reversible reaction between NO_3 (ads) and the adsorbed water (R3.21).

$$NO_3^- (ads) + H_2O (ads) \rightleftharpoons HNO_3 (ads) + \text{--}OH \quad (R3.21)$$

Under dry conditions (RH<60%), interactions between HNO_3(ads), $CaCO_3$, and $(NH_4)_2SO_4$ in the mixture (R3.22) can consume HNO_3 and shift the equilibrium to the right, which promotes the regeneration of --OH groups.

$$2HNO_3 (ads) + CaCO_3 + (NH_4)_2SO_4 \rightarrow CaSO_4 (s) + 2NH_4NO_3 + H_2O + CO_2 \quad (R3.22)$$

Under humid conditions, $CaCO_3$ can directly react with $(NH_4)_2SO_4$ without involving HNO_3; thus, the uptake of NO_2 may be controlled the direct reactions between NO_2(ads) and H_2O (ads).

Ma et al. (2017) studied the uptake of NO_2 on MgO and found that SO_2-aged MgO has $\gamma(NO_2)$ that is (1) 2-3 orders of magnitude higher than that on fresh MgO and (2) independent of NO_2 (g) and RH. They proposed a mechanism that involves reactions between SO_2 (g) and surface oxygen groups ($\text{--}O^{2-}$) on MgO surface.

$$SO_2 (g) + \text{--}O^{2-} \rightarrow SO_3^{2-} (ads) \quad (R3.23)$$

$$SO_3^{2-} (ads) + 2NO_2 (g) \rightarrow 2NO_2^- (ads) + SO_4^{2-} (ads) \quad (R3.24)$$

In the presence of H_2O (ads), adsorbed nitrite can obtain the H^+ to form HONO, which then leaves the surface in gas phase and frees up a reactive site on surface. In an earlier laboratory study, Chang Liu et al. (2012) also found that NO_2 can promote the oxidation of SO_2 on different

types of dry mineral oxides. Their mechanism contains a step similar to R3.23 but requires the formation of N_2O_4 on the surface. The final products from Chang Liu et al. (2012)'s mechanism are SO_4^{2-} (ads), NO_3^- (ads), NO (g), and NO_2 (g). The potential importance of the synergistic heterogeneous reactions between SO_2 and NO_2 in haze events has discussed frequently in the recent literature (e.g., Shao et al., 2019; Junfeng Wang et al., 2020; Xue et al., 2016). Many mechanisms for coupling the heterogeneous chemistry of SO_2 and NO_2 have been proposed, but not all of them involves the surface uptake of NO_2 (g). For example, in the mechanism proposed by Gen et al. (2019), the NO_2 for SO_2 oxidation is generated from the photolysis of nitrate in the aerosols instead.

3.2.3 *Redox reactions with metal ions/complexes*

Kebede et al. (2016) proposed that, in iron-bearing minerals in surface soil, Fe^{2+} in ionic or metal-complex form can reduce NO_2 to NO_2^-, which can then form HONO(g) by protonation. At low soil pH (about 3 to 5), aqueous Fe^{2+} ions exist and react with adsorbed NO_2 to produce nitrite and Fe^{3+} (R3.25). Nitrite can form HONO (g) by reacting with protonated water (R3.26).

$$NO_2\ (ads) + Fe^{2+}\ (aq) \rightarrow NO_2^-\ (aq) + Fe^{3+}(aq) \qquad (R3.25)$$

$$NO_2^-\ (aq) + H_3O^+\ (aq) \rightarrow HONO\ (g) + H_2O\ (g) \qquad (R3.26)$$

At higher soil pH (>5), Kebede et al. (2016) suggested that structural or complexed Fe^{2+} may still react with NO_2 to produce NO_2^-. The resulted NO_2^- then reacts with $-OH_2^+$ surface groups to form HONO(g).

If R3.25 is efficient in the real atmosphere, the heterogeneous uptake of NO_2 might have large influence on the uptake of HO_2 on aerosols, the cycling between HO_2 and H_2O_2, and the solubility of iron in aerosols. However, more recent laboratory experiments by R. Li et al. (2020) showed that the heterogeneous uptake of NO_2 on hematite, magnetite, and goethite has negligible effects on nitrate formation and iron solubility.

3.2.4 *Photoelectrochemical reactions on titanium dioxide surface*

Several studies reported NO_2-to-HONO conversion on UV-illuminated TiO_2 surfaces (Beaumont et al., 2009; H. Chen et al., 2012; Gustafsson et al., 2006; Langridge et al., 2009; Ndour et al., 2008). Beaumont et al. (2009) proposed a mechanism for explaining the observed photocatalytic formation of HONO and H_2O_2 (R3.27 - R3.31).

$$h\boldsymbol{\nu}\ (<387\ nm) + TiO_2 \rightarrow e^- + h^+ \qquad (R3.27)$$

$$e^- + NO_2\ (ads) \rightarrow NO_2^-\ (ads) \qquad (R3.28)$$

$$h^+ + H_2O\ (ads) \rightarrow H^+(ads) + OH\cdot \qquad (R3.29)$$

NO_2^- (ads) + H^+ (ads) → HONO (g) (R3.30)

OH· (ads) + OH· (ads) → H_2O_2 (g) (R3.31)

It is noted that the symbol "h^+" in the chemical equation stands for valence band hole and should not be confused with "H^+", which stands for hydrogen ion (H^+). Since TiO_2 is a common component of dust aerosol, this mechanism can be potentially important during a dust episode. Modeling results from Ndour et al. (2008) showed that NO_2-to-HONO conversion on UV-illuminated dust aerosol can reduce NO_2 level by up to 37% during a dust episode in West Sahara.

Similar to the cases for the other metal oxides, surface-group-mediated reactions might also be relevant for the uptake of NO_2 on TiO_2. Chang Liu et al. (2017) explained the uptake of NO_2 on amorphous TiO_2 nanoparticles by the interactions between NO_2 and --OH surface groups. However, it is important to note that NO_2 is not the only common atmospheric species that interacts with --OH surface groups on TiO_2 particle surfaces. --OH surface groups also react with SO_2 to form adsorbed sulfite and involves in the adsorption of alcohols and carbonyls (H. Chen et al., 2012). Different species likely compete for reaction sites on the TiO_2 aerosols in the atmosphere, so a large proportion of the --OH surface groups may not be available for NO_2 uptake.

3.2.5 *Redox reactions with reduced compounds and/or surface groups on soot particles and organic surfaces*

To explain the observed uptake of NO_2 on soot or carbonaceous surfaces, several laboratory studies suggested NO_2 can oxidize the organic compounds adsorbed on surfaces and/or the surface groups rapidly (R3.32 and R3.33) (Ammann et al., 1998; Bröske et al., 2003; Gerecke et al., 1998; Kalberer et al., 1999; Kleffmann et al., 1999). NO_2 uptake on soot mainly produces HONO, while some studies also reported the detection of NO and N_2O in reaction products (Chughtai et al., 1990; Gerecke et al., 1998; Kleffmann et al., 1999; Monge et al., 2010).

$$NO_2\ (g/ads) + \text{reduced compound (ads)} \rightarrow HONO\ (g) + \text{oxidized compound} \qquad (R3.32)$$

$$NO_2\ (g/ads) + \text{reduced group} \rightarrow HONO\ (g) + \text{oxidized group} \qquad (R3.33)$$

It is important to note that the surface species are reactants instead of catalysts in R3.32 and R3.33. As R3.32 and R3.33 proceed, the soot surfaces will gradually lose its reducing power. Observed $\gamma(NO_2)$ on fresh soot and the corresponding HONO-formation rate decrease to negligible levels within minutes to hours (Gerecke et al., 1998; Kalberer et al., 1999; Kleffmann et al., 1999). NO_2 uptake rate and the yield of HONO also depends on humidity, but the observed RH-dependence differs between studies (Kalberer et al., 1999; Kleffmann et al., 1999).

Many laboratory studies reported that solar radiation can promote NO_2-to-HONO conversion on soot particles (George et al., 2005; Monge et al., 2010; Stemmler et al., 2006). When soot particles or organic-film-coated surfaces are irradiated by visible light or UV radiation, higher

rates of NO_2 uptake and/or HONO formation were observed than the control experiments in the dark (George et al., 2005; Monge et al., 2010; Stemmler et al., 2006). These studies attributed the observed photo-enhancing effects to the presence of more complex organic compounds, such as polycyclic phenols, aromatic hydrocarbons, and humic acids. These complex organic compounds can be activated by solar radiation, become stronger electron donors, and hence promote the reduction of NO_2 (g) under sunlight.

3.3 Uncertainty in the uptake coefficient of NO_2

Given the large variety of possible NO_2-uptake mechanisms, it would not be surprising to see a huge range of $\gamma(NO_2)$ used in photochemical models (e.g., Holmes et al., 2019; Li Zhang et al., 2016). The more important questions to ask perhaps are (1) which mechanisms are relevant to the atmosphere, especially during haze events and (2) how to parametrize these mechanisms and their environmental dependence in photochemical models.

One of the largest discrepancies among laboratory studies is how the uptake of NO_2 on surfaces depends on humidity. Some laboratory studies noted that the loss of NO_2 on surfaces is more efficient under humid conditions (B. J. Finlayson-Pitts et al., 2003; Barbara J. Finlayson-Pitts, 2009). There are several explanations for the positive relationship between RH and NO_2-uptake rate:

1. [H_2O] (ads) controls the reaction rate when the amount of water on surfaces is not in excess for the reactions with NO_2 (g)

2. Water is hypothesized to be essential for the isomerization and autoionization of N_2O_4

3. Water is essential in the cycling of the surface groups on metal oxides in some mechanism (e.g., Yongchun Liu et al. (2015)'s mechanism)

4. Water speeds up the production of HONO (g) by the protonation of NO_2^-. Gas-phase HONO then leave the surface and free up reactive sites.

In contrast, several laboratory studies of the uptake of NO_2 on mineral-dust-like surfaces found that high RH may inhibits the reactions. Their arguments include:

5. Excess H_2O (g) competes for the limiting reactive sites on surfaces, which ultimately inhibits the adsorption of NO_2 (g).

6. As RH goes up, water film may form on surfaces, and aerosols may even undergo deliquescence. These processes terminate the original "dry" mechanisms that are more efficient.

While (5) and (6) might explain the apparent suppression of NO_2 uptake in Beijing in more intense haze (inferred from the higher $\Delta^{17}O(NO_3^-)$ in observations), there is no strong qualitative

reason to reject claims (1) to (4) for the environment in wintertime Beijing. More observational constraints and quantitative analysis are required to establish the linkage between the actual chemical mechanism for NO_2 uptake in Beijing and the observed relationship between RH and $\gamma(NO_2)$.

3.4 UNCERTAINTY IN THE YIELD OF NITRATE AND HONO FROM NO_2 UPTAKE

Nitrate and HONO are the final products for NO_2 uptake reactions in various hypothesized mechanisms, but the predicted yield varies greatly among different studies. For mechanisms in which NO_2 undergoes disproportionation-like reactions, the ratio of nitrate production rate and HONO production rate should be close to 1:1 (i.e., yield of nitrate ≈ yield of HONO). This is also the assumption behind the standard parametrization for NO_2 uptake in the GC model. In contrast, for mechanisms in which NO_2 behaves like an oxidizing-agent (e.g., in the oxidation of organic compounds on soot particles and SO_3^{2-}), HONO, which is more reduced than NO_2, should be the dominant product (i.e., yield of nitrate ≈ 0 % & yield of HONO ≈ 100%).

Nitrate photolysis may complicate the interpretation of some of the observations and laboratory findings. Under sunlight, some nitrate produced via NO_2 uptake may undergo photolysis to form HONO. If nitrate photolysis becomes an important source of HONO in an experimental set-up or an environment, it would be difficult to distinguish whether the observed HONO originates directly from NO_2 uptake reactions or the subsequent nitrate photolysis.

3.5 Uncertainty in the $\Delta^{17}O$ of the nitrate produced from NO_2 uptake

The $\Delta^{17}O$ associated with NO_2-uptake pathway is determined by the origin of the three oxygen atoms in nitrate, which depends on the detailed mechanism of NO_2 hydrolysis. For the calculations of modeled $\Delta^{17}O(NO_3^-)$ related to NO_2 hydrolysis ($\Delta^{17}O(NO_3^-$, NO_2 hydrolysis), we currently assume that two oxygen atoms in nitrate originate from the NO_2 molecule, while the remaining one oxygen atom comes from the water molecule involved in the heterogeneous reaction. This presumed flow of oxygen atoms is consistent with the mechanisms that based on direct NO_2 hydrolysis and OH-surface-group reactions. Since $\Delta^{17}O(H_2O)$ is very close to zero in the lower troposphere, the modeled $\Delta^{17}O(NO_3^-$, NO_2 hydrolysis) will also carry lower $\Delta^{17}O$ than those produced via N_2O_5 hydrolysis. This approach of estimating $\Delta^{17}O(NO_3^-$, NO_2 hydrolysis) has also been adopted by most of the previous $\Delta^{17}O$ studies (e.g., Alexander et al., 2020; He et al., 2018, 2020). However, this assumption about the origin of oxygen atoms in nitrate may not be consistent with some of the proposed NO_2-uptake mechanisms that involve N_2O_4.

If N_2O_4 is indeed the key intermediate in the mechanisms of NO_2 uptake, $\Delta^{17}O(NO_3^-$, NO_2 hydrolysis) will likely be higher. In environments where ozone is the dominant oxidant in NO-to-NO_2 conversion, $\Delta^{17}O(NO_2)$ is close to the $\Delta^{17}O$ of the terminal oxygen atoms of ozone (~39 ‰). If we assume that (i) the adsorption and dimerization of NO_2 do not change $\Delta^{17}O$ and (ii) N_2O_4 does not exchange oxygen atoms with other species until it undergoes hydrolysis, then the resulted nitrate will inherit the high $\Delta^{17}O$ in NO_2 because all the three oxygen atoms originate from N_2O_4. Meanwhile, the HONO produced from the same mechanism will have a lower $\Delta^{17}O$

because one out of two oxygen atoms in HONO originates from water. This hypothesized flow of oxygen atom from H_2O to HONO is supported by some early isotope-labeling studies of NO_2 hydrolysis using $H_2{}^{18}O$ (Sakamaki et al., 1983; Svensson et al., 1987). If B. J. Finlayson-Pitts et al. (2003)'s proposed mechanism dominates the production of nitrate via NO_2 uptake and assumptions (i) and (ii) hold in the real atmosphere, then $\Delta^{17}O(NO_3^-$, NO_2 hydrolysis) should be higher than our currently assumed values. This could affect our interpretation of $\Delta^{17}O(NO_3^-)$ observations in Beijing because we currently assume that the higher $\Delta^{17}O(NO_3^-)$ observed in more intense haze is not consistent with the base model's prediction of higher contribution of NO_2 hydrolysis to nitrate production. Nevertheless, as demonstrated in Section 3.2.1, direct uptake of N_2O_4 (g) on surfaces is not likely to be an important source of nitrate in wintertime Beijing because of the expected low [N_2O_4 (g)].

The potential exchange of oxygen atoms between nitrite and water on surfaces may further complicate the estimation of $\Delta^{17}O(NO_3^-$, NO_2 hydrolysis). While the isotopic composition of nitrate is relatively stable against abiotic processes, it has long been known that aqueous nitrite can exchange oxygen atoms with water molecules (Buchwald & Casciotti, 2013; Casciotti et al., 2007). Laboratory studies showed that nitrite and water molecules can establish oxygen-isotopic equilibrium within weeks to months in seawater (Buchwald & Casciotti, 2013). Some of the proposed NO_2-uptake mechanisms also involve adsorbed nitrite. It is unclear whether the exchange of oxygen atoms between nitrite and water can occur on aerosol surfaces. Even less is known about the exchange rate and influence on the final isotopic composition of nitrate. If (i) nitrite is an important intermediate for nitrate formation via NO_2 uptake and (ii) oxygen-exchanging process is fast relative to the lifetime of aerosols, we may expect a larger influence

on $\Delta^{17}O(NO_3^-)$ from aerosol water; thus, a lower $\Delta^{17}O(NO_3^-$, NO_2 hydrolysis) should be expected.

3.6 IMPLICATIONS AND SUGGESTIONS FOR FUTURE STUDIES

The literature on the heterogeneous reactions of NO_2 demonstrates that the uptake of NO_2 on aerosols is a very complicated process and can proceed via vastly different pathways. Given the current observations, it is still unclear which chemical mechanism for NO_2 uptake actually dominates in the real atmosphere and whether the importance of different mechanisms shift as the aerosol concentration or composition changes. Apart from producing nitrate, NO_2 uptake may also contribute to the daytime production of HONO and the rapid oxidation of SO_2 in extreme haze, which are of great interest to atmospheric chemists who are studying the extreme haze events in wintertime North China and other polluted airmass. The recent progress in understanding the heterogeneous reactions of NO_2 has been made largely through computer simulations (both molecular dynamics simulation and atmospheric simulation) and idealized laboratory experiments. To validate various hypotheses for NO_2 uptake mechanisms proposed in modeling and laboratory studies, the designers of future observation campaigns in polluted regions can consider the following measurements:

(1) Measurements of N_2O_4 in gas phase or aerosol. The detection or lack of detection of N_2O_4 gives hints on the validity of Finlayson-Pitts's mechanism, in which N_2O_4 is the critical intermediate for efficient NO_2 hydrolysis.

(2) Observations of the response of NO_y species to dust aerosols. Metal oxides in dust aerosols are required to explain the heterogeneous reactions of NO_2 in several mechanisms that involve the reaction of surface-groups.

(3) Measurement of phenols, humic acids, and polycyclic aromatic hydrocarbons in intense haze. These complex organic species may become photoactivated under sunlight and efficiently consume the NO_2 in aerosol phase. The same set of measurements will also benefit the studies of organic aerosols.

Chapter 4. CONCLUSION

In this work, we re-interpret the observations of ^{17}O-Excess of nitrate ($\Delta^{17}O(NO_3^-)$) and other chemistry metrics in Beijing using GEOS-Chem, a state-of-the-art 3D chemical transport model. Analysis of stable oxygen isotopes has long been proven to be a promising tool for understanding the chemical origins of nitrate in various environments and recently applied to study air pollution in wintertime North China. Three studies have reported observations of $\Delta^{17}O(NO_3^-)$ in Beijing during winter haze events, but their interpretation of isotopic observations relied on highly simplified representations of reactive-nitrogen chemistry and oxidant concentrations. We use the GEOS-Chem model to perform more comprehensive simulations of wintertime haze events in North China and conduct a series of model experiments to examine how the uncertainties in heterogeneous chemistry affect nitrate production during haze events. Our work provides a comprehensive assessment on how the nitrate production chemistry over North China shifts as haze intensifies.

Our study reveals that the model's current parametrization overestimates the importance of heterogeneous chemistry of NO_2 on aerosols, and the N_2O_5 uptake in aerosols and clouds is likely the dominant nitrate-production pathway in intense haze. We also demonstrate that nitrate production via N_2O_5 uptake is limited by ozone in intense haze, suggesting that the NO_x-VOC-ozone non-linear interactions may explain the persistence of nitrate pollution observed in Beijing during the 2010s and, more recently, during the COVID-19 lockdown period when NO_x emissions declined.

To further understand the uncertainties associated with the uptake of NO_2 on aerosols, we review the literature on the NO_2 uptake and categorize the hypothesized chemical mechanisms into five major groups. We discuss how the uptake rate, the products yield, and their dependence on environmental conditions vary among different mechanisms. Although there are not enough observational constraints for deducing which mechanism is the most important in intense haze in wintertime Beijing, we consider some possibly observable features of different NO_2 uptake mechanisms and provide recommendations for future laboratory studies.

Based on the findings from this project, I recommend the future studies that look into NO_y chemistry in wintertime urban haze to (1) explore the possible sources of VOCs in winter and study how the VOCs mixed with the NO_x-rich air and (2) find observational constraints for NO_2 uptake on soot, SOA, and mineral dust aerosols. As air-pollution mitigation proceeds, NO_x emissions will continue decrease, and VOCs are becoming more important in controlling wintertime production of ozone and nitrate over many cities. However, apart from vehicle emissions and combustions, other sources of VOCs (e.g., volatile chemical products) in winter remain quite uncertain and are usually overlooked in current modeling studies. Better representation of VOCs emissions in chemical transport models will improve the simulation of NO_x-VOC-ozone interactions in urban air, which can lead to better model prediction for ozone and nitrate. While our analysis shows that N_2O_5 hydrolysis is likely a more important source of nitrate in winter, NO_2 uptake on soot, SOA, and mineral dust may explain the missing source of daytime HONO and haze-event sulfate observed in North China and other polluted regions. Current information about NO_2 uptake on soot, SOA, and mineral dust mostly come from

laboratory studies, so field studies that observe how NO_2 (g) interacts with these aerosols in polluted environments will validate a lot of the current hypothesized mechanisms.

BIBLIOGRAPHY

Acton, W. J. F., Huang, Z., Davison, B., Drysdale, W. S., Fu, P., Hollaway, M., et al. (2020). Surface–atmosphere fluxes of volatile organic compounds in Beijing. *Atmospheric Chemistry and Physics*, *20*(23), 15101–15125. https://doi.org/10.5194/acp-20-15101-2020

Alexander, B., Sherwen, T., Holmes, C. D., Fisher, J. A., Chen, Q., Evans, M. J., & Kasibhatla, P. (2020). Global inorganic nitrate production mechanisms: comparison of a global model with nitrate isotope observations. *Atmospheric Chemistry and Physics*, *20*(6), 3859–3877. https://doi.org/10.5194/acp-20-3859-2020

Ammann, M., Kalberer, M., Jost, D. T., Tobler, L., Rössler, E., Piguet, D., et al. (1998). Heterogeneous production of nitrous acid on soot in polluted air masses. *Nature*, *395*(6698), 157–160. https://doi.org/10.1038/25965

Ammann, M., Cox, R. A., Crowley, J. N., Jenkin, M. E., Mellouki, A., Rossi, M. J., et al. (2013). Evaluated kinetic and photochemical data for atmospheric chemistry: Volume VI – heterogeneous reactions with liquid substrates. *Atmospheric Chemistry and Physics*, *13*(16), 8045–8228. https://doi.org/10.5194/acp-13-8045-2013

An, Z., Huang, R.-J., Zhang, R., Tie, X., Li, G., Cao, J., et al. (2019). Severe haze in northern China: A synergy of anthropogenic emissions and atmospheric processes. *Proceedings of the National Academy of Sciences of the United States of America*, *116*(18), 8657–8666. https://doi.org/10.1073/pnas.1900125116

Atkinson, R., Baulch, D. L., Cox, R. A., Crowley, J. N., Hampson, R. F., Hynes, R. G., et al. (2004). Evaluated kinetic and photochemical data for atmospheric chemistry: Volume I - gas phase reactions of O_x, HO_x,

NO_x and SO_x species. *Atmospheric Chemistry and Physics*, *4*(6), 1461–1738. https://doi.org/10.5194/acp-4-1461-2004

Bao, F., Li, M., Zhang, Y., Chen, C., & Zhao, J. (2018). Photochemical Aging of Beijing Urban PM 2.5 : HONO Production. *Environmental Science & Technology*, *52*(11), 6309–6316. https://doi.org/10.1021/acs.est.8b00538

Bates, K. H., & Jacob, D. J. (2020). An Expanded Definition of the Odd Oxygen Family for Tropospheric Ozone Budgets: Implications for Ozone Lifetime and Stratospheric Influence. *Geophysical Research Letters*, *47*(4). https://doi.org/10.1029/2019GL084486

Beaumont, S. K., Gustafsson, R. J., & Lambert, R. M. (2009). Heterogeneous Photochemistry Relevant to the Troposphere: H 2 O 2 Production during the Photochemical Reduction of NO 2 to HONO on UV-Illuminated TiO 2 Surfaces. *ChemPhysChem*, *10*(2), 331–333. https://doi.org/10.1002/cphc.200800613

Bertram, T. H., & Thornton, J. A. (2009). Toward a general parameterization of N2O5 reactivity on aqueous particles: The competing effects of particle liquid water, nitrate and chloride. *Atmospheric Chemistry and Physics*, *9*(21), 8351–8363. https://doi.org/10.5194/acp-9-8351-2009

Bröske, R., Kleffmann, J., & Wiesen, P. (2003). Heterogeneous conversion of NO2 on secondary organic aerosol surfaces: A possible source of nitrous acid (HONO) in the atmosphere? *Atmospheric Chemistry and Physics*, *3*(3), 469–474. https://doi.org/10.5194/acp-3-469-2003

Buchwald, C., & Casciotti, K. L. (2013). Isotopic ratios of nitrite as tracers of the sources and age of oceanic nitrite. *Nature Geoscience*, *6*(4), 308–313. https://doi.org/10.1038/ngeo1745

Casciotti, K. L., Böhlke, J. K., McIlvin, M. R., Mroczkowski, S. J., & Hannon, J. E. (2007). Oxygen Isotopes in Nitrite: Analysis, Calibration, and Equilibration. *Analytical Chemistry*,

79(6), 2427–2436. https://doi.org/10.1021/ac061598h

Chen, H., Nanayakkara, C. E., & Grassian, V. H. (2012). Titanium Dioxide Photocatalysis in Atmospheric Chemistry. *Chemical Reviews*, *112*(11), 5919–5948. https://doi.org/10.1021/cr3002092

Chen, S., Wang, H., Lu, K., Zeng, L., Hu, M., & Zhang, Y. (2020). The trend of surface ozone in Beijing from 2013 to 2019: Indications of the persisting strong atmospheric oxidation capacity. *Atmospheric Environment*, *242*, 117801. https://doi.org/10.1016/j.atmosenv.2020.117801

Chen, Y., Ebenstein, A., Greenstone, M., & Li, H. (2013). Evidence on the impact of sustained exposure to air pollution on life expectancy from China's Huai River policy. *Proceedings of the National Academy of Sciences of the United States of America*, *110*(32), 12936–12941. https://doi.org/10.1073/pnas.1300018110

Chughtai, A. R., Welch, W. F., Akhter, M. S., & Smith, D. M. (1990). A Spectroscopic Study of Gaseous Products of Soot-Oxides of Nitrogen/Water Reactions. *Applied Spectroscopy*, *44*(2), 294–298. https://doi.org/10.1366/0003702904085598

Crowley, J. N., Ammann, M., Cox, R. A., Hynes, R. G., Jenkin, M. E., Mellouki, A., et al. (2010). Evaluated kinetic and photochemical data for atmospheric chemistry: Volume v - heterogeneous reactions on solid substrates. *Atmospheric Chemistry and Physics*, *10*(18), 9059–9223. https://doi.org/10.5194/acp-10-9059-2010

Diamond, M. S., & Wood, R. (2020). Limited Regional Aerosol and Cloud Microphysical Changes Despite Unprecedented Decline in Nitrogen Oxide Pollution During the February 2020 COVID-19 Shutdown in China. *Geophysical Research Letters*, *47*(17). https://doi.org/10.1029/2020GL088913

Ding, J., Zhao, P., Su, J., Dong, Q., Du, X., & Zhang, Y. (2019). Aerosol pH and its driving factors in Beijing. *Atmospheric Chemistry and Physics*, *19*(12), 7939–7954. https://doi.org/10.5194/acp-19-7939-2019

Eastham, S. D., Weisenstein, D. K., & Barrett, S. R. H. (2014). Development and evaluation of the unified tropospheric–stratospheric chemistry extension (UCX) for the global chemistry-transport model GEOS-Chem. *Atmospheric Environment*, *89*, 52–63. https://doi.org/10.1016/j.atmosenv.2014.02.001

Finlayson-Pitts, B. J., Wingen, L. M., Sumner, A. L., Syomin, D., & Ramazan, K. A. (2003). The heterogeneous hydrolysis of NO2 in laboratory systems and in outdoor and indoor atmospheres: An integrated mechanism. *Physical Chemistry Chemical Physics*, *5*(2), 223–242. https://doi.org/10.1039/b208564j

Finlayson-Pitts, Barbara J. (2009, September 2). Reactions at surfaces in the atmosphere: Integration of experiments and theory as necessary (but not necessarily sufficient) for predicting the physical chemistry of aerosols. *Physical Chemistry Chemical Physics*. Abadleh. https://doi.org/10.1039/b906540g

Fisher, J. A., Atlas, E. L., Barletta, B., Meinardi, S., Blake, D. R., Thompson, C. R., et al. (2018). Methyl, Ethyl, and Propyl Nitrates: Global Distribution and Impacts on Reactive Nitrogen in Remote Marine Environments. *Journal of Geophysical Research: Atmospheres*, *123*(21), 12,429-12,451. https://doi.org/10.1029/2018JD029046

Fountoukis, C., & Nenes, A. (2007). *Atmospheric Chemistry and Physics ISORROPIA II: a computationally efficient thermodynamic equilibrium model for K +-Ca 2+-Mg 2+-NH + 4-Na +-SO 2− 4-NO − 3-Cl −-H 2 O aerosols*. *Atmos. Chem. Phys* (Vol. 7). Retrieved from www.atmos-chem-phys.net/7/4639/2007/

Fu, X., Wang, T., Zhang, L., Li, Q., Wang, Z., Xia, M., et al. (2019). The significant contribution of HONO to secondary pollutants during a severe winter pollution event in southern China. *Atmospheric Chemistry and Physics*, *19*(1), 1–14. https://doi.org/10.5194/acp-19-1-2019

Fu, X., Wang, T., Gao, J., Wang, P., Liu, Y., Wang, S., et al. (2020). Persistent Heavy Winter Nitrate Pollution Driven by Increased Photochemical Oxidants in Northern China. *Environmental Science and Technology*, *54*(7), 3881–3889. https://doi.org/10.1021/acs.est.9b07248

Gaston, C. J., Thornton, J. A., & Ng, N. L. (2014). Reactive uptake of N $_2$ O $_5$ to internally mixed inorganic and organic particles: the role of organic carbon oxidation state and inferred organic phase separations. *Atmospheric Chemistry and Physics*, *14*(11), 5693–5707. https://doi.org/10.5194/acp-14-5693-2014

Gen, M., Zhang, R., Huang, D. D., Li, Y., & Chan, C. K. (2019). Heterogeneous SO 2 Oxidation in Sulfate Formation by Photolysis of Particulate Nitrate. *Environmental Science & Technology Letters*, *6*(2), 86–91. https://doi.org/10.1021/acs.estlett.8b00681

Geng, L., Murray, L. T., Mickley, L. J., Lin, P., Fu, Q., Schauer, A. J., & Alexander, B. (2017). Isotopic evidence of multiple controls on atmospheric oxidants over climate transitions. *Nature*, *546*(7656), 133–136. https://doi.org/10.1038/nature22340

George, C., Strekowski, R. S., Kleffmann, J., Stemmler, K., & Ammann, M. (2005). Photoenhanced uptake of gaseous NO2 on solid organic compounds: A photochemical source of HONO? In *Faraday Discussions* (Vol. 130, pp. 195–210). The Royal Society of Chemistry. https://doi.org/10.1039/b417888m

Gerecke, A., Thielmann, A., Gutzwiller, L., & Rossi, M. J. (1998). The chemical kinetics of HONO formation resulting from heterogeneous interaction of NO 2 with flame soot.

Geophysical Research Letters, *25*(13), 2453–2456. https://doi.org/10.1029/98GL01796

Guo, J., Wang, Z., Tao Wang, & Zhang, X. (2019). Theoretical evaluation of different factors affecting the HO2 uptake coefficient driven by aqueous-phase first-order loss reaction. *Science of The Total Environment*, *683*, 146–153. https://doi.org/10.1016/j.scitotenv.2019.05.237

Gustafsson, R. J., Orlov, A., Griffiths, P. T., Cox, R. A., & Lambert, R. M. (2006). Reduction of NO2 to nitrous acid on illuminated titanium dioxide aerosol surfaces: implications for photocatalysis and atmospheric chemistry. *Chemical Communications*, (37), 3936. https://doi.org/10.1039/b609005b

Gustafsson, R. J., Kyriakou, G., & Lambert, R. M. (2008). The molecular mechanism of tropospheric nitrous acid production on mineral dust surfaces. *ChemPhysChem*, *9*(10), 1390–1393. https://doi.org/10.1002/cphc.200800259

Haskins, J. D., Lopez-Hilfiker, F. D., Lee, B. H., Shah, V., Wolfe, G. M., DiGangi, J., et al. (2019). Anthropogenic Control Over Wintertime Oxidation of Atmospheric Pollutants. *Geophysical Research Letters*, *46*(24), 14826–14835. https://doi.org/10.1029/2019GL085498

He, P., Xie, Z., Chi, X., Yu, X., Fan, S., Kang, H., et al. (2018). Atmospheric Δ 17 O(NO 3 −) reveals nocturnal chemistry dominates nitrate production in Beijing haze. *Atmospheric Chemistry and Physics*, *18*(19), 14465–14476. https://doi.org/10.5194/acp-18-14465-2018

He, P., Xie, Z., Yu, X., Wang, L., Kang, H., & Yue, F. (2020). The observation of isotopic compositions of atmospheric nitrate in Shanghai China and its implication for reactive nitrogen chemistry. *Science of the Total Environment*, *714*, 136727. https://doi.org/10.1016/j.scitotenv.2020.136727

Hoesly, R. M., Smith, S. J., Feng, L., Klimont, Z., Janssens-Maenhout, G., Pitkanen, T., et al. (2018). Historical (1750–2014) anthropogenic emissions of reactive gases and aerosols from the Community Emissions Data System (CEDS). *Geoscientific Model Development*, *11*(1), 369–408. https://doi.org/10.5194/gmd-11-369-2018

Hoffmann, E. H., Tilgner, A., Vogelsberg, U., Wolke, R., & Herrmann, H. (2019). Near-Explicit Multiphase Modeling of Halogen Chemistry in a Mixed Urban and Maritime Coastal Area. *ACS Earth and Space Chemistry*, *3*(11), 2452–2471. https://doi.org/10.1021/acsearthspacechem.9b00184

Hollaway, M., Wild, O., Yang, T., Sun, Y., Xu, W., Xie, C., et al. (2019). Photochemical impacts of haze pollution in an urban environment. *Atmospheric Chemistry and Physics*, *19*(15), 9699–9714. https://doi.org/10.5194/acp-19-9699-2019

Holmes, C. D., Bertram, T. H., Confer, K. L., Graham, K. A., Ronan, A. C., Wirks, C. K., & Shah, V. (2019). The Role of Clouds in the Tropospheric NOx Cycle: A New Modeling Approach for Cloud Chemistry and Its Global Implications. *Geophysical Research Letters*, *46*(9), 4980–4990. https://doi.org/10.1029/2019GL081990

Huang, X., Ding, A., Gao, J., Zheng, B., Zhou, D., Qi, X., et al. (2020). Enhanced secondary pollution offset reduction of primary emissions during COVID-19 lockdown in China. *National Science Review*. https://doi.org/10.1093/nsr/nwaa137

Hudman, R. C., Moore, N. E., Mebust, A. K., Martin, R. V, Russell, A. R., Valin, L. C., & Cohen, R. C. (2012). Steps towards a mechanistic model of global soil nitric oxide emissions: implementation and space based-constraints. *Atmospheric Chemistry and Physics*, *12*(16), 7779–7795. https://doi.org/10.5194/acp-12-7779-2012

Itahashi, S., Yumimoto, K., Uno, I., Hayami, H., Fujita, S., Pan, Y., & Wang, Y. (2018). A 15-

year record (2001–2015) of the ratio of nitrate to non-sea-salt sulfate in precipitation over East Asia. *Atmospheric Chemistry and Physics*, *18*(4), 2835–2852. https://doi.org/10.5194/acp-18-2835-2018

Jaeglé, L., Shah, V., Thornton, J. A., Lopez-Hilfiker, F. D., Lee, B. H., McDuffie, E. E., et al. (2018). Nitrogen Oxides Emissions, Chemistry, Deposition, and Export Over the Northeast United States During the WINTER Aircraft Campaign. *Journal of Geophysical Research: Atmospheres*, *123*(21), 12,368-12,393. https://doi.org/10.1029/2018JD029133

Kalberer, M., Ammann, M., Arens, F., Gäggeler, H. W., & Baltensperger, U. (1999). Heterogeneous formation of nitrous acid (HONO) on soot aerosol particles. *Journal of Geophysical Research: Atmospheres*, *104*(D11), 13825–13832. https://doi.org/10.1029/1999JD900141

Kasibhatla, P., Sherwen, T., Evans, M. J., Carpenter, L. J., Reed, C., Alexander, B., et al. (2018). Global impact of nitrate photolysis in sea-salt aerosol on NOx, OH, and O3 in the marine boundary layer. *Atmospheric Chemistry and Physics*, *18*(15), 11185–11203. https://doi.org/10.5194/acp-18-11185-2018

Kebede, M. A., Bish, D. L., Losovyj, Y., Engelhard, M. H., & Raff, J. D. (2016). The Role of Iron-Bearing Minerals in NO2 to HONO Conversion on Soil Surfaces. *Environmental Science and Technology*, *50*(16), 8649–8660. https://doi.org/10.1021/acs.est.6b01915

Kenagy, H. S., Sparks, T. L., Ebben, C. J., Wooldrige, P. J., Lopez-Hilfiker, F. D., Lee, B. H., et al. (2018). NO x Lifetime and NO y Partitioning During WINTER. *Journal of Geophysical Research: Atmospheres*, *123*(17), 9813–9827. https://doi.org/10.1029/2018JD028736

Kim, S.-K., & Kang, H. (2010). Efficient Conversion of Nitrogen Dioxide into Nitrous Acid on Ice Surfaces. *The Journal of Physical Chemistry Letters*, *1*(20), 3085–3089.

https://doi.org/10.1021/jz1011669

Kleffmann, J., Becker, K. H., Lackhoff, M., & Wiesen, P. (1999). Heterogeneous conversion of NO2 on carbonaceous surfaces. *Physical Chemistry Chemical Physics*, *1*(24), 5443–5450. https://doi.org/10.1039/a905545b

Lamsal, L. N., Martin, R. V., van Donkelaar, A., Steinbacher, M., Celarier, E. A., Bucsela, E., et al. (2008). Ground-level nitrogen dioxide concentrations inferred from the satellite-borne Ozone Monitoring Instrument. *Journal of Geophysical Research*, *113*(D16), D16308. https://doi.org/10.1029/2007JD009235

Langridge, J. M., Gustafsson, R. J., Griffiths, P. T., Cox, R. A., Lambert, R. M., & Jones, R. L. (2009). Solar driven nitrous acid formation on building material surfaces containing titanium dioxide: A concern for air quality in urban areas? *Atmospheric Environment*, *43*(32), 5128–5131. https://doi.org/10.1016/j.atmosenv.2009.06.046

Le, T., Wang, Y., Liu, L., Yang, J., Yung, Y. L., Li, G., & Seinfeld, J. H. (2020). Unexpected air pollution with marked emission reductions during the COVID-19 outbreak in China. *Science*, *369*(6504), 702–706. https://doi.org/10.1126/science.abb7431

Lelieveld, J., Evans, J. S., Fnais, M., Giannadaki, D., & Pozzer, A. (2015). The contribution of outdoor air pollution sources to premature mortality on a global scale. *Nature*, *525*(7569), 367–371. https://doi.org/10.1038/nature15371

Leung, D. M., Shi, H., Zhao, B., Wang, J., Ding, E. M., Gu, Y., et al. (2020). Wintertime Particulate Matter Decrease Buffered by Unfavorable Chemical Processes Despite Emissions Reductions in China. *Geophysical Research Letters*, *47*(14). https://doi.org/10.1029/2020GL087721

Li, D., Xue, L., Wen, L., Wang, X., Chen, T., Mellouki, A., et al. (2018). Characteristics and

sources of nitrous acid in an urban atmosphere of northern China: Results from 1-yr continuous observations. *Atmospheric Environment*, *182*, 296–306. https://doi.org/10.1016/J.ATMOSENV.2018.03.033

Li, H., Cheng, J., Zhang, Q., Zheng, B., Zhang, Y., Zheng, G., & He, K. (2019). Rapid transition in winter aerosol composition in Beijing from 2014 to 2017: response to clean air actions. *Atmospheric Chemistry and Physics*, *19*(17), 11485–11499. https://doi.org/10.5194/acp-19-11485-2019

Li, H. J., Zhu, T., Zhao, D. F., Zhang, Z. F., & Chen, Z. M. (2010). Kinetics and mechanisms of heterogeneous reaction of NO₂ on CaCO₃ surfaces under dry and wet conditions. *Atmospheric Chemistry and Physics*, *10*(2), 463–474. https://doi.org/10.5194/acp-10-463-2010

Li, J., Xie, S. D., Zeng, L. M., Li, L. Y., Li, Y. Q., & Wu, R. R. (2015). Characterization of ambient volatile organic compounds and their sources in Beijing, before, during, and after Asia-Pacific Economic Cooperation China 2014. *Atmospheric Chemistry and Physics*, *15*(14), 7945–7959. https://doi.org/10.5194/acp-15-7945-2015

Li, Jie, Chen, X., Wang, Z., Du, H., Yang, W., Sun, Y., et al. (2018). Radiative and heterogeneous chemical effects of aerosols on ozone and inorganic aerosols over East Asia. *Science of the Total Environment*, *622–623*, 1327–1342. https://doi.org/10.1016/j.scitotenv.2017.12.041

Li, Ke, Jacob, D. J., Liao, H., Zhu, J., Shah, V., Shen, L., et al. (2019). A two-pollutant strategy for improving ozone and particulate air quality in China. *Nature Geoscience*, *12*(11), 906–910. https://doi.org/10.1038/s41561-019-0464-x

Li, Ke, Jacob, D. J., Liao, H., Shen, L., Zhang, Q., & Bates, K. H. (2019). Anthropogenic drivers of 2013-2017 trends in summer surface ozone in China. *Proceedings of the National Academy of Sciences of the United States of America*, *116*(2), 422–427. https://doi.org/10.1073/pnas.1812168116

Li, Kun, Li, J., Tong, S., Wang, W., Huang, R.-J., & Ge, M. (2019). Characteristics of wintertime VOCs in suburban and urban Beijing: concentrations, emission ratios, and festival effects. *Atmospheric Chemistry and Physics*, *19*(12), 8021–8036. https://doi.org/10.5194/acp-19-8021-2019

Li, L., Hoffmann, M. R., & Colussi, A. J. (2018). Role of Nitrogen Dioxide in the Production of Sulfate during Chinese Haze-Aerosol Episodes. *Environmental Science & Technology*, *52*(5), 2686–2693. https://doi.org/10.1021/acs.est.7b05222

Li, M., Zhang, Q., Kurokawa, J., Woo, J.-H., He, K., Lu, Z., et al. (2017). MIX: a mosaic Asian anthropogenic emission inventory under the international collaboration framework of the MICS-Asia and HTAP. *Atmospheric Chemistry and Physics*, *17*(2), 935–963. https://doi.org/10.5194/acp-17-935-2017

Li, Q., Badia, A., Wang, T., Sarwar, G., Fu, X., Zhang, L., et al. (2020). Potential Effect of Halogens on Atmospheric Oxidation and Air Quality in China. *Journal of Geophysical Research: Atmospheres*, *125*(9). https://doi.org/10.1029/2019JD032058

Li, R., Jia, X., Wang, F., Ren, Y., Wang, X., Zhang, H., et al. (2020). Heterogeneous reaction of NO2 with hematite, goethite and magnetite: Implications for nitrate formation and iron solubility enhancement. *Chemosphere*, *242*, 125273. https://doi.org/10.1016/j.chemosphere.2019.125273

Lin, J. T., & McElroy, M. B. (2010). Impacts of boundary layer mixing on pollutant vertical

profiles in the lower troposphere: Implications to satellite remote sensing. *Atmospheric Environment*, *44*(14), 1726–1739. https://doi.org/10.1016/j.atmosenv.2010.02.009

Liu, Chang, Ma, Q., Liu, Y., Ma, J., & He, H. (2012). Synergistic reaction between SO2 and NO2 on mineral oxides: a potential formation pathway of sulfate aerosol. *Phys. Chem. Chem. Phys.*, *14*(5), 1668–1676. https://doi.org/10.1039/C1CP22217A

Liu, Chang, Ma, Q., He, H., He, G., Ma, J., Liu, Y., & Wu, Y. (2017). Structure-activity relationship of surface hydroxyl groups during NO2 adsorption and transformation on TiO2 nanoparticles. *Environmental Science: Nano*, *4*(12), 2388–2394. https://doi.org/10.1039/c7en00920h

Liu, Chengtang, Ma, Z., Mu, Y., Liu, J., Zhang, C., Zhang, Y., et al. (2017). The levels, variation characteristics, and sources of atmospheric non-methane hydrocarbon compounds during wintertime in Beijing, China. *Atmospheric Chemistry and Physics*, *17*(17), 10633–10649. https://doi.org/10.5194/acp-17-10633-2017

Liu, H., Jacob, D. J., Bey, I., & Yantosca, R. M. (2001). Constraints from 210 Pb and 7 Be on wet deposition and transport in a global three-dimensional chemical tracer model driven by assimilated meteorological fields. *Journal of Geophysical Research: Atmospheres*, *106*(D11), 12109–12128. https://doi.org/10.1029/2000JD900839

Liu, P., Ye, C., Xue, C., Zhang, C., Mu, Y., & Sun, X. (2020). Formation mechanisms of atmospheric nitrate and sulfate during the winter haze pollution periods in Beijing: gas-phase, heterogeneous and aqueous-phase chemistry. *Atmospheric Chemistry and Physics*, *20*(7), 4153–4165. https://doi.org/10.5194/acp-20-4153-2020

Liu, Yongchun, Han, C., Ma, J., Bao, X., & He, H. (2015). Influence of relative humidity on heterogeneous kinetics of NO2 on kaolin and hematite. *Physical Chemistry Chemical*

Physics, *17*(29), 19424–19431. https://doi.org/10.1039/c5cp02223a

Liu, Yuhan, Lu, K., Li, X., Dong, H., Tan, Z., Wang, H., et al. (2019). A Comprehensive Model Test of the HONO Sources Constrained to Field Measurements at Rural North China Plain. *Environmental Science & Technology*, *53*(7), 3517–3525. https://doi.org/10.1021/acs.est.8b06367

Lu, K., Fuchs, H., Hofzumahaus, A., Tan, Z., Wang, H., Zhang, L., et al. (2019). Fast Photochemistry in Wintertime Haze: Consequences for Pollution Mitigation Strategies. *Environmental Science & Technology*, *53*(18), 10676–10684. https://doi.org/10.1021/acs.est.9b02422

Ma, Q., Wang, T., Liu, C., He, H., Wang, Z., Wang, W., & Liang, Y. (2017). SO 2 Initiates the Efficient Conversion of NO 2 to HONO on MgO Surface. *Environmental Science & Technology*, *51*(7), 3767–3775. https://doi.org/10.1021/acs.est.6b05724

Mao, J., Fan, S., Jacob, D. J., & Travis, K. R. (2013). Radical loss in the atmosphere from Cu-Fe redox coupling in aerosols. *Atmospheric Chemistry and Physics*, *13*(2), 509–519. https://doi.org/10.5194/acp-13-509-2013

Marais, E. A., & Wiedinmyer, C. (2016). Air Quality Impact of Diffuse and Inefficient Combustion Emissions in Africa (DICE-Africa). *Environmental Science & Technology*, *50*(19), 10739–10745. https://doi.org/10.1021/acs.est.6b02602

McCulloch, A., Aucott, M. L., Benkovitz, C. M., Graedel, T. E., Kleiman, G., Midgley, P. M., & Li, Y.-F. (1999). Global emissions of hydrogen chloride and chloromethane from coal combustion, incineration and industrial activities: Reactive Chlorine Emissions Inventory. *Journal of Geophysical Research: Atmospheres*, *104*(D7), 8391–8403. https://doi.org/10.1029/1999JD900025

McDonald, B. C., De Gouw, J. A., Gilman, J. B., Jathar, S. H., Akherati, A., Cappa, C. D., et al. (2018). Volatile chemical products emerging as largest petrochemical source of urban organic emissions. *Science*, *359*(6377), 760–764. https://doi.org/10.1126/science.aaq0524

McDuffie, E. E., Fibiger, D. L., Dubé, W. P., Lopez-Hilfiker, F., Lee, B. H., Thornton, J. A., et al. (2018). Heterogeneous N2O5 Uptake During Winter: Aircraft Measurements During the 2015 WINTER Campaign and Critical Evaluation of Current Parameterizations. *Journal of Geophysical Research: Atmospheres*, *123*(8), 4345–4372. https://doi.org/10.1002/2018JD028336

Michalski, G., Scott, Z., Kabiling, M., & Thiemens, M. H. (2003). First measurements and modeling of Δ 17 O in atmospheric nitrate. *Geophysical Research Letters*, *30*(16). https://doi.org/10.1029/2003GL017015

Miller, Y., Finlayson-Pitts, B. J., & Gerber, R. B. (2009). Ionization of N2O4 in contact with water: Mechanism, time scales and atmospheric implications. *Journal of the American Chemical Society*, *131*(34), 12180–12185. https://doi.org/10.1021/ja900350g

Monge, M. E., D'Anna, B., Mazri, L., Giroir-Fendler, A., Ammann, M., Donaldson, D. J., & George, C. (2010). Light changes the atmospheric reactivity of soot. *Proceedings of the National Academy of Sciences*, *107*(15), 6605–6609. https://doi.org/10.1073/pnas.0908341107

Morin, S., Sander, R., & Savarino, J. (2011). Simulation of the diurnal variations of the oxygen isotope anomaly (Δ17O) of reactive atmospheric species. *Atmospheric Chemistry and Physics*, *11*(8), 3653–3671. https://doi.org/10.5194/acp-11-3653-2011

Murray, L. T., Jacob, D. J., Logan, J. A., Hudman, R. C., & Koshak, W. J. (2012). Optimized regional and interannual variability of lightning in a global chemical transport model

constrained by LIS/OTD satellite data. *Journal of Geophysical Research: Atmospheres*, *117*(D20). https://doi.org/10.1029/2012JD017934

Ndour, M., D'Anna, B., George, C., Ka, O., Balkanski, Y., Kleffmann, J., et al. (2008). Photoenhanced uptake of NO 2 on mineral dust: Laboratory experiments and model simulations. *Geophysical Research Letters*, *35*(5), L05812. https://doi.org/10.1029/2007GL032006

Neu, J. L., Prather, M. J., & Penner, J. E. (2007). Global atmospheric chemistry: Integrating over fractional cloud cover. *Journal of Geophysical Research*, *112*(D11), D11306. https://doi.org/10.1029/2006JD008007

Ramazan, K. A., Syomin, D., & Finlayson-Pitts, B. J. (2004). The photochemical production of HONO during the heterogeneous hydrolysis of NO2. *Physical Chemistry Chemical Physics*, *6*(14), 3836. https://doi.org/10.1039/b402195a

Reed, C., Evans, M. J., Di Carlo, P., Lee, J. D., & Carpenter, L. J. (2016). Interferences in photolytic NO₂ measurements: explanation for an apparent missing oxidant? *Atmospheric Chemistry and Physics*, *16*(7), 4707–4724. https://doi.org/10.5194/acp-16-4707-2016

Romer, P. S., Wooldridge, P. J., Crounse, J. D., Kim, M. J., Wennberg, P. O., Dibb, J. E., et al. (2018). Constraints on Aerosol Nitrate Photolysis as a Potential Source of HONO and NO x. *Environmental Science & Technology*, *52*(23), 13738–13746. https://doi.org/10.1021/acs.est.8b03861

Sakamaki, F., Hatakeyama, S., & Akimoto, H. (1983). Formation of nitrous acid and nitric oxide in the heterogeneous dark reaction of nitrogen dioxide and water vapor in a smog chamber. *International Journal of Chemical Kinetics*, *15*(10), 1013–1029.

https://doi.org/10.1002/kin.550151006

Sander, R. (2015). Compilation of Henry's law constants (version 4.0) for water as solvent. *Atmospheric Chemistry and Physics*, *15*(8), 4399–4981. https://doi.org/10.5194/acp-15-4399-2015

Savarino, J., Morin, S., Erbland, J., Grannec, F., Patey, M. D., Vicars, W., et al. (2013). Isotopic composition of atmospheric nitrate in a tropical marine boundary layer. *Proceedings of the National Academy of Sciences*, *110*(44), 17668–17673. https://doi.org/10.1073/pnas.1216639110

Shah, V., Jaeglé, L., Thornton, J. A., Lopez-Hilfiker, F. D., Lee, B. H., Schroder, J. C., et al. (2018). Chemical feedbacks weaken the wintertime response of particulate sulfate and nitrate to emissions reductions over the eastern United States. *Proceedings of the National Academy of Sciences of the United States of America*, *115*(32), 8110–8115. https://doi.org/10.1073/pnas.1803295115

Shah, V., Jacob, D. J., Li, K., Silvern, R. F., Zhai, S., Liu, M., et al. (2020). Effect of changing NOx lifetime on the seasonality and long-term trends of satellite-observed tropospheric NO2 columns over China. *Atmospheric Chemistry and Physics*, *20*(3), 1483–1495. https://doi.org/10.5194/acp-20-1483-2020

Shao, J., Chen, Q., Wang, Y., Lu, X., He, P., Sun, Y., et al. (2019). Heterogeneous sulfate aerosol formation mechanisms during wintertime Chinese haze events: air quality model assessment using observations of sulfate oxygen isotopes in Beijing. *Atmospheric Chemistry and Physics*, *19*(9), 6107–6123. https://doi.org/10.5194/acp-19-6107-2019

Sheng, J., Zhao, D., Ding, D., Li, X., Huang, M., Gao, Y., et al. (2018). Characterizing the level, photochemical reactivity, emission, and source contribution of the volatile organic

compounds based on PTR-TOF-MS during winter haze period in Beijing, China. *Atmospheric Research*, *212*, 54–63. https://doi.org/10.1016/j.atmosres.2018.05.005

Sherwen, T., Evans, M. J., Sommariva, R., Hollis, L. D. J., Ball, S. M., Monks, P. S., et al. (2017). Effects of halogens on European air-quality. *Faraday Discussions*, *200*, 75–100. https://doi.org/10.1039/C7FD00026J

Shi, G., Xu, J., Shi, X., Liu, B., Bi, X., Xiao, Z., et al. (2019). Aerosol pH Dynamics During Haze Periods in an Urban Environment in China: Use of Detailed, Hourly, Speciated Observations to Study the Role of Ammonia Availability and Secondary Aerosol Formation and Urban Environment. *Journal of Geophysical Research: Atmospheres*, *124*(16), 9730–9742. https://doi.org/10.1029/2018JD029976

Shi, Y., Hu, F., Xiao, Z., Fan, G., & Zhang, Z. (2020). Comparison of four different types of planetary boundary layer heights during a haze episode in Beijing. *Science of the Total Environment*, *711*, 134928. https://doi.org/10.1016/j.scitotenv.2019.134928

Song, C., He, J., Wu, L., Jin, T., Chen, X., Li, R., et al. (2017). Health burden attributable to ambient PM2.5 in China. *Environmental Pollution*, *223*, 575–586. https://doi.org/10.1016/J.ENVPOL.2017.01.060

Song, W., Liu, X.-Y., Wang, Y.-L., Tong, Y.-D., Bai, Z.-P., & Liu, C.-Q. (2020). Nitrogen isotope differences between atmospheric nitrate and corresponding nitrogen oxides: A new constraint using oxygen isotopes. *Science of The Total Environment*, *701*, 134515. https://doi.org/10.1016/j.scitotenv.2019.134515

Stemmler, K., Ammann, M., Donders, C., Kleffmann, J., & George, C. (2006). Photosensitized reduction of nitrogen dioxide on humic acid as a source of nitrous acid. *Nature*, *440*(7081), 195–198. https://doi.org/10.1038/nature04603

Su, T., Li, Z., & Kahn, R. (2018). Relationships between the planetary boundary layer height and surface pollutants derived from lidar observations over China: regional pattern and influencing factors. *Atmospheric Chemistry and Physics*, *18*(21), 15921–15935. https://doi.org/10.5194/acp-18-15921-2018

Sun, J., Wang, Y., Wu, F., Tang, G., Wang, L., Wang, Y., & Yang, Y. (2018). Vertical characteristics of VOCs in the lower troposphere over the North China Plain during pollution periods. *Environmental Pollution*, *236*, 907–915. https://doi.org/10.1016/j.envpol.2017.10.051

Sun, Y., Lei, L., Zhou, W., Chen, C., He, Y., Sun, J., et al. (2020). A chemical cocktail during the COVID-19 outbreak in Beijing, China: Insights from six-year aerosol particle composition measurements during the Chinese New Year holiday. *Science of the Total Environment*, *742*, 140739. https://doi.org/10.1016/j.scitotenv.2020.140739

Svensson, R., Ljungström, E., & Lindqvist, O. (1987). Kinetics of the reaction between nitrogen dioxide and water vapour. *Atmospheric Environment (1967)*, *21*(7), 1529–1539. https://doi.org/10.1016/0004-6981(87)90315-5

Tan, F., Tong, S., Jing, B., Hou, S., Liu, Q., Li, K., et al. (2016). Heterogeneous reactions of NO 2 with CaCO 3 –(NH 4) 2 SO 4 mixtures at different relative humidities. *Atmospheric Chemistry and Physics*, *16*(13), 8081–8093. https://doi.org/10.5194/acp-16-8081-2016

Tan, F., Jing, B., Tong, S., & Ge, M. (2017). The effects of coexisting Na2SO4 on heterogeneous uptake of NO2 on CaCO3 particles at various RHs. *Science of the Total Environment*, *586*, 930–938. https://doi.org/10.1016/j.scitotenv.2017.02.072

Tan, Z., Lu, K., Jiang, M., Su, R., Wang, H., Lou, S., et al. (2019). Daytime atmospheric oxidation capacity in four Chinese megacities during the photochemically polluted season: a

case study based on box model simulation. *Atmospheric Chemistry and Physics*, *19*(6), 3493–3513. https://doi.org/10.5194/acp-19-3493-2019

Tang, G., Zhang, J., Zhu, X., Song, T., Münkel, C., Hu, B., et al. (2016). Mixing layer height and its implications for air pollution over Beijing, China. *Atmospheric Chemistry and Physics*, *16*(4), 2459–2475. https://doi.org/10.5194/acp-16-2459-2016

Tham, Y. J., Wang, Z., Li, Q., Yun, H., Wang, W., Wang, X., et al. (2016). Significant concentrations of nitryl chloride sustained in the morning: investigations of the causes and impacts on ozone production in a polluted region of northern China. *Atmospheric Chemistry and Physics*, *16*(23), 14959–14977. https://doi.org/10.5194/acp-16-14959-2016

Thornton, J., & Abbatt, J. P. D. (2005). Measurements of HO 2 uptake to aqueous aerosol: Mass accommodation coefficients and net reactive loss. *Journal of Geophysical Research*, *110*(D8), D08309. https://doi.org/10.1029/2004JD005402

Underwood, G. M., Song, C. H., Phadnis, M., Carmichael, G. R., & Grassian, V. H. (2001). Heterogeneous reactions of NO 2 and HNO 3 on oxides and mineral dust: A combined laboratory and modeling study. *Journal of Geophysical Research: Atmospheres*, *106*(D16), 18055–18066. https://doi.org/10.1029/2000JD900552

Vicars, W. C., & Savarino, J. (2014). Quantitative constraints on the 17O-excess (Δ17O) signature of surface ozone: Ambient measurements from 50°N to 50°S using the nitrite-coated filter technique. *Geochimica et Cosmochimica Acta*, *135*, 270–287. https://doi.org/10.1016/j.gca.2014.03.023

Wang, Jiaqi, Zhang, X., Guo, J., Wang, Z., & Zhang, M. (2017). Observation of nitrous acid (HONO) in Beijing, China: Seasonal variation, nocturnal formation and daytime budget. *Science of The Total Environment*, *587–588*, 350–359.

https://doi.org/10.1016/j.scitotenv.2017.02.159

Wang, Junfeng, Li, J., Ye, J., Zhao, J., Wu, Y., Hu, J., et al. (2020). Fast sulfate formation from oxidation of SO2 by NO2 and HONO observed in Beijing haze. *Nature Communications*, *11*(1), 2844. https://doi.org/10.1038/s41467-020-16683-x

Wang, W., Li, X., Shao, M., Hu, M., Zeng, L., Wu, Y., & Tan, T. (2019). The impact of aerosols on photolysis frequencies and ozone production in Beijing during the 4-year period 2012–2015. *Atmospheric Chemistry and Physics*, *19*(14), 9413–9429. https://doi.org/10.5194/acp-19-9413-2019

Wang, X., Jacob, D. J., Eastham, S. D., Sulprizio, M. P., Zhu, L., Chen, Q., et al. (2019). The role of chlorine in global tropospheric chemistry. *Atmospheric Chemistry and Physics*, *19*(6), 3981–4003. https://doi.org/10.5194/acp-19-3981-2019

Wang, X., Jacob, D. J., Fu, X., Wang, T., Le Breton, M., Hallquist, M., et al. (2020). Effects of anthropogenic chlorine on PM 2.5 and ozone air quality in China. *Environmental Science & Technology*, acs.est.0c02296. https://doi.org/10.1021/acs.est.0c02296

Wang, Yan-Li, Song, W., Yang, W., Sun, X., Tong, Y., Wang, X., et al. (2019). Influences of Atmospheric Pollution on the Contributions of Major Oxidation Pathways to PM 2.5 Nitrate Formation in Beijing. *Journal of Geophysical Research: Atmospheres*, *124*(7), 4174–4185. https://doi.org/10.1029/2019JD030284

Wang, Yuhang, Jacob, D. J., & Logan, J. A. (1998). Global simulation of tropospheric O3-NOx-hydrocarbon chemistry: 1. Model formulation. *Journal of Geophysical Research: Atmospheres*, *103*(D9), 10713–10725. https://doi.org/10.1029/98JD00158

van der Werf, G. R., Randerson, J. T., Giglio, L., van Leeuwen, T. T., Chen, Y., Rogers, B. M., et al. (2017). Global fire emissions estimates during 1997–2016. *Earth System Science*

Data, *9*(2), 697–720. https://doi.org/10.5194/essd-9-697-2017

Womack, C. C., McDuffie, E. E., Edwards, P. M., Bares, R., Gouw, J. A., Docherty, K. S., et al. (2019). An Odd Oxygen Framework for Wintertime Ammonium Nitrate Aerosol Pollution in Urban Areas: NOx and VOC Control as Mitigation Strategies. *Geophysical Research Letters*, *46*(9), 4971–4979. https://doi.org/10.1029/2019GL082028

Xia, M., Wang, W., Wang, Z., Gao, J., Li, H., Liang, Y., et al. (2019). Heterogeneous uptake of N2O5 in sand dust and urban aerosols observed during the dry season in Beijing. *Atmosphere*, *10*(4), 204. https://doi.org/10.3390/ATMOS10040204

Xiang, Y., Zhang, T., Liu, J., Lv, L., Dong, Y., & Chen, Z. (2019). Atmosphere boundary layer height and its effect on air pollutants in Beijing during winter heavy pollution. *Atmospheric Research*, *215*, 305–316. https://doi.org/10.1016/j.atmosres.2018.09.014

Xu, Q., Wang, S., Jiang, J., Bhattarai, N., Li, X., Chang, X., et al. (2019). Nitrate dominates the chemical composition of PM2.5 during haze event in Beijing, China. *Science of the Total Environment*, *689*, 1293–1303. https://doi.org/10.1016/j.scitotenv.2019.06.294

Xue, J., Yuan, Z., Griffith, S. M., Yu, X., Lau, A. K. H., & Yu, J. Z. (2016). Sulfate Formation Enhanced by a Cocktail of High NOx, SO2, Particulate Matter, and Droplet pH during Haze-Fog Events in Megacities in China: An Observation-Based Modeling Investigation. *Environmental Science and Technology*, *50*(14), 7325–7334. https://doi.org/10.1021/acs.est.6b00768

Yan, Y., Peng, L., Li, R., Li, Y., Li, L., & Bai, H. (2017). Concentration, ozone formation potential and source analysis of volatile organic compounds (VOCs) in a thermal power station centralized area: A study in Shuozhou, China. *Environmental Pollution*, *223*, 295–304. https://doi.org/10.1016/j.envpol.2017.01.026

Ye, C., Zhang, N., Gao, H., & Zhou, X. (2017). Photolysis of Particulate Nitrate as a Source of HONO and NOx. *Environmental Science & Technology*, *51*(12), 6849–6856. https://doi.org/10.1021/acs.est.7b00387

Yu, C., Wang, Z., Xia, M., Fu, X., Wang, W., Tham, Y. J., et al. (2020). Heterogeneous N2O5 reactions on atmospheric aerosols at four Chinese sites: improving model representation of uptake parameters. *Atmospheric Chemistry and Physics*, *20*(7), 4367–4378. https://doi.org/10.5194/acp-20-4367-2020

Yu, D., Tan, Z., Lu, K., Ma, X., Li, X., Chen, S., et al. (2020). An explicit study of local ozone budget and NOx-VOCs sensitivity in Shenzhen China. *Atmospheric Environment*, *224*, 117304. https://doi.org/10.1016/j.atmosenv.2020.117304

Zhang, B., Zhao, B., Zuo, P., Huang, Z., & Zhang, J. (2017). Ambient peroxyacyl nitrate concentration and regional transportation in Beijing. *Atmospheric Environment*, *166*, 543–550. https://doi.org/10.1016/j.atmosenv.2017.07.053

Zhang, G., Xia, L., Zang, K., Xu, W., Zhang, F., Liang, L., et al. (2020). The abundance and inter-relationship of atmospheric peroxyacetyl nitrate (PAN), peroxypropionyl nitrate (PPN), O3, and NOy during the wintertime in Beijing, China. *Science of the Total Environment*, *718*, 137388. https://doi.org/10.1016/j.scitotenv.2020.137388

Zhang, H., Xu, X., Lin, W., & Wang, Y. (2014). Wintertime peroxyacetyl nitrate (PAN) in the megacity Beijing: Role of photochemical and meteorological processes. *Journal of Environmental Sciences (China)*, *26*(1), 83–96. https://doi.org/10.1016/S1001-0742(13)60384-8

Zhang, J., An, J., Qu, Y., Liu, X., & Chen, Y. (2019). Impacts of potential HONO sources on the concentrations of oxidants and secondary organic aerosols in the Beijing-Tianjin-Hebei

region of China. *Science of The Total Environment*, *647*, 836–852. https://doi.org/10.1016/j.scitotenv.2018.08.030

Zhang, Leiming, Gong, S., Padro, J., & Barrie, L. (2001). A size-segregated particle dry deposition scheme for an atmospheric aerosol module. *Atmospheric Environment*, *35*(3), 549–560. https://doi.org/10.1016/S1352-2310(00)00326-5

Zhang, Li, Wang, T., Zhang, Q., Zheng, J., Xu, Z., & Lv, M. (2016). Potential sources of nitrous acid (HONO) and their impacts on ozone: A WRF-Chem study in a polluted subtropical region. *Journal of Geophysical Research*, *121*(7), 3645–3662. https://doi.org/10.1002/2015JD024468

Zhang, Y.-L., & Cao, F. (2015). Fine particulate matter (PM2.5) in China at a city level. *Scientific Reports*, *5*(1), 14884. https://doi.org/10.1038/srep14884

Zheng, B., Tong, D., Li, M., Liu, F., Hong, C., Geng, G., et al. (2018). Trends in China's anthropogenic emissions since 2010 as the consequence of clean air actions. *Atmospheric Chemistry and Physics*, *18*(19), 14095–14111. https://doi.org/10.5194/acp-18-14095-2018

Zhou, W., Zhao, J., Ouyang, B., Mehra, A., Xu, W., Wang, Y., et al. (2018). Production of N2O5 and ClNO2 in summer in urban Beijing, China. *Atmospheric Chemistry and Physics*, *18*(16), 11581–11597. https://doi.org/10.5194/acp-18-11581-2018

Zhou, W., Gao, M., He, Y., Wang, Q., Xie, C., Xu, W., et al. (2019). Response of aerosol chemistry to clean air action in Beijing, China: Insights from two-year ACSM measurements and model simulations. *Environmental Pollution*, *255*, 113345. https://doi.org/10.1016/j.envpol.2019.113345

A. APPENDIX A

A.1 SUPPLEMENTARY TEXTS FOR CHAPTER 2

A.1.1 Model suggests that NO3 + VOCs reactions are not important in wintertime Beijing

Previous interpretation of $\Delta^{17}O$-observations in Beijing suggested that NO_3 + VOCs (Figure **2-1**b, R12) might contribute over 30% of nitrate production during wintertime haze events (He et al., 2018; W. Song et al., 2020; Yan-Li Wang et al., 2019). However, R12 contributes only 0.2% to nitrate production in Beijing on average in the model and rate of nitrate production via R12 decreases as the haze events become more intense (Figure **A-15** and Figure **A-16**) because R12 is limited by NO_3, not VOCs. VOCs can also contribute to nitrate production in urban air through the formation of organic nitrates (R15 and R16). Hydrolysis of organic nitrate, which yields low $\Delta^{17}O(NO_3^-)$ values, is a more important source of inorganic nitrate in Beijing than the NO_3 + VOC reactions (R12) (See Figure **A-15**), although it still accounts for only 0.4% of total nitrate production on average. Thus, model biases in reactions between NO_3 and VOCs are unlikely to explain the model's underestimate in $\Delta^{17}O(NO_3^-)$ during haze events.

A.1.2 Results from other model sensitivity experiments

In this section, we discuss the set-ups and the motivations of two model sensitivity experiments and the findings from these simulations.

A.1.2.1 + p-NO_3^- photolysis simulation

In this section, we hypothesize that the model underestimate of [O_x] and overestimate of NOR is driven by the lack of renoxification (i.e., the processes that convert NO_3^- back to NO_x and HONO) in the model. Observations in North China show high concentrations of [HONO] during the daytime that cannot be solely explained by direct emission and formation via NO + OH (e.g., D. Li et al., 2018; J. Wang et al., 2017). Photolysis of particulate nitrate, which converts p-NO_3^- into HONO and NO_x, is a proposed mechanism to explain observations of [HONO] in Beijing and other regions in North China (e.g., Bao et al., 2018; Y. Liu et al., 2019; J. Wang et al., 2017; Ye et al., 2017). To evaluate the role of renoxification on [O_x], NOR, and $\Delta^{17}O$, we perform a sensitivity simulation by scaling the photolysis rate coefficient of p-NO_3^- (J(p-NO_3^-)) to 100×(J(HNO_3)). This photolysis scheme is applied to p-NO_3^- in both $PM_{2.5}$ and coarse-mode sea-salt aerosols. The scale factor we choose (100) is similar to Fu et al. (2019) (~119), but much higher than estimates in Kasibhatla et al (2018) (25) and Romer et al. (2018) (<30). We further assume that p-NO_3^- photolysis produces HONO only, not NO_2. This HONO yield of 100% is higher than used in previous modeling studies (67% in Kasibhatla et al. (2018) and Fu et al. (2019)), but it is more consistent with the high HONO:NO_2 ratio found in the laboratory studies of nitrate photolysis using the aerosols sampled in urban air (Bao et al., 2018; Ye et al., 2017). Although our model configurations may overestimate the rate of p-NO_3^- photolysis and the yield of HONO, this

simulation can shed light on the maximum potential impacts of renoxification on NO_y chemistry in North China.

p-NO_3^- photolysis reduces modeled $\Delta^{17}O(NO_3^-)$ in moderate haze and severe haze while increasing $\Delta^{17}O(NO_3^-)$ in extreme haze relative to the base model (Figure **A-17**). Compared to the base model, the modeled median $\Delta^{17}O(NO_3^-)$ in moderate haze, severe haze, and extreme haze changed by −0.9‰, −0.6‰, and +0.7‰, respectively. Including p-NO_3^- photolysis in the simulation reduces the model-observation discrepancy in $\Delta^{17}O(NO_3^-)$ in moderate haze and extreme haze but not in severe haze. Similar to the previous two simulations, the model with p-NO_3^- photolysis predicts a decrease in $\Delta^{17}O(NO_3^-)$ as $[PM_{2.5}]$ increases, although the decreasing trend is weaker than in the base model. Modeled median $\Delta^{17}O(NO_3^-)$ in extreme haze is only 0.6‰ lower than that in moderate haze.

The lower modeled $\Delta^{17}O(NO_3^-)$ in the + p-NO_3^- photolysis simulation is mainly driven by increased OH produced from HONO photolysis. Gas-phase oxidation of NO_2 by OH contributes over 40% to nitrate production in all haze regimes, while the relative importance of all heterogeneous pathways decreases compared with the base simulation (Figure **A-18**). Although NO_2 + OH overwhelms the overall changes in modeled $\Delta^{17}O(NO_3^-)$, it is still important to note that the absolute rate of N_2O_5 hydrolysis does increase in the + p-NO_3^- photolysis simulation. The faster nitrate production via` N_2O_5 hydrolysis in this simulation is largely attributed to the higher rate of N_2O_5 production (Figure **A-19**) driven by higher $[O_x]$ (Figure **A-20**).

After we introduce the renoxification source of HONO into the model, the modeled [O_x] under all haze regimes increases, but the O_x speciation and NOR remains similar to the base model (Figure **A-20** and Figure **A-21**). The modeled [O_x] increases by about 24% in intense haze; thus, the average bias in modeled [$O_{x,\ major}$] in intense haze reduces to −23%. The modeled NOR is not sensitive to the nitrate photolysis chemistry under all haze regimes (Figure **A-21**). The overall average modeled NOR during intense haze events in the nitrate photolysis simulation remains the same as in the base simulation (0.33). Adding renoxification into the model does not decrease the relative abundance of nitrate in Beijing because the absolute rate of nitrate production scales up as [O_x] increases (Figure **A-18**). The extra OH and O_3 resulting from nitrate photolysis reacts with NO_2 to produce nitrate again. In contrast, p-NO_3^- photolysis does not increase the modeled abundance of sulfate and organic aerosol, suggesting that their production rate is not limited by O_x (Figure **A-22**).

A.1.2.2 +Cl chem simulation

In this section, we hypothesize that the underestimate of $\Delta^{17}O(NO_3^-)$ in extreme haze, the underestimate of [O_x], and the overestimate of NOR are caused by the lack of anthropogenic emission of HCl and the inadequate representation of the chemistry of gas-phase chlorine species (Cl_y = Cl + Cl_2 + HCl + HOCl + $ClNO_2$ + $ClNO_3$ + BrCl + ICl) in the base simulation. To investigate the potential influence of anthropogenic HCl and chlorine activation on NO_y chemistry in North China, we adopt the global HCl emission inventory from McCulloch et al. (1999), which includes HCl emissions from coal combustion, incineration, and industrial activities. We also update the modeled Cl_y chemistry following X. Wang et al. (2019). In particular, in the updated

model, the chloride content of fine-mode aerosol now modulates the partitioning between p-NO_3^- and HNO_3, the uptake coefficient of N_2O_5, and the production of $ClNO_2$ via $N_2O_5 + Cl^-$. Moreover, nitrate production from the hydrolysis of halogen nitrates and $N_2O_5 + Cl^-$ yield high $\Delta^{17}O$; an underestimate in these reactions could lead to an underestimate of modeled $\Delta^{17}O$ (See Figure **A-2**). In our simulations, the majority of Cl_y in Beijing is in the form of HCl and $ClNO_2$ (Figure **A-23**), but more minor Cl_y species (e.g. Cl and $ClNO_3$) may also have significant impacts on NO_y chemistry (Haskins et al., 2019; Hoffmann et al., 2019; X. Wang et al., 2019). The modeled [Cl_y] in Beijing increases by about two orders of magnitude after we include emissions of anthropogenic HCl and update the Cl_y chemistry (Figure **A-23**). The model results from X. Wang et al. (2019) suggested that the McCulloch et al. (1999)'s HCl emission inventory overestimates boundary-layer [HCl] in their global simulation, suggesting that our sensitivity simulation provides a high-end estimate of the potential effects of anthropogenic HCl on NO_y chemistry in North China.

The +Cl chem simulation predicts a higher $\Delta^{17}O(NO_3^-)$ compared with the base simulation, but still underestimates the $\Delta^{17}O(NO_3^-)$ in extreme haze (Figure **A-17**). The modeled median $\Delta^{17}O(NO_3^-)$ in intense haze is 29.6‰, which is 0.4‰ higher than that in the base simulation. The model still exhibits an inverse relationship between $\Delta^{17}O(NO_3^-)$ and [$PM_{2.5}$]. The modeled median $\Delta^{17}O(NO_3^-)$ decreases from 30.0‰ in moderate haze to 28.1‰ in extreme haze. The increase in modeled $\Delta^{17}O(NO_3^-)$ in +Cl Chem compared to the base simulation is mostly attributed to the higher $\Delta^{17}O$ associated with $N_2O_5 + Cl^-$ channel and the higher rate of N_2O_5 uptake onto aerosol (Figure **A-18** and Figure **A-19**). Nitrate produced via the $N_2O_5 + Cl^-$ pathway contributes 6.9% to the total nitrate production on average in intense haze and has higher $\Delta^{17}O$ than those formed via the $N_2O_5 + H_2O$ pathway (Alexander et al., 2020). The median rate of N_2O_5 uptake on aerosol

increases by 8.7%, 57.2%, and 62.3% in moderate haze, severe haze, and extreme haze, respectively, compared to the base simulation due to the increase in calculated $\gamma(N_2O_5)$ and the rate of N_2O_5 production via $NO_3 + NO_2$. $\gamma(N_2O_5)$ increases in the +Cl Chem simulation because the model now considers the promoting effects of chloride on the uptake of N_2O_5 on aerosols (Bertram & Thornton, 2009). The median $\gamma(N_2O_5)$ increases by 87.4%, 68.6%, and 23.2% in moderate haze, severe haze, and extreme haze, respectively, compared to the base model. In contrast, the changes in the modeled rate of N_2O_5 production are more moderate (Figure **A-19**). The median changes by −30.7%, −7.9%, and +21.8% in moderate haze, severe haze, and extreme haze, respectively, compared to the base model. The small changes in the rate of N_2O_5 production prevents the rate of N_2O_5 uptake from scaling up with the much higher $\gamma(N_2O_5)$ in moderate and severe haze. Results from both the +Cl chem and +p-NO_3^- photolysis simulations show that the rate of nitrate production via N_2O_5 uptake is more sensitive to the supply of N_2O_5 than the magnitude of $\gamma(N_2O_5)$ in Beijing.

The emission and the chemistry of anthropogenic Cl_y only have minor effects on the modeled $[O_x]$ and NOR (Figure **A-20** and Figure **A-21**). Compared with the base simulation, the modeled median $[O_x]$ increases by 2.3 ppb on average in intense haze. The largest increase in modeled $[O_x]$ is found in extreme haze (median increases by + 6.4 ppb compared with that in the base simulation), which is driven by the increase in modeled $[O_3]$ and $[NO_2]$ (Figure **A-20**). Our simulation suggests that including anthropogenic Cl_y would increase the wintertime $[O_3]$ in Beijing by 12% on average, which is higher the predictions from the simulations done by Q. Li et al. (2020) (up to +10%) and (X. Wang et al., 2020) (+3.2%), likely because of our overestimate of HCl emissions. The modeled NOR in intense haze has an average value of 0.31, which is higher than the observations (0.21),

particularly during extreme haze (Figure **A-21**). The relationship between NOR and $PM_{2.5}$ in the + Cl chem simulation is very similar to what we see in the base simulation and + p-NO_3^- photolysis simulation (Figure **A-21**).

The small change in modeled NOR in +Cl chem relative to the base simulation is caused by the higher overall rate of nitrate production and the competing effects from $ClNO_2$ production via the N_2O_5 + Cl^- pathway. In the base model, the hydrolysis of N_2O_5 produces only HNO_3, which quickly forms p-NO_3^- in Beijing. In the +Cl Chem simulation, the N_2O_5 + Cl^- channel allows some of the N_2O_5 uptake on aerosols to recycle back to NO_2 via the production of $ClNO_2$ and its subsequent photolysis during the daytime. This conversion of N_2O_5 to NO_2 via the chemistry of $ClNO_2$ can potentially reduce modeled NOR. However, the simultaneous increase in the overall rate of nitrate production causes the modeled overestimate of NOR to persist. Moreover, the higher aerosol water content in severe haze and extreme haze reduces the yield of $ClNO_2$ from the N_2O_5 uptake on aerosols suppressing the conversion of N_2O_5 to NO_2 (See Figure **A-24**).

A.2 Supplementary Figures for Chapter 2 and Appendix A.1

A.1 (a)


G7
G6
G110
G110
G6
CHANGPING

A.1 (b)

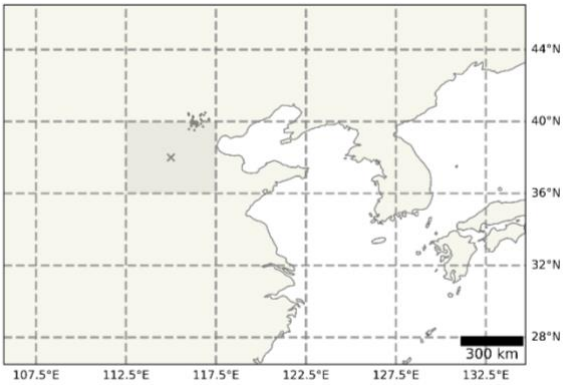
44°N
40°N
36°N
32°N
28°N
300 km
107.5°E
112.5°E
117.5°E
122.5°E
127.5°E
132.5°E

A.1 (c)

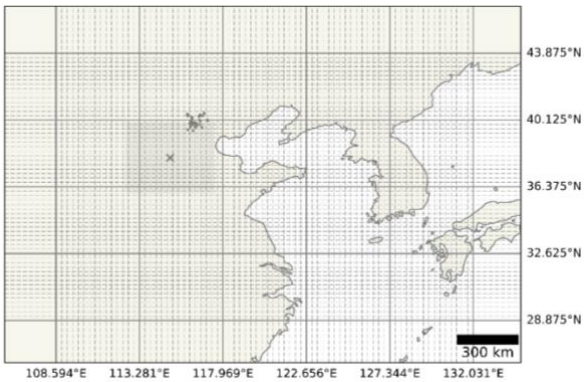
43.875°N
40.125°N
36.375°N
32.625°N
28.875°N
300 km
108.594°E
113.281°E
117.969°E
122.656°E
127.344°E
132.031°E

Figure A-1 Geographic information of the observations used in this work.

A-1(a) shows the location of air quality monitoring sites in Beijing and the measurement sites in He et al. (2018), Y. Wang et al. (2019), and W. Song et al. (2020). A-1(b) shows the locations of observation sites and the grid cells over North China in the GC 4°x5° simulations. A-1(c) is similar to A-1(b), but it shows the grid cells in GC nested-grid simulations. In the GC 4°x5° simulations, the gridbox centering at (38°N, 115°E) is chosen to represent Beijing and is marked with an "x". The gridbox centering at (42°N, 115°E) covers mostly mountainous terrain north of Beijing, resulting in poor agreement between modeled and observed [$PM_{2.5}$].

A-2

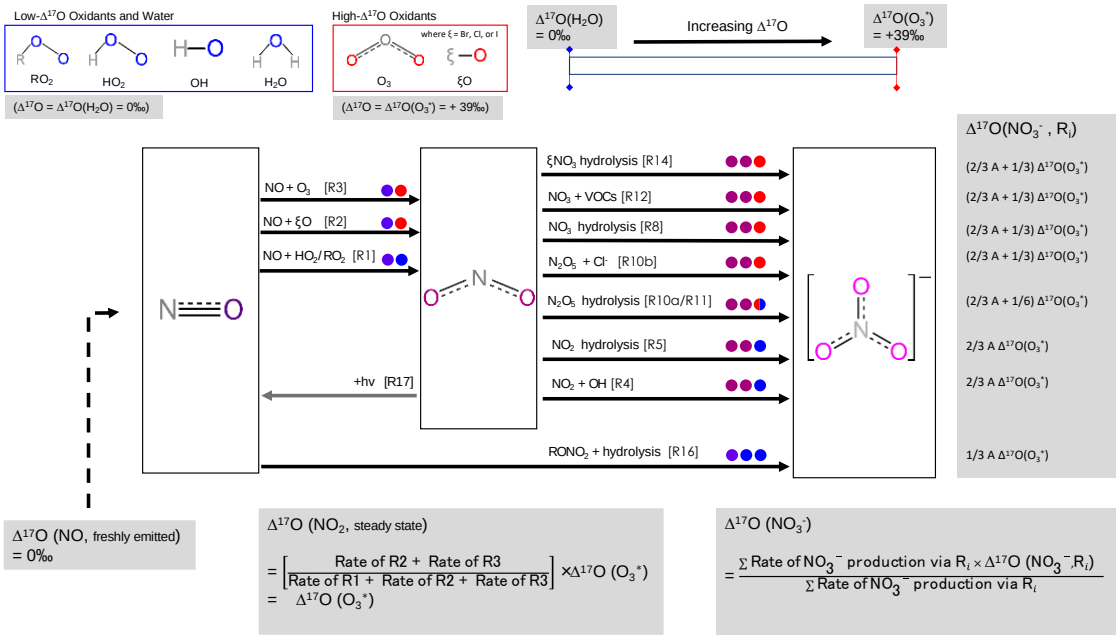

Figure A-2 A cartoon demonstrating model calculation of $\Delta^{17}O(NO_3^-)$ from the local rate of different nitrate-production pathways and assumptions for the $\Delta^{17}O$ of different oxidants.

$\Delta^{17}O(O_3^*)$ refers to the $\Delta^{17}O$ of an ozone molecule's terminal oxygen atoms, which are also assumed to be the oxygen atoms transferred to the other species during oxidation. $\Delta^{17}O(O_3^*) = 3/2 \times \Delta^{17}O(O_3) = 1.5*26‰ = 39‰$. We assume that the oxygen atom in halogen monoxide (ξO, ξ = Cl, Br, or I) originated from ozone and carries a $\Delta^{17}O$ of 39‰. We further assume that the oxygen atoms in HO_2, RO_2, and OH carry an $\Delta^{17}O$ that is very close to $\Delta^{17}O(H_2O)$, which is equal to 0‰. The colors of the filled circles indicate the $\Delta^{17}O$ of the oxygen atoms in the NO_2 or NO_3^- produced via a particular reaction. Other description of the calculation for $\Delta^{17}O(NO_3^-)$ can be found in Section 2.2.3 and in Alexander et al. (2020). The chemical equation and other details of the reactions R1 to R17 can be found in Table **A-1**.

A-3 (a)

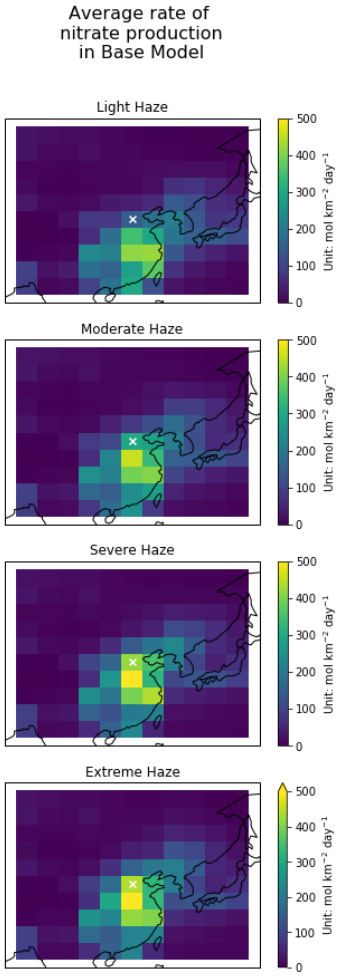

A-3 (b)

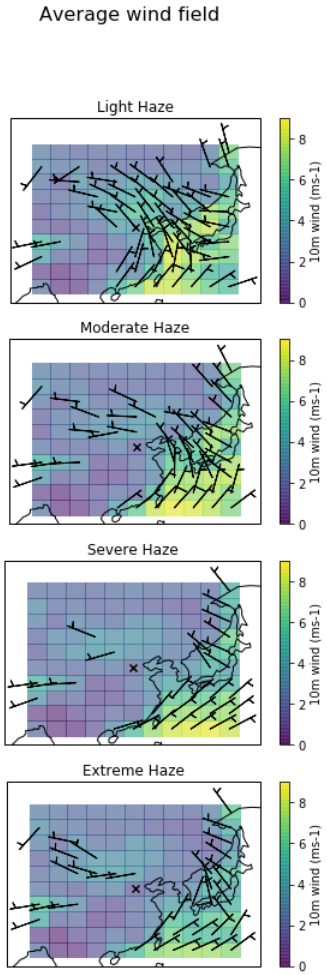

A-3 (c)

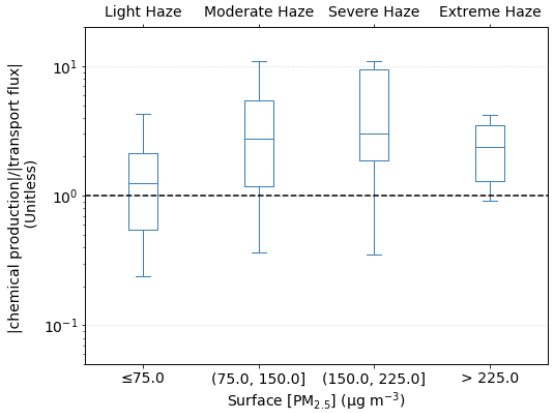

Figure A-3 Relationship between modeled nitrate production and atmospheric transport in different haze regimes in the base model simulation.

A.3(a) shows the spatial patterns of the average total rate of nitrate production predicted by the base model. A.3(b) shows the average wind field from meteorological data assimilation products regridded for the global simulation. A.3(c) shows the ratio of the magnitude of chemical production of NO_3^- to the magnitude of transport flux of NO_3^- in the planetary boundary layer over Beijing in the base model simulation. The ratio equals to 1 when the the magnitude of chemical production equals to the magnitude of transport flux (shown as the dashed line in A-3(c)).

A-4 (a)

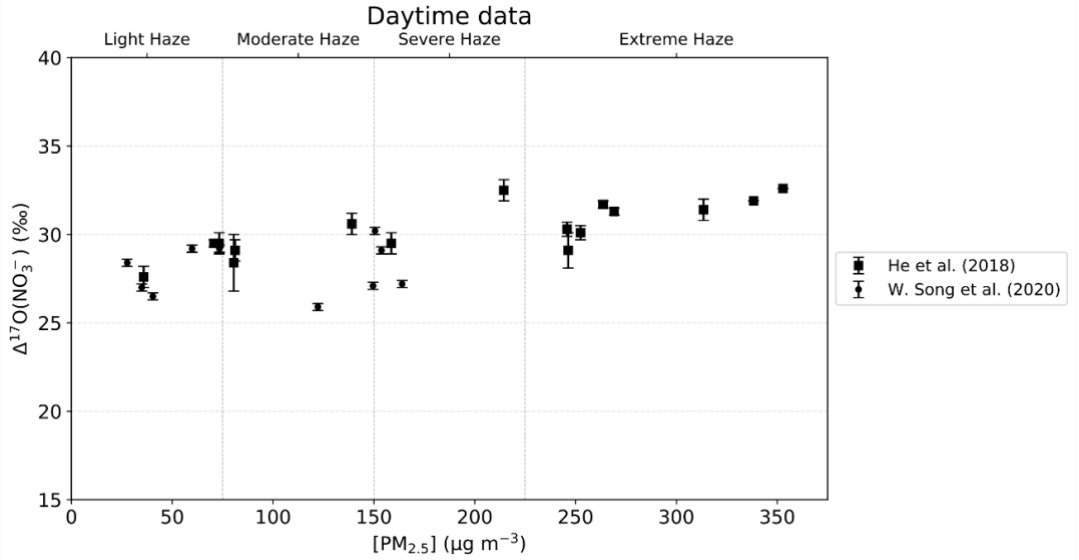

A-4 (b)

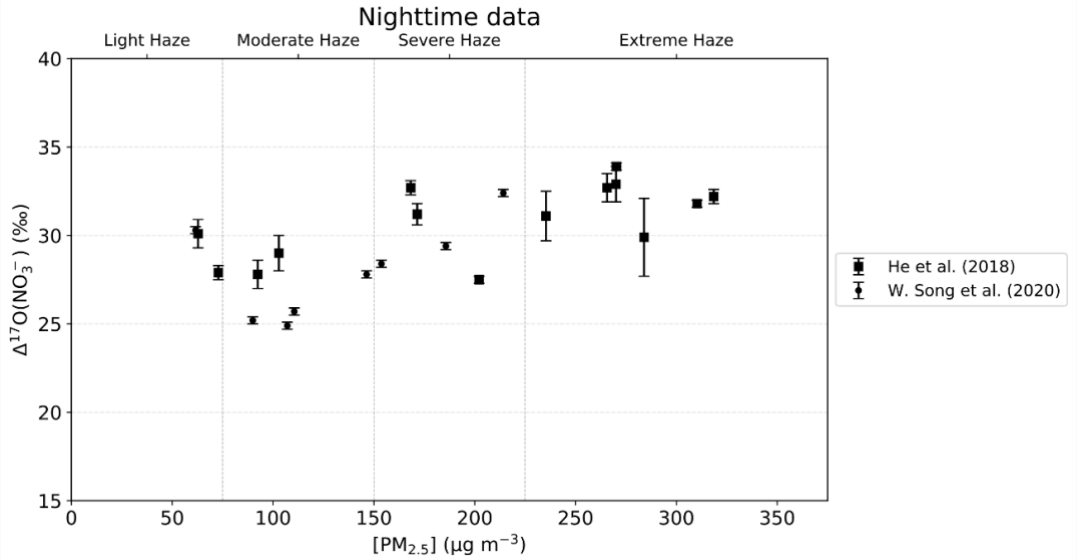

Figure A-4 Relationship between $\Delta^{17}O(NO_3^-)$ and $PM_{2.5}$ concentration in the (a) daytime and (b) nighttime observations.

For the observations from He et al. (2018), "daytime" and "nighttime" sampling are conducted during 8am-8pm and 8pm-8am, respectively. For the observations from W. Song et al. (2020), "daytime" and "nighttime" sampling are conducted during 8:30am-8:30pm and 8:30pm-8:30am, respectively.

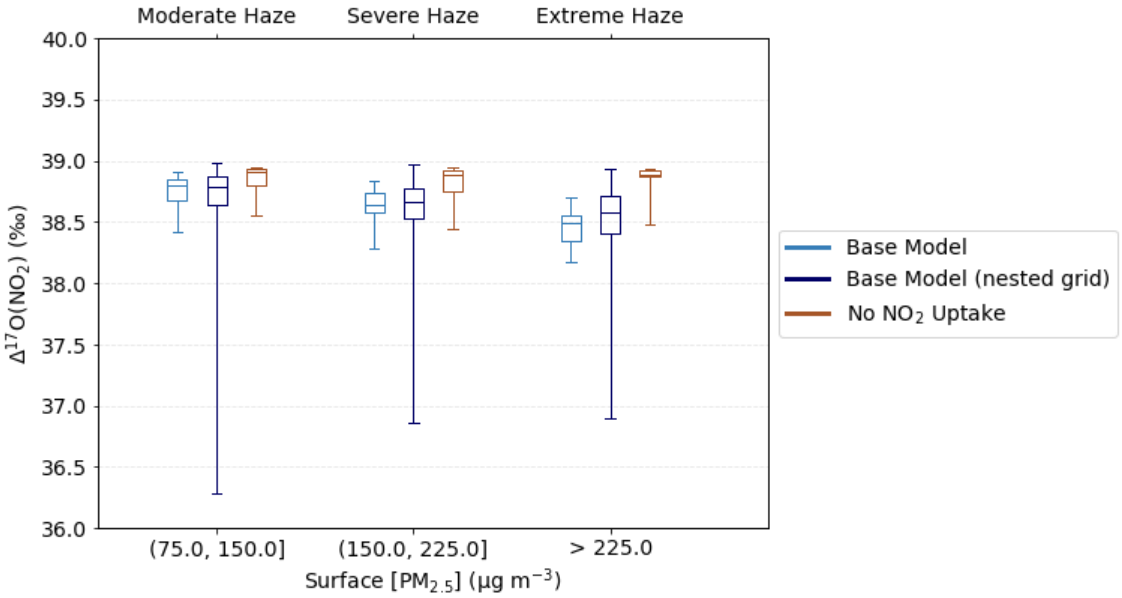

Figure A-5 Comparison of $\Delta^{17}O(NO_2)$ in simulations under different haze regimes.

A-6 (a)

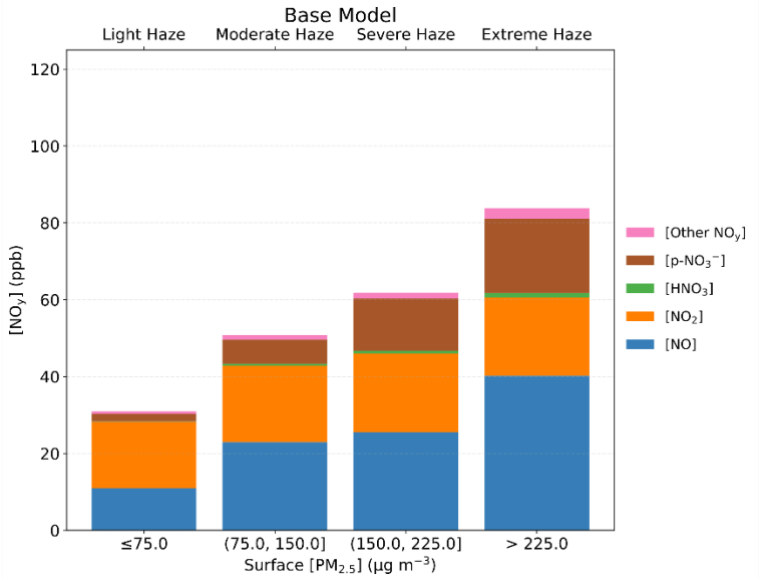

A-6 (b)

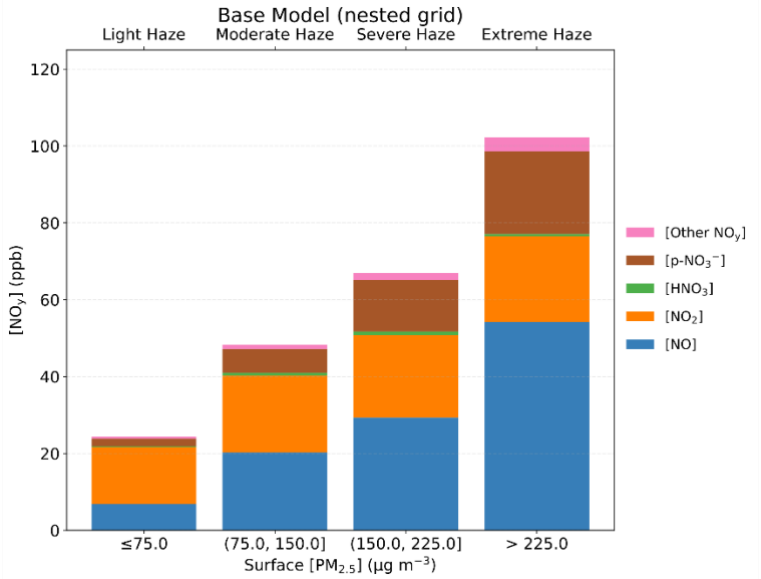

Figure A-6 Concentration and speciation of NO_y predicted by the base model under different haze regimes in (a) the global simulation and (b) the nested-grid simulation.

A-7 (a)

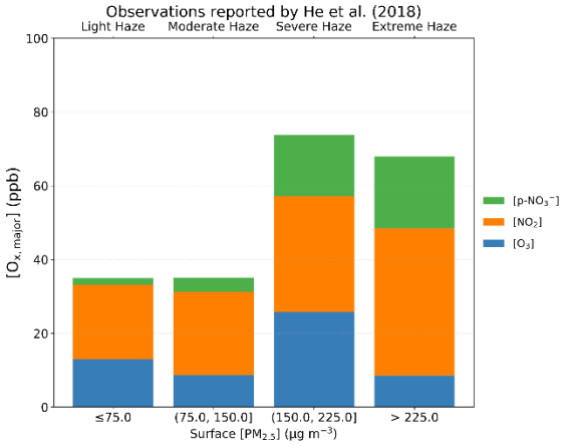

A-7 (b)

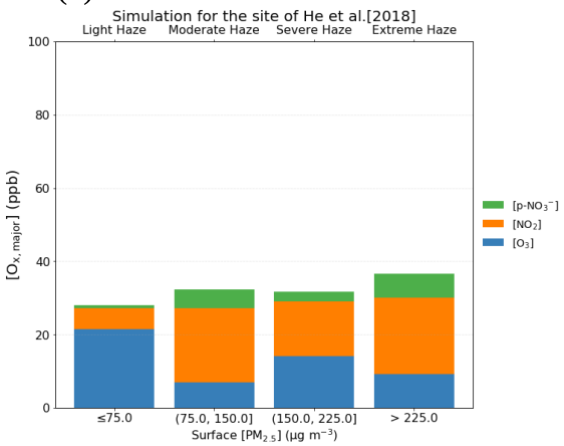

A-7 (c)

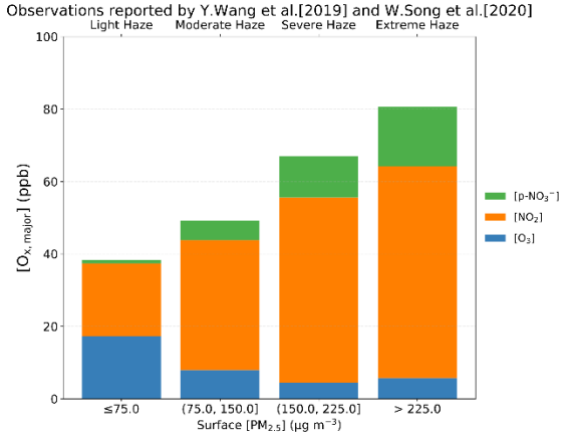

A-7 (d)

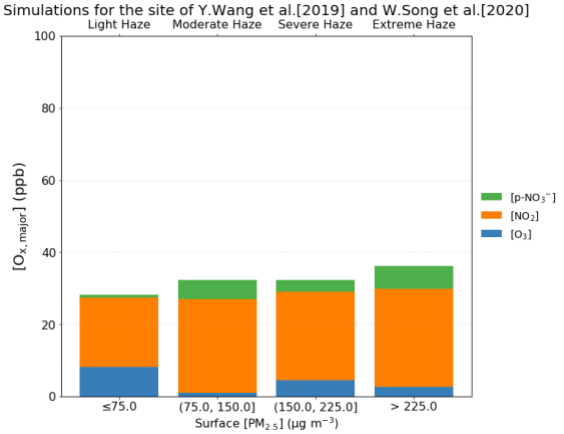

Figure A-7 Site-level comparison for the concentration and speciation of O_x under different haze regimes.

Observations from Y. Wang et al. (2019) and W. Song et al. (2020) are shown in the same plot because they are measured at the same location. The values shown in A-7 (b) and A-7 (d) are taken from the gridboxes that are closest to the two observation sites in the base-model simulation run at 0.25° latitude × 0.3125° longitude resolution.

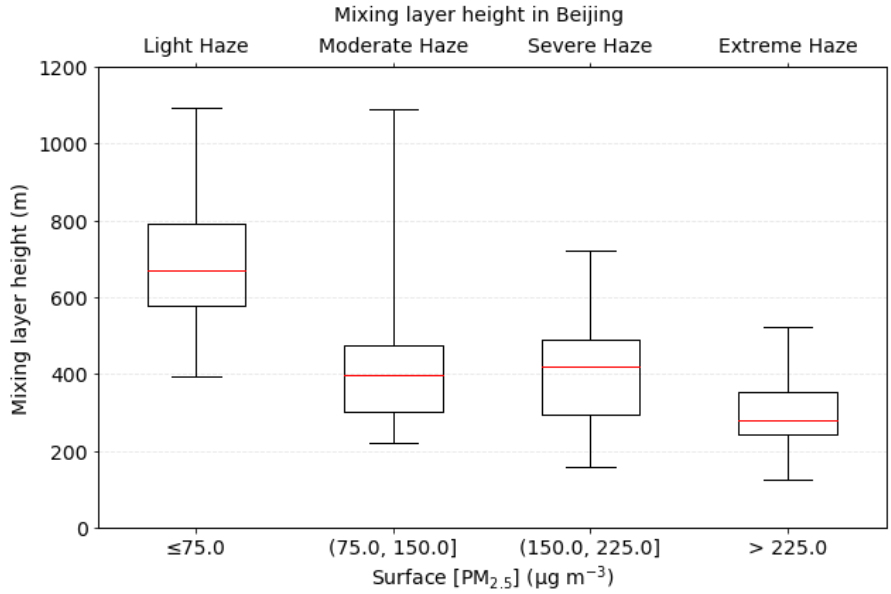

Figure A-8. The statistics of GEOS-FP mixing depth in Beijing under different haze regimes.

To examine whether the underestimate of modeled [NO_2], [O_3], and [O_x] at the surface is caused by a model bias in simulating vertical mixing in the boundary layer, we compare the mixing depth in GEOS-FP with local observations in Beijing. Mixing depth is proportional to the extent of dilution of trace gases in the boundary layer: a model overestimate of mixing depth would lead to an underestimate of surface concentrations of trace species. [$PM_{2.5}$] increases with decreasing GEOS-FP mixing depth. The median mixing depth in Beijing decreases from 670 m in light haze to 280 m in extreme haze, which are consistent with the observations reported in Tang et al. (2016) (664 m in "clean days" and 320 m in "heavy haze"). Although other recent observational studies reported different estimates of mixing depth and boundary layer height in Beijing (e.g., Shi et al., 2020; Su et al., 2018; Xiang et al., 2019), none of the observations suggest that GEOS-FP systematically overestimates the mixing depth in wintertime Beijing. Our analysis shows

that the modeled underestimate of [NO_2], [O_3], and [O_x] at the surface in the base simulation is likely not caused by a misrepresentation of boundary layer depths.

A-9

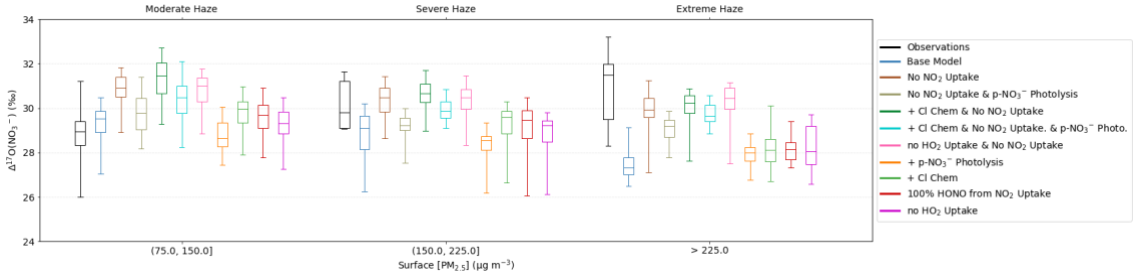

Figure A-9. Comparison of $\Delta^{17}O(NO_3^-)$ in observations and all model simulations under different haze regimes.

This figure is similar to Figure **2-3** but includes all the model sensitivity simulations that we conducted.

A-10

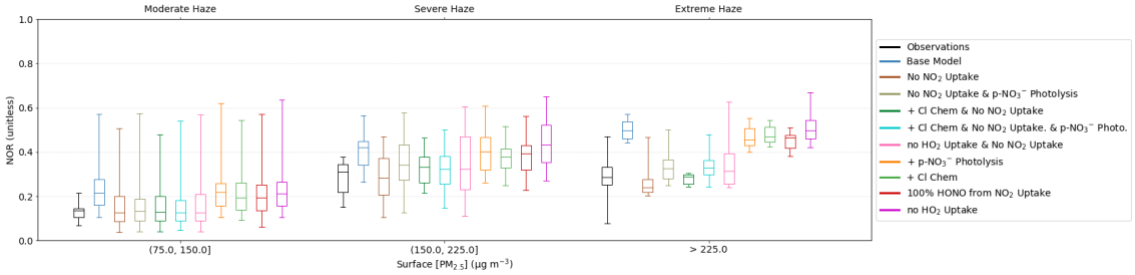

Figure A-10 Comparison of NOR in observations and all model simulations under different haze regimes.

This figure is similar to Figure **2-5** but includes all the model sensitivity simulations that we conducted.

A-11

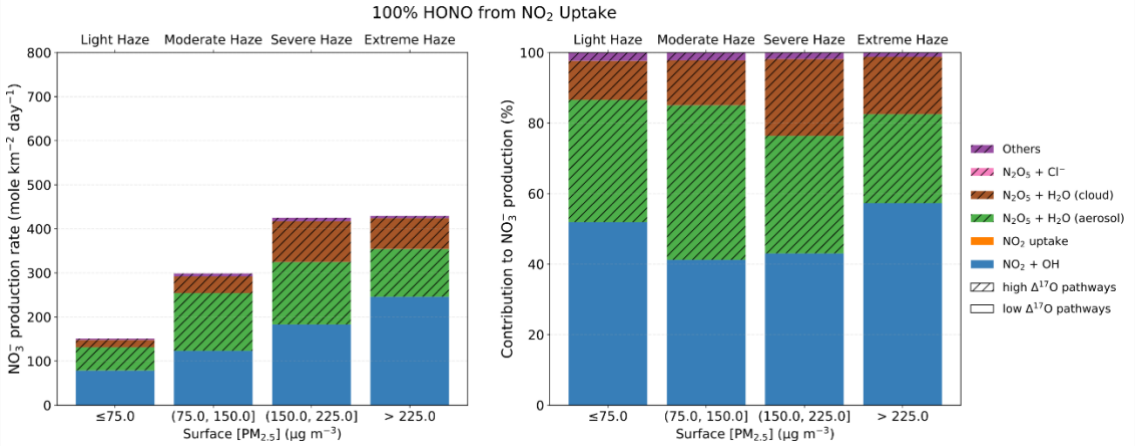

Figure A-11 Average rate of different near-surface nitrate production pathways (left) and their relative contribution in Beijing under different haze regimes (right) in the 100% HONO from NO_2 Uptake.

A-12

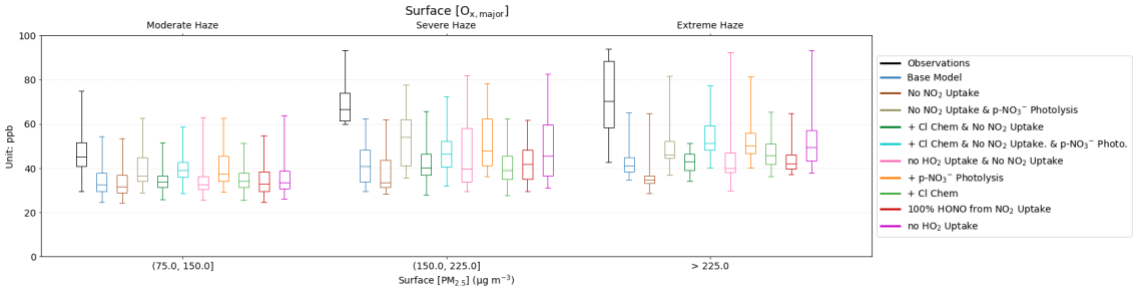

Figure A-12. Comparison of $[O_{x,\,major}]$ ($\equiv [NO_2] + [O_3] + [p\text{-}NO_3^-]$) in observations and simulations under different haze regimes.

A-13

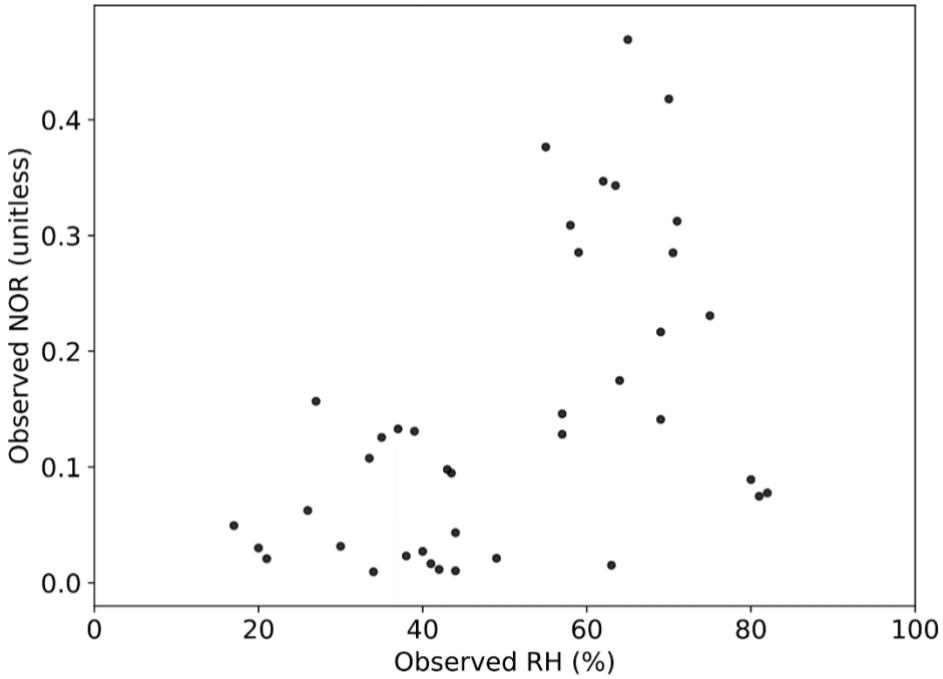

Figure A-13 Relationship between the observed NOR and surface RH in Beijing.

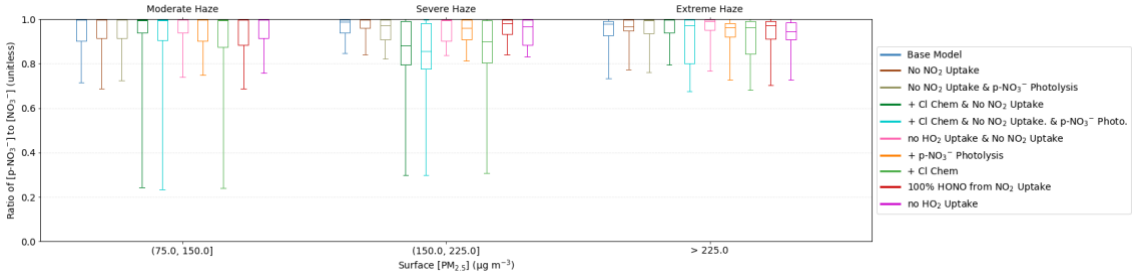

Figure A-14 Comparison of p-NO_3^- to NO_3^- ratio (≡ [p-NO_3^-]/([p-NO_3^-] + [HNO_3])) in observations and simulations under different haze regimes.

A-15 (a)

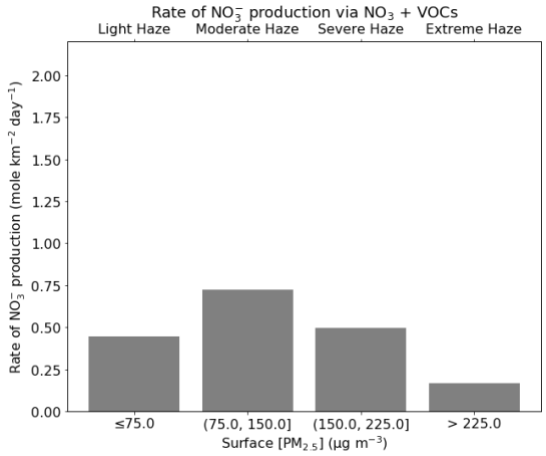

A-15 (b)

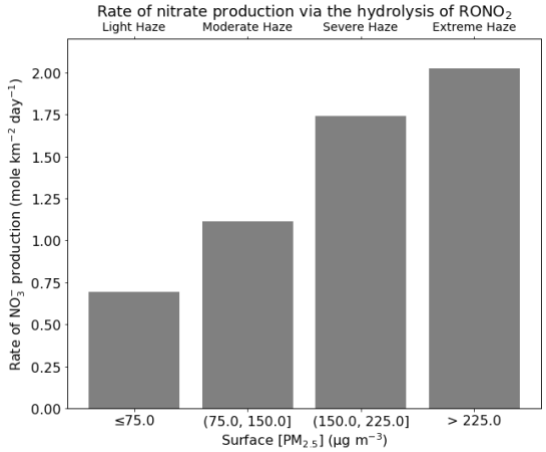

Figure A-15 Average rate of nitrate production via (a) all NO_3 + VOC reactions (R12) and (b) the hydrolysis of organic nitrates (R13) in Beijing under different haze regimes in the base simulation.

A-16

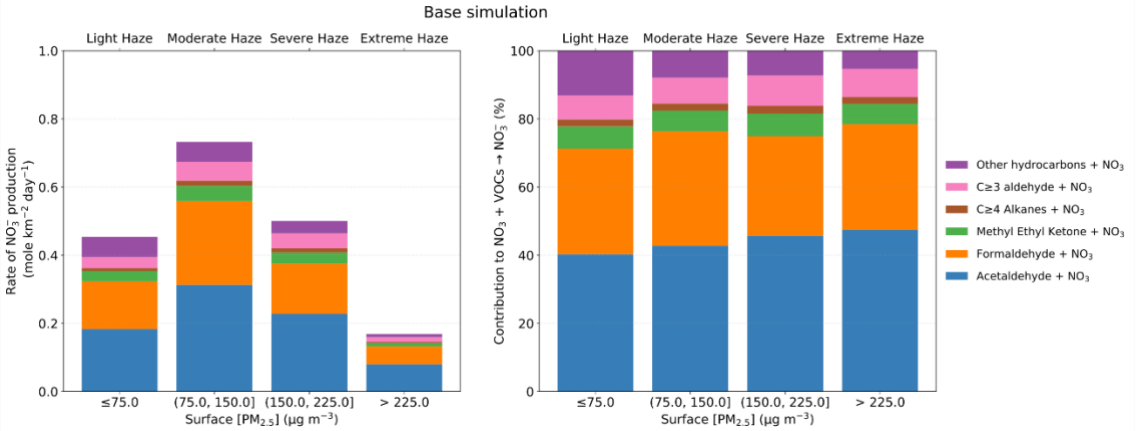

Figure A-16 Average rate of nitrate production via different NO_3 + VOC reactions (left) and their relative contribution in Beijing under different haze regimes (right) in the base simulation.

A-17

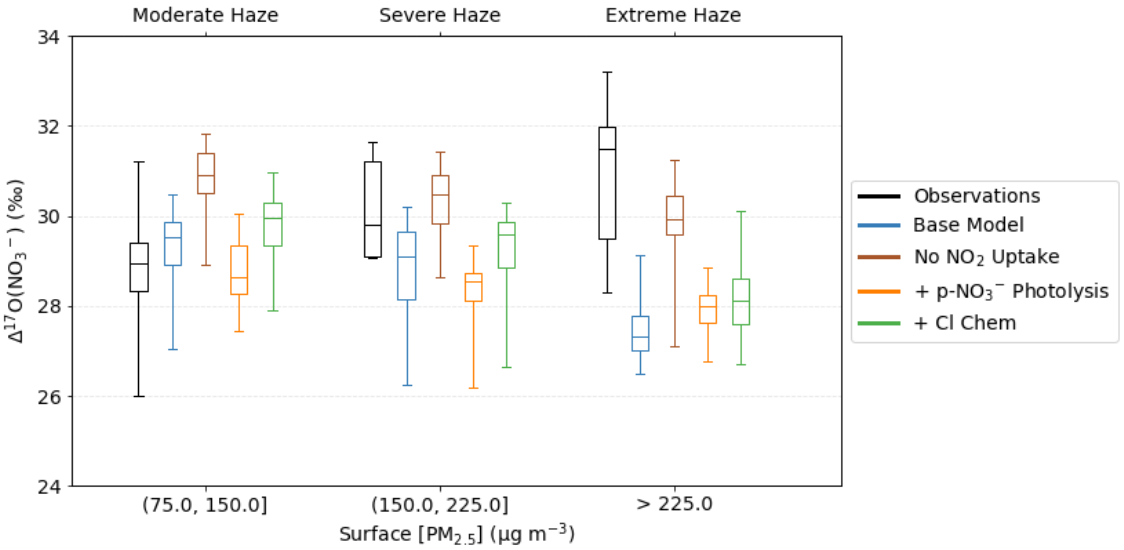

Figure A-17 Comparison of $\Delta^{17}O(NO_3^-)$ in observations and model simulations under different haze regimes.

A-18 (a)

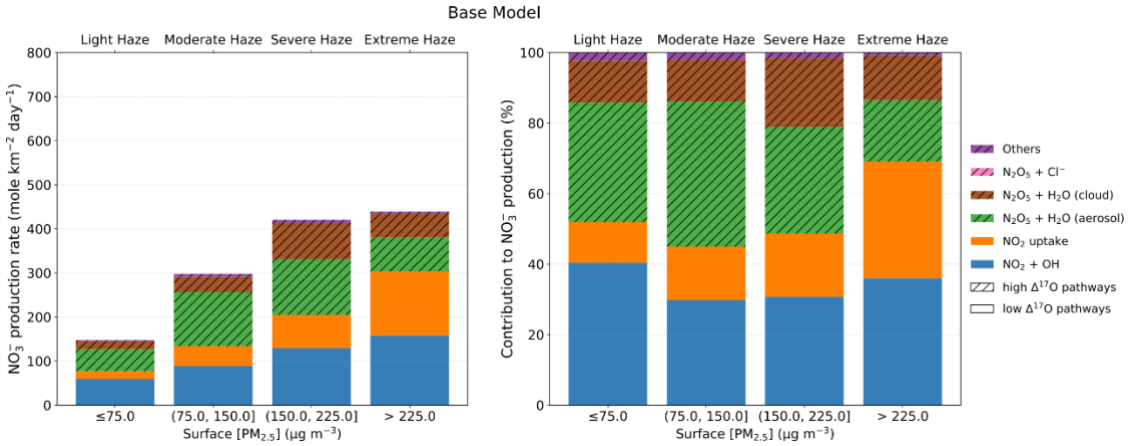

A-18 (b)

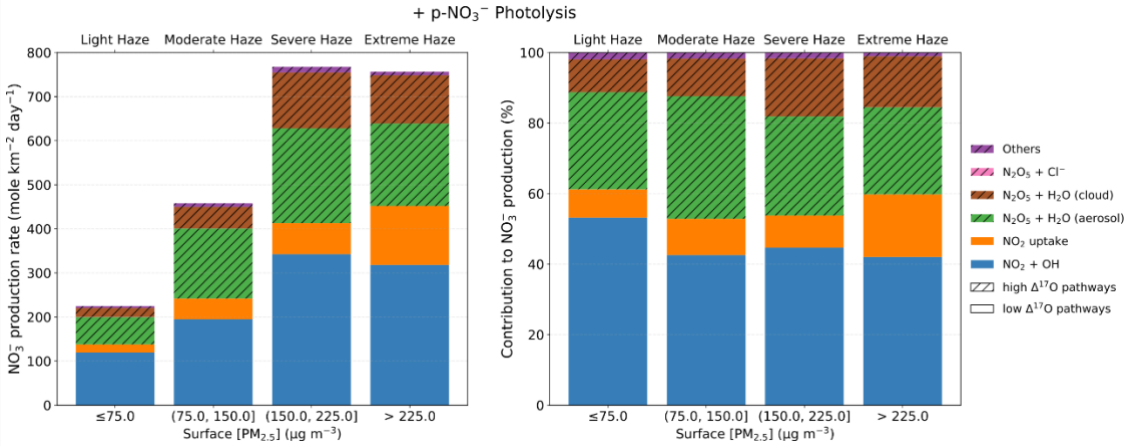

A-18 (c)

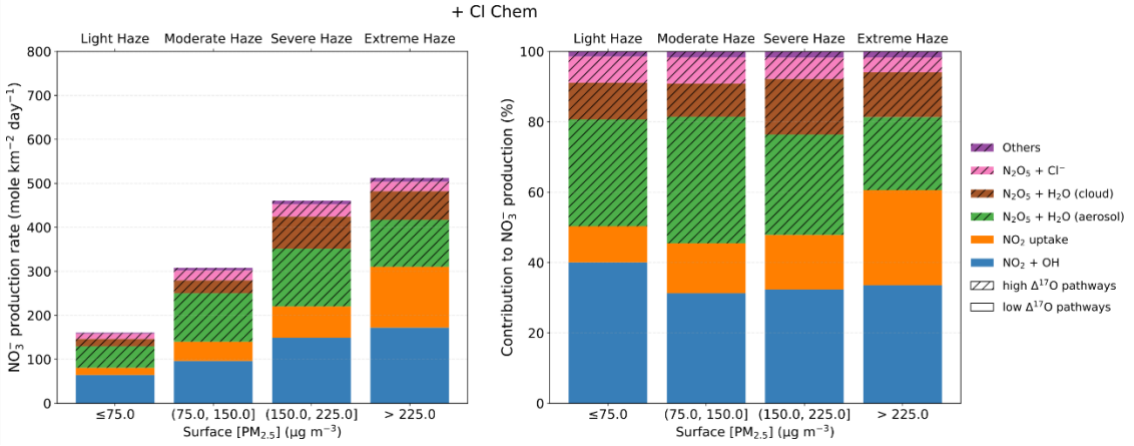

Figure A-18 Average rate of different near-surface nitrate production pathways (left) and their relative contribution in Beijing under different haze regimes (right) in (a) the base simulation, (b) + p-NO_3^- Photolysis simulation, and (c) + Cl Chem simulation.

"Near-surface" is defined as the sum over the ten lowest vertical levels in model, which on average corresponds to the altitudes between 0 to 1300 m. Denser hatching (//-filled bars) indicates high-Δ^{17}O pathways.

A-19 (a)

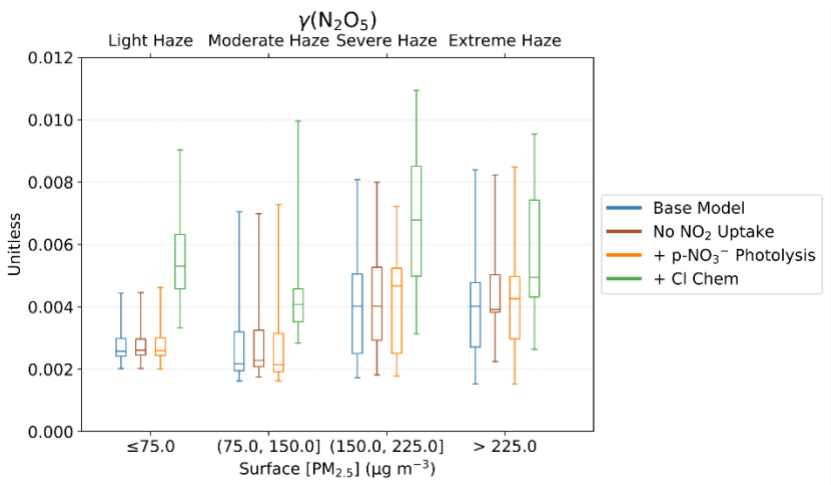

A-19 (b)

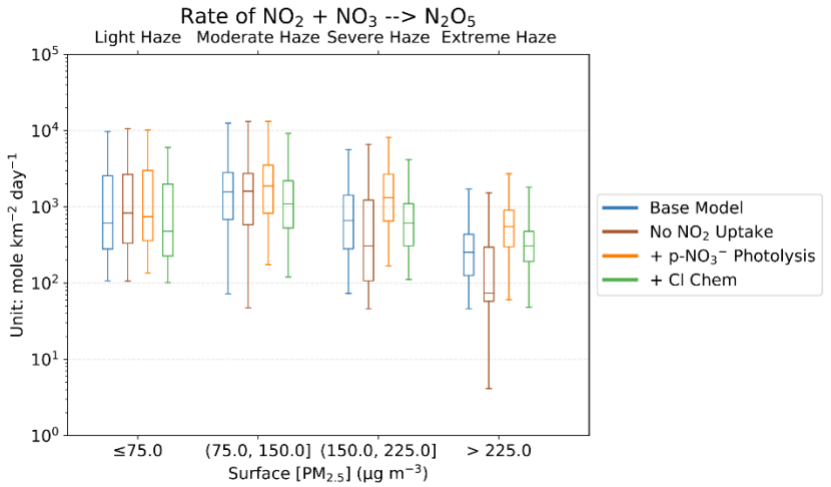

A-19 (c)

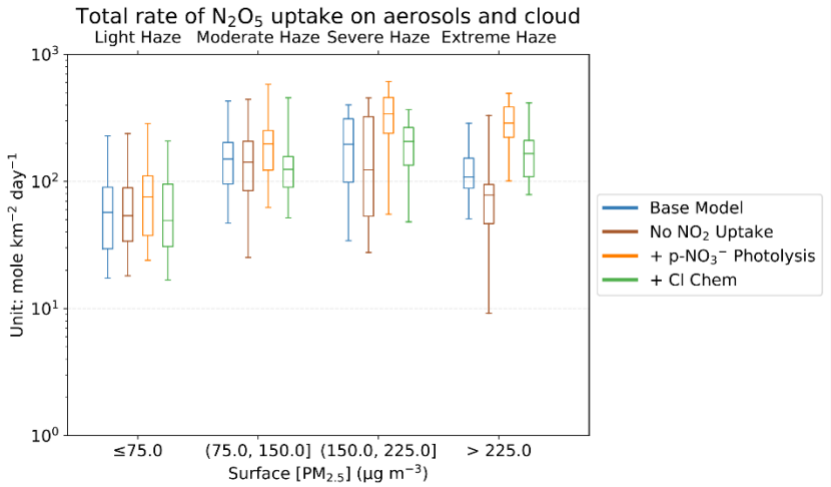

Figure A-19 Factors controlling the near-surface rate of nitrate production via N_2O_5 hydrolysis in four simulations (Base, No NO_2 uptake, + p-NO3− Photolysis, and + Cl Chem).

A-19(a) shows the average uptake coefficient of N_2O_5 on aerosols. A-19(b) shows the average rate of N_2O_5 production. A-19(c) shows the average total rate of N_2O_5 uptake on aerosols and cloud.

A-20 (a)

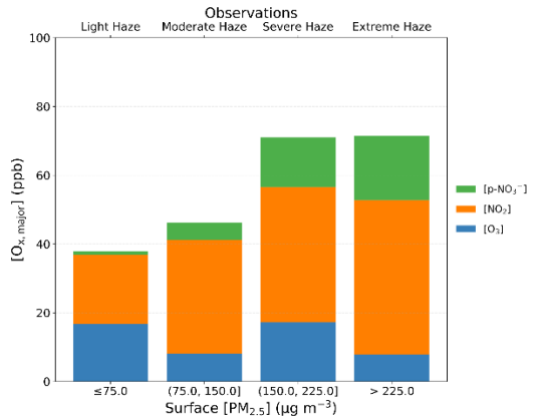

A-20 (b)

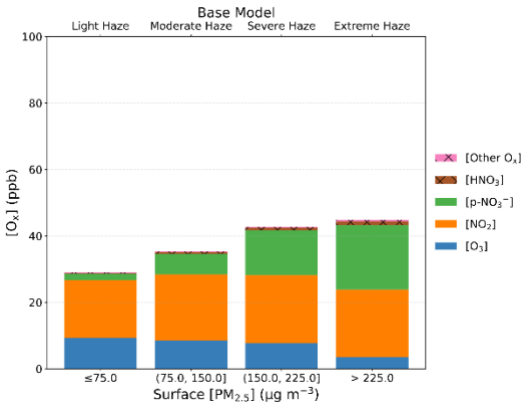

A-20(c)

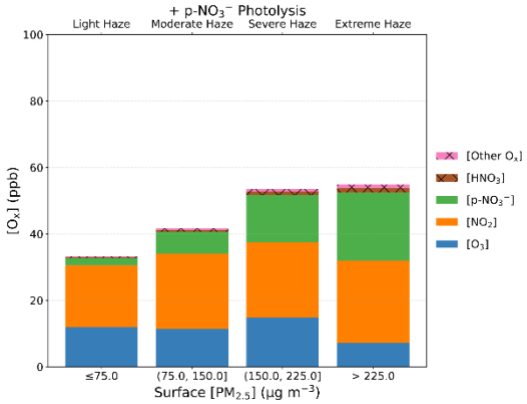

A-20(d)

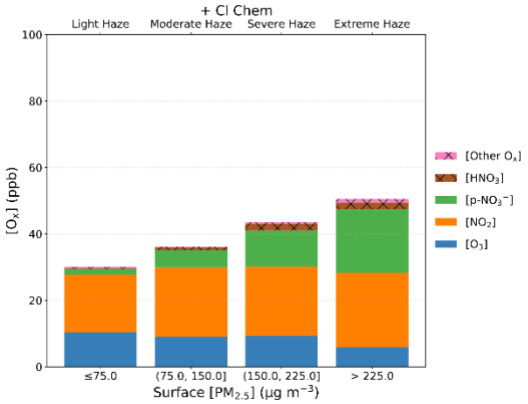

Figure A-20 Concentration and speciation of O_x under different haze regimes in (a) observations, (b) base simulation, (c) + p-NO_3^- Photolysis simulation, and (d) + Cl Chem simulation.

Hatching (x-filled bars) indicates the O_x species that were not measured at the sites.

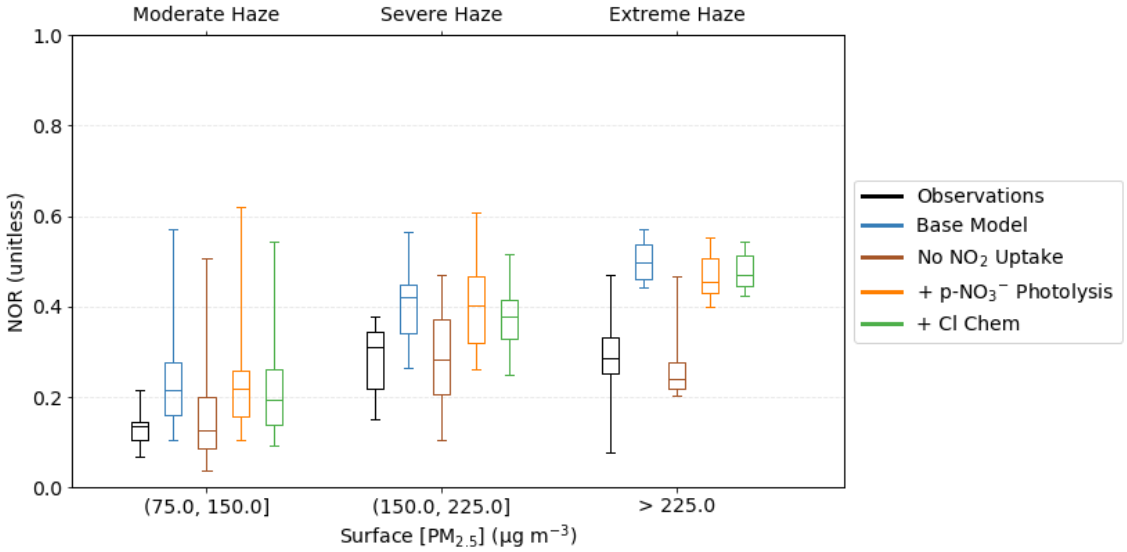

Figure A-21 Comparison of nitrogen oxidation ratio (NOR) in observations and four simulations (Base, No NO_2 uptake, + p-$NO3^-$ Photolysis, and + Cl Chem). under different haze regimes.

A-22 (a)

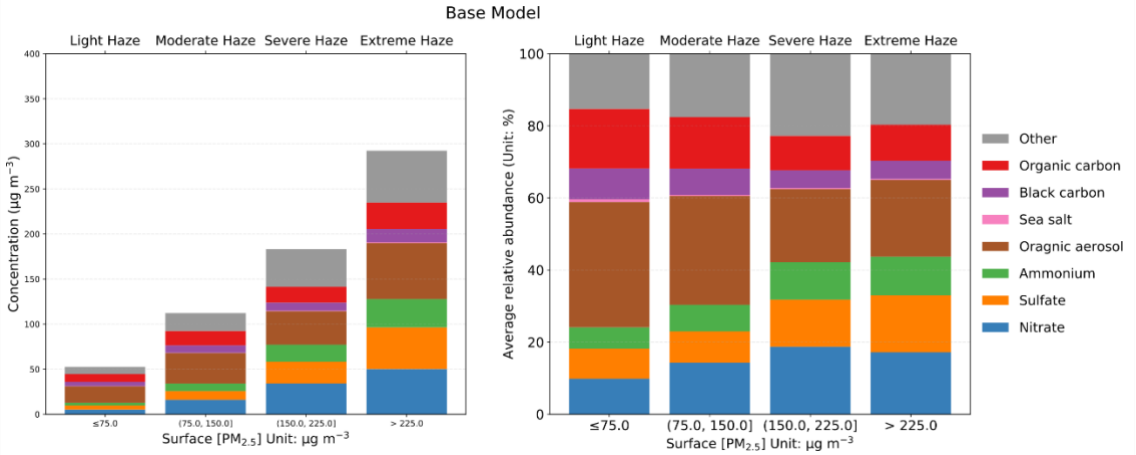

A-22 (b)

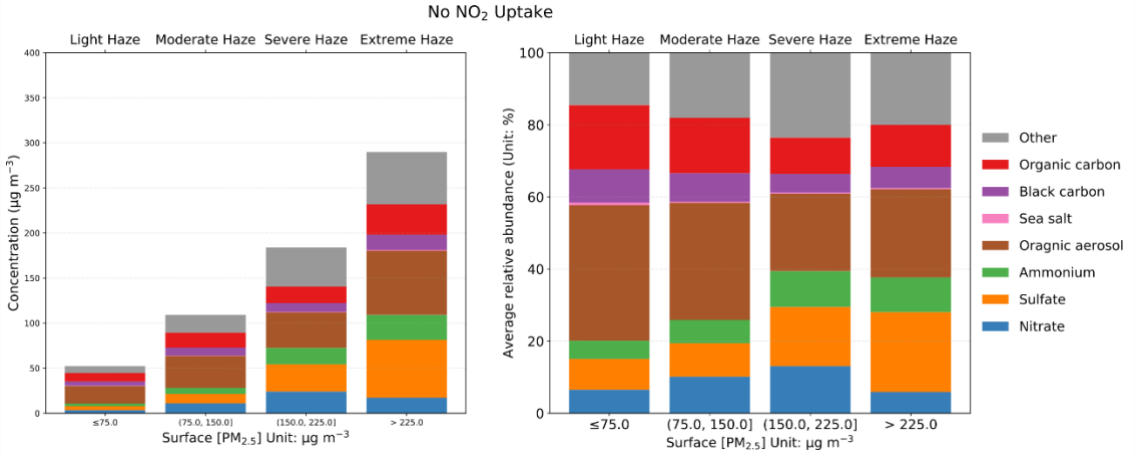

A-22 ©

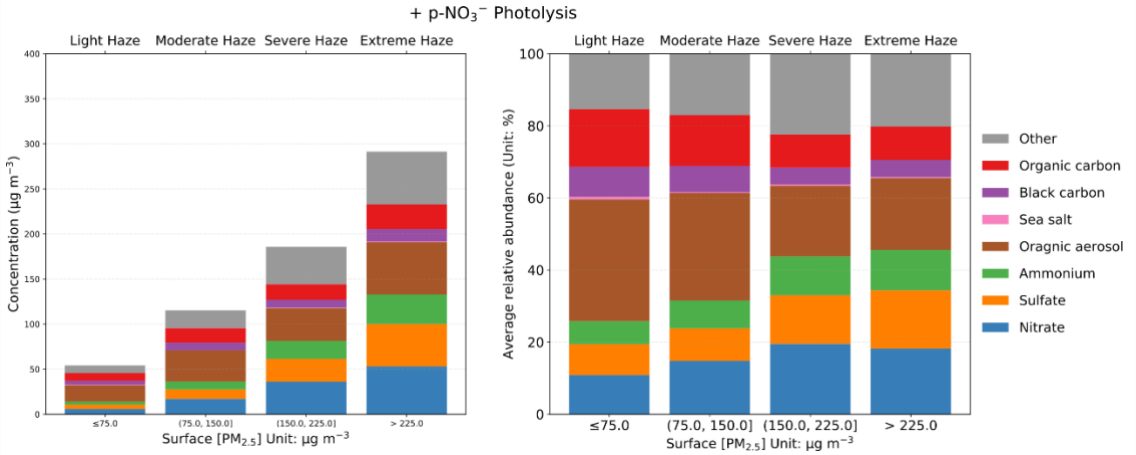

A-22 (d)

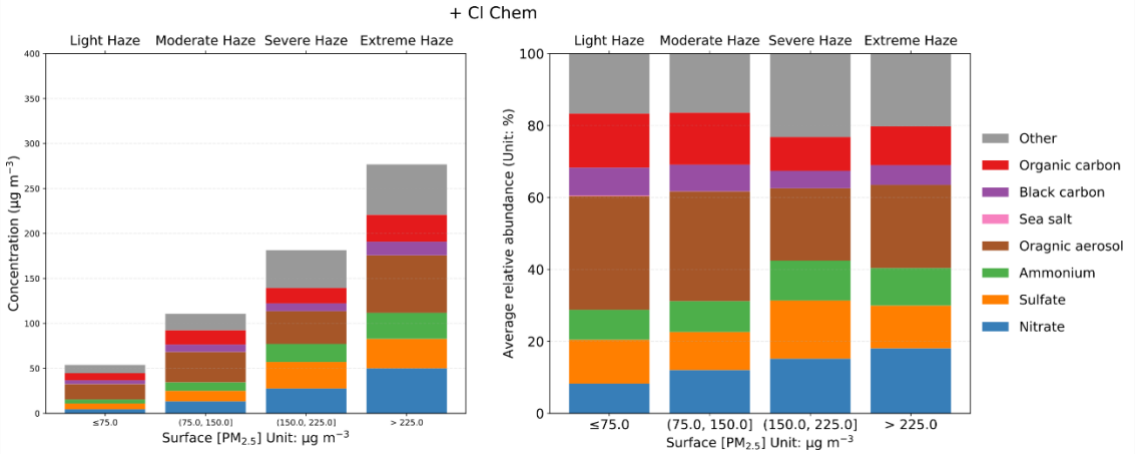

Figure A-22. Simulated speciation of $PM_{2.5}$ under different haze regimes in (a) base simulation, (b) No NO_2 Uptake simulation, (c) + p-NO_3^- Photolysis simulation, and (d) + Cl Chem simulation.

A-23 (a)

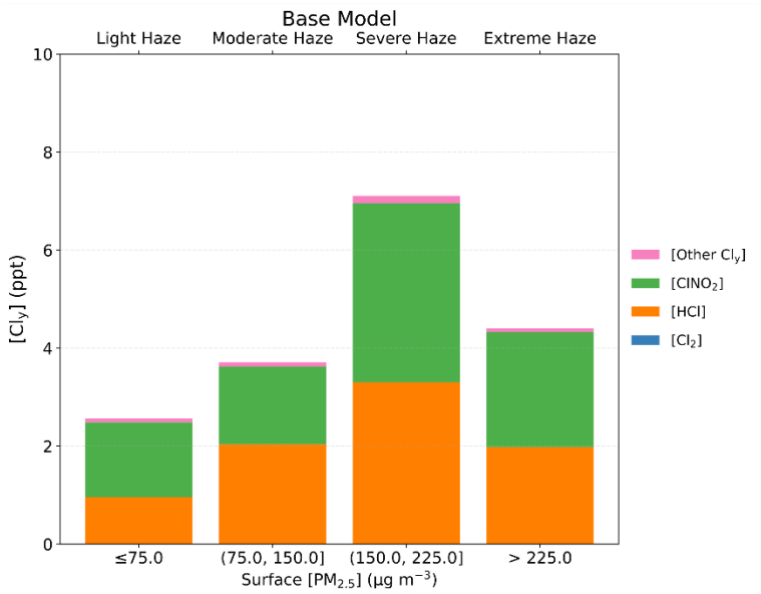

A-23 (b)

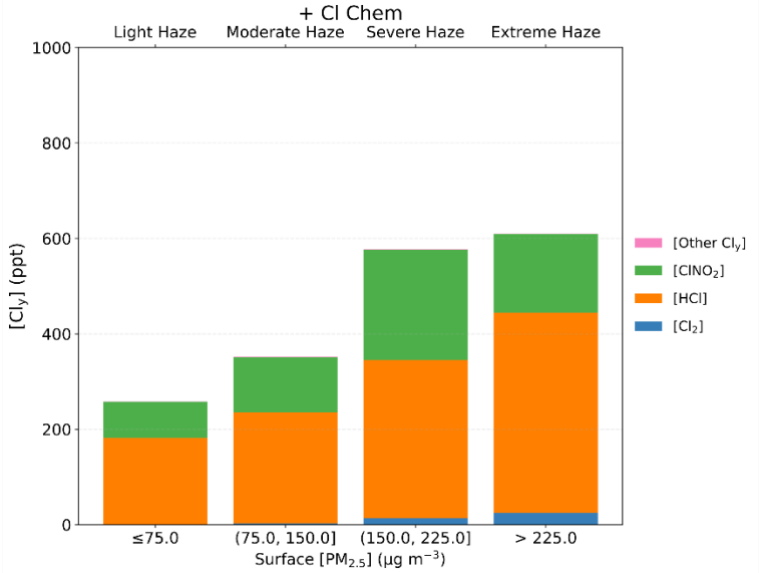

Figure A-23. Concentration and speciation of Cl_y under different haze regimes in (a) base simulation and (b) + Cl Chem simulation.

Other Cl_y includes Cl, HOCl, $ClNO_3$, BrCl, and ICl. The y-axes in A-23(a) and A-23(b) differ by a factor of 100.

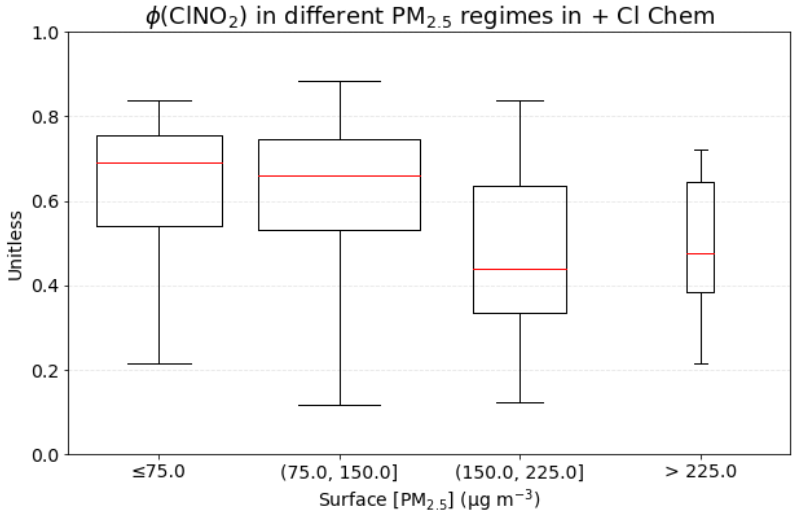

Figure A-24. The modeled yield of $ClNO_2$ ($\phi(ClNO_2)$) from the uptake of N_2O_5 (R10) on aerosol in the + Cl Chem simulation.

$\phi(ClNO_2)$ also indicates the relative importance of the N_2O_5 + Cl- pathway because $\phi(ClNO_2) = \frac{\text{rate of R10b}}{\text{rate of R10a+ rate of R10b}}$. The width of boxes scales with the number of samples in each haze regime.

A.3 SUPPLEMENTARY TABLES FOR CHAPTER 2 AND APPENDIX A.1

Table A-1 Summary of the important reactions of NO_y family species in the troposphere.

Additional notes: ᵅ Although most of the parameterization presented above list HNO_3(g) as the product of the uptake reaction, the GC model re-computes the partition between HNO_3(g) and p-NO_3^- (aerosol) at each timestep. The GC model predicts p-NO_3^- to be the dominant form of NO_3^- in wintertime Beijing (See more in Figure **A-14** and Section 2.4.3).

	Chemical reaction	**Effect on final** $\Delta^{17}O(NO_3^-)$	**Notes**
Gas-phase reactions			
R1	$NO + HO_2 \rightarrow NO_2 + OH$ $NO + RO_2 \rightarrow NO_2 + RO$	Decrease	
R2	$NO + \xi O \rightarrow NO_2 + \xi$	Increase	ξ stands for halogen (Br/Cl/I)
R3	$NO + O_3 \rightarrow NO_2 + O_2$	Increase	
R4	$NO_2 + OH \rightarrow HNO_3$	Decrease	
R6	$NO_2 + O_3 \rightarrow NO_3 + O_2$	Increase	
R9	$NO_3 + NO2 \rightarrow N_2O_5$	Increase	
R12	$NO_3 + VOCs \rightarrow HNO_3$ + other products	Increase	
R13	$NO_2 + \xi O \rightarrow \xi NO_3$	Increase	ξ stands for halogen (Br/Cl/I)
R15	$NO_2 + RO_2 \rightarrow RONO_2$	Decrease	
Photolysis reactions			
R7	NO_3 (g) + hv → NO_2 (g) + O (g) NO_3 (g) + hv → NO (g) + O_2 (g)	N/A	

R17	NO_2 (g) + hv → NO (g) + O (g)	N/A	
Heterogeneous reactions (model's parameterization) [α]			
R5	NO_2 (g) $\xrightarrow[\text{aerosol, } H_2O]{}$ 0.5 HNO_3 (g) + 0.5 HONO (g)	Decrease	Uptake of NO_2 (g) takes place on sulfate-nitrate-ammonium (SNA), black carbon, organic carbon, mineral dust and sea-salt aerosols in the GC model.
R8	NO_3 (g) $\xrightarrow[\text{aerosol}]{}$ p-NO_3^- (aerosol)	Increase	Uptake of NO_3 (g) takes place on SNA, black carbon, organic carbon, and sea-salt aerosols in the GC model.
R10 (a)	N_2O_5 (g) $\xrightarrow[\text{aerosol, } H_2O]{}$ 2HNO_3 (g)	Increase	This channel for N_2O_5 uptake is always activated on SNA, black carbon, organic carbon, mineral dust and sea-salt aerosols in the GC model.
R10 (b)	N_2O_5 (g) $\xrightarrow[\text{aerosol, } H_2O, Cl^-]{}$ HNO_3 (g) + $ClNO_2$ (g)	Increase	This channel for N_2O_5 uptake is activated when chloride is present in modeled fine-mode aerosol (0.01 μm ≤ radius ≤ 0.5 μm).
R11	N_2O_5 (g) $\xrightarrow[\text{cloud}]{}$ 2HNO_3 (g)	Increase	
R14	ξNO_3 (g) $\xrightarrow[\text{aerosol, } H_2O]{}$ HNO_3 (g)	Increase	Uptake of ξNO3(g) takes place on SNA and sea-salt aerosols in the GC model.
R16	RONO2 (g) $\xrightarrow[\text{aerosol, } H_2O]{}$ HNO_3 (g) + other products	Decrease	Uptake of ξNO3(g) takes place on SNA aerosols in the GC model.

Table A-2. Frequency of different haze regimes (unit: number of days).

The observations with aerosol samples cover 51 days from 1 October 2014 and 15 January 2015. The air-quality station observations cover 123 days from 1 October 2014 to 31 January 2015. The main simulations cover 123 days from 1 October 2014 to 31 January 2015.

	Light Haze	**Moderate Haze**	**Severe Haze**	**Extreme Haze**
Observations (days with aerosol samples only)	21	14	5	11
Observations	64	33	14	14
Base Model	34	48	25	16
No NO_2 Uptake	38	49	28	8
+ p-NO_3^- Photolysis	34	46	24	19
+ Cl Chem	30	48	30	15

Table A-3. Model-observation comparison of wintertime concentration of various volatile organic compounds in Beijing. The predictions from our base simulation are used as the "modeled values" in this table. [a] Statistics of the observations of C. Liu et al. (2017) at the Research Center for Eco-Environmental Sciences (RCEES) site in Beijing, which cover from December 15, 2015 to January 14, 2015. [b] The statistics of the observations of K. Li et al. (2019) at the National Center for Nanoscience and Technology of China (NCNST site) in Beijing, which cover from January 31, 2015 to February 15, 2015. [c] Statistics of the observations of J. Li et al. (2015) at the Peking University (PKU) site in Beijing, which cover from October 18, 2014 to November 22, 2014. [d] Statistics of the wintertime observations of Acton et al. (2020) from a 325 m high meteorological mast located on the campus of the Institute of Atmospheric Physics, Chinese Academy of Sciences (IAP) in Beijing, which cover from November 12, 2016 to December 10, 2016.

	Whole Simulation	**C. Liu et al. (2017)[a]**	**K. Li et al. (2019)[b]**	**J. Li et al. (2015)[c]**	**Acton et al. (2020)[d]**	**Light Haze**	**Moderate Haze**	**Severe Haze**	**Extreme Haze**	**C. Liu et al. (2017)[a]**	**Acton et al. (2020)[d]**
	Modeled Mean ± S.D.	**Observed Mean ± S.D.**				**Modeled Range**				**Observed Maximum**	
Aromatic compounds											
Benzene	0.907 ± 0.571	1.810 ± 1.199	1.930 ± 1.610	1.622	2.000 ± 1.740	0.226-0.959	0.322-1.527	0.443-1.814	0.577-3.386	8.270	9.110
Toluene	1.353 ± 0.620	1.670 ± 1.143	1.510 ± 1.140	2.425	1.940 ± 1.870	0.276-1.285	0.646-2.022	0.815-2.375	1.194-4.044	8.410	9.430
Xylene	1.378 ± 0.577	1.116		1.245		0.284-1.471	0.507-2.123	0.632-2.375	1.054-3.432		
Alkanes											
Ethane	3.430 ± 0.777	9.764 ± 5.647		9.922		2.128-3.727	2.615-4.221	2.940-4.651	3.700-6.815		
Propane	3.586 ± 1.746	6.570 ± 4.023		5.415		0.956-3.318	1.691-5.133	2.372-6.083	3.052-11.149	28.510	
C≥4 alkanes	5.224 ± 2.049	8.434		11.062		1.542-4.969	2.686-6.960	3.810-8.506	5.051-13.475		
Alkenes											
Ethylene		8.001 ± 5.129		7.906						31.650	
C≥3 alkenes	2.552 ± 1.206	3.753		2.404		0.530-2.893	0.722-4.328	0.853-4.764	1.542-6.486		
Isoprene	0.007 ± 0.009	0.115 ± 0.045	0.220 ± 0.130	0.080	1.210 ± 1.030	0.000-0.032	0.001-0.043	0.001-0.044	0.001-0.023		

Monoterpenes	0.007 ± 0.006		0.060 ± 0.060			0.001-0.020	0.001-0.021	0.003-0.041	0.003-0.022		
Alcohols											
Methanol	1.624 ± 0.681		12.860 ± 6.030			0.396-1.407	1.034-2.271	1.064-2.786	1.494-4.409		
Ethanol	1.523 ± 0.773				24.320 ± 20.830	0.331-1.514	0.561-2.408	0.704-2.886	1.274-4.775		93.980
Aldehydes											
Formaldehyde	1.444 ± 0.916					0.320-1.042	0.656-1.880	1.080-2.588	1.945-6.290		
Acetaldehyde	0.955 ± 0.556		1.880 ± 0.970		4.920 ± 3.660	0.247-0.731	0.490-1.333	0.810-1.694	1.056-3.608		17.420
C≥3 aldehydes	0.010 ± 0.007			0.930		0.002-0.008	0.003-0.020	0.008-0.025	0.013-0.035		
Ketones											
Acetone	1.178 ± 0.371		4.180 ± 1.720	3.007	2.800 ± 2.000	0.579-1.066	0.803-1.717	1.002-2.127	1.249-2.169		9.660
Methylethylketone (MEK)	0.234 ± 0.082		1.890 ± 0.670	1.058		0.108-0.227	0.154-0.324	0.215-0.431	0.263-0.552		
Methylvinylketone(MVK) + Methacrolein(MACR)	0.010 ± 0.015		0.310 ± 0.210	0.301		0.000-0.026	0.001-0.046	0.002-0.060	0.002-0.050		
Other VOCs											
Formic acid	2.369 ± 1.564		4.390 ± 1.490			0.413-2.642	0.553-4.498	0.690-5.345	1.446-8.477		
Acetic acid	0.009 ± 0.003		4.500 ± 2.800			0.004-0.009	0.005-0.016	0.006-0.020	0.009-0.020		